

AD-A076 497

VIRGINIA POLYTECHNIC INST AND STATE UNIV BLACKSBURG F/G 11/4  
DEFECT-PROPERTY RELATIONSHIPS IN COMPOSITE MATERIALS. PART IV.(U)  
JUN 79 K L REIFSNIDER , E G HENNEKE F33615-77-C-5044

UNCLASSIFIED

AFML-TR-76-81-PT-4

NL

1 OF 2

AD  
A076497



AFML-TR-76-81  
Part IV

② LEVEL III  
A062611

**A076497**

DEFECT-PROPERTY RELATIONSHIPS IN COMPOSITE MATERIALS

K. L. Reifsnider, E. G. Herneke, II and W. W. Stinchcomb

Virginia Polytechnic Institute & State University  
Blacksburg, Virginia 24061

JUNE 1979

DDC FILE COPY

Final Report

February 1977 - February 1979

Approved for public release; distribution unlimited.

AIR FORCE MATERIALS LABORATORY  
AIR FORCE WRIGHT AERONAUTICAL LABORATORIES  
AIR FORCE SYSTEMS COMMAND  
WRIGHT-PATTERSON AIR FORCE BASE, OHIO 45433

DDC  
RECEIVED  
NOV 14 1979  
B

79 13 11 345

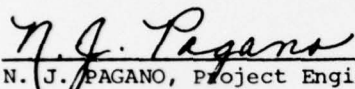


NOTICE

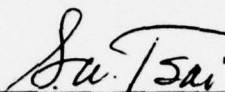
When Government drawings, specifications, or other data are used for any purpose other than in connection with a definitely related Government procurement operation, the United States Government thereby incurs no responsibility nor any obligation whatsoever; and the fact that the government may have formulated, furnished, or in any way supplied the said drawings, specifications, or other data, is not to be regarded by implication or otherwise as in any manner licensing the holder or any other person or corporation, or conveying any rights or permission to manufacture, use, or sell any patented invention that may in any way be related thereto.

This report has been reviewed by the Information Office (OI) and is releasable to the National Technical Information Service (NTIS). At NTIS, it will be available to the general public, including foreign nations.

This technical report has been reviewed and is approved for publication.

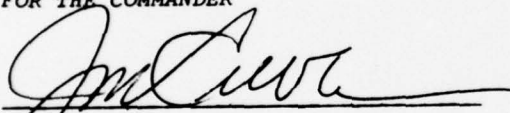


N. J. PAGANO, Project Engineer  
Mechanics & Surface Interactions Branch  
Nonmetallic Materials Division



S. W. TSAI, Chief  
Mechanics & Surface Interactions Branch  
Nonmetallic Materials Division

FOR THE COMMANDER



J. M. KELBLE, Chief  
Nonmetallic Materials Division

"If your address has changed, if you wish to be removed from our mailing list, or if the addressee is no longer employed by your organization please notify AFML/MBM, W-PAFB, OH 45433 to help us maintain a current mailing list".

Copies of this report should not be returned unless return is required by security considerations, contractual obligations, or notice on a specific document.

UNCLASSIFIED

SECURITY CLASSIFICATION OF THIS PAGE (When Data Entered)

REPORT DOCUMENTATION PAGE		READ INSTRUCTIONS BEFORE COMPLETING FORM	
1. REPORT NUMBER 18 AFML TR-76-81 (Part IV)	2. GOVT ACCESSION NO.	3. RECIPIENT'S CATALOG NUMBER	
4. TITLE (and Subtitle) 6 DEFECT-PROPERTY RELATIONSHIPS IN COMPOSITE MATERIALS. Part IV.	5. TYPE OF REPORT & PERIOD COVERED 9 Technical Final rept. 7 Feb 77 - 6 Feb 79	6. PERFORMING ORG. REPORT NUMBER	
7. AUTHOR(s) 10 K. L. Reifsnider E. G. Henneke, II W. W. Stinchcomb	8. CONTRACT OR GRANT NUMBER(s) 15 F33615-77-C-5044	9. PROGRAM ELEMENT, PROJECT, TASK AREA & WORK UNIT NUMBERS 16 2419-03-13	17 1703
11. CONTROLLING OFFICE NAME AND ADDRESS Air Force Materials Laboratory (MBM) Wright-Patterson AF Base, Ohio 45433	12. REPORT DATE 11 June 1979	13. NUMBER OF PAGES 139	14. SECURITY CLASS. (of this report) UNCLASSIFIED
14. MONITORING AGENCY NAME & ADDRESS (if different from Controlling Office) 12 146	15. SECURITY CLASS. (of this report) UNCLASSIFIED	16. DISTRIBUTION STATEMENT (of this Report) Approved for public release; distribution unlimited.	17. DISTRIBUTION STATEMENT (of the abstract entered in Block 20, if different from Report) 62102F
18. SUPPLEMENTARY NOTES B			
19. KEY WORDS (Continue on reverse side if necessary and identify by block number) Composite Materials, Graphite-epoxy, Defects, Properties, First Ply Failure, Nondestructive Testing, Delamination, Cracking			
20. ABSTRACT (Continue on reverse side if necessary and identify by block number) This report describes the results of an investigation of the nature of damage in two graphite-epoxy laminates under various loading histories, with special attention to the changes in mechanical properties caused by specific damage mechanisms. The results include several new findings, the development of unique investigative methods and some substantial deviations from common model predictions. The discovery of a "characteristic damage state" is reported.			

DD FORM 1 JAN 73 1473

EDITION OF 1 NOV 65 IS OBSOLETE

UNCLASSIFIED

SECURITY CLASSIFICATION OF THIS PAGE (When Data Entered)

407 206

JLW

## PREFACE

This is the final report of work completed under Contract F33615-77-C-5044 from the Air Force Materials Laboratory, Wright Patterson AFB between February 7, 1977 and February 6, 1979. The technical monitor of the contract was Dr. N. J. Pagano. The work was executed at Virginia Polytechnic Institute and State University under the direction of Drs. K. L. Reifsnider, E. G. Henneke, II and W. W. Stinchcomb. The authors gratefully acknowledge the support of the Air Force Materials Laboratory, and the enthusiastic encouragement and guidance provided by Dr. Pagano during the course of this work.

Appreciation is also extended to Phyllis Schmidt for typing this manuscript.

ACCESSION for	
NTIS	White Section <input checked="" type="checkbox"/>
DDC	Buff Section <input type="checkbox"/>
UNANNOUNCED	<input type="checkbox"/>
JUSTIFICATION _____	
BY _____	
DISTRIBUTION/AVAILABILITY CODES	
Dist.	AVAIL. and/or SPECIAL
A	

# TABLE OF CONTENTS

SECTION		PAGE
I	Introduction. . . . .	1
II	Approach. . . . .	5
	Development of New Test Methods . . . . .	12
III	Static Test Results . . . . .	17
	Test Results: Fatigue Loading. . . . .	52
	Survey Tests on Comparison Laminates. . . . .	73
IV	Mechanics of the "Characteristic Damage State". . .	78
V	Summary and Closure . . . . .	124
	Appendix A. . . . .	129
	REFERENCES. . . . .	135

# LIST OF ILLUSTRATIONS

FIGURE		PAGE
1 A-D.	Crack Patterns in Type I Laminates . . . . .	18
1 E-H.	Crack Patterns in Type I Laminates . . . . .	19
1 I-K.	Crack Patterns in Type I Laminates . . . . .	21
2 A-D.	Crack Patterns in Type II Laminates. . . . .	23
2 E-G.	Crack Patterns in Type II Laminates. . . . .	25
3.	Number of Cracks Observed in Each 90° Lamina at Edge I of Type II Specimen 2652-14 . . . . .	28
4.	Number of Cracks Observed in Each 90° Lamina at Edge II of Type II Specimen 2652-14. . . . .	29
5.	Number of Cracks Observed in 90°, +45° and -45° Lamina of Type I Specimen I-6. . . . .	31
6.	Number of Cracks Observed in 90°, +45° and -45° Lamina of Type II Specimen 2652-10 . . . . .	32
7.	Average Crack Spacing in 90° and +45° Laminae for Edges I and II of Specimen 2652-14 . . . . .	34
8.	Average Crack Spacings in 90° (bottom curve) and -45° (top curve) Lamina for Specimen No. I-6 . . .	35
9.	Average Crack Spacing in 90° (bottom curve) and -45° (top curve) Laminae for Specimen No. I-9. . .	36
10.	Average Crack Spacings in 90° Laminate for Five Type I Specimens. . . . .	38
11.	Average Crack Spacings in -45° Laminae for Five Type I Specimens. . . . .	39
12.	Average Crack Spacings in 90°, +45° and -45° Laminae for Type II Specimen No. 2652-10 . . . . .	43
13.	Average Crack Spacings for 90°, +45° and -45° Laminae for Type II Specimen No. 2652-8. . . . .	44
14.	Average Crack Spacing in 90° Laminae for Four Type II Specimens. . . . .	46
15.	Average Crack Spacings in +45° Laminae for Four Type II Specimens. . . . .	47



FIGURE	PAGE
16. Average Crack Spacings in $-45^\circ$ Laminae for Four Type II Specimens. . . . .	48
17. Schematic Diagram of Sectioning and Data Collecting Scheme for Cyclic Testing. . . . .	53
18. Number of Observed Cracks as a Function of Cycles of Loading at 40 ksi (275.6 MPa) for Specimen I-15, in the $90^\circ$ Plies (top curve), $-45^\circ$ Plies (middle curve) and $+45^\circ$ Plies (bottom curve) . . . . .	55
19. Spacing of Cracks as a Function of Cycles of Loading for Specimen I-15, in the $+45^\circ$ (top), $-45^\circ$ (middle) and $90^\circ$ (bottom) Plies . . . . .	57
20. Crack Spacings as a Function of Cycles of Loading at 40 ksi (275.6 MPa) in the $90^\circ$ Plies of Several Type I Laminates . . . . .	59
21. Crack Spacings as a Function of Cycles of Loading at 40 ksi (275.6 MPa) in the $-45^\circ$ Plies of Several Type I Laminates . . . . .	60
22. Crack Spacings as a Function of Cycles of Loading at 40 ksi (275.6 MPa) in the $+45^\circ$ Plies of Several Type I Laminates . . . . .	61
23. Number of Observed Cracks as a Function of Cycles of Loading at 40 ksi (275.6 MPa) for Specimen II-20 in the $90^\circ$ Plies (top curve), $+45^\circ$ Plies (middle curve) and $-45^\circ$ Plies (bottom curve) . . . . .	62
24. Spacing of Cracks as a Function of Cycles of Loading for Specimen II-20 in the $90^\circ$ (bottom), $+45^\circ$ (middle) and $-45^\circ$ (top) Plies . . . . .	63
25. Crack Spacings in the $90^\circ$ Plies of Several Type II Specimens as a Function of Cycles of Loading . . . . .	65
26. Crack Spacings in the $+45^\circ$ Plies of Several Type II Specimens as a Function of Cycles of Loading . . . . .	66
27. Crack Spacings in the $-45^\circ$ Plies of Several Type II Specimens as a Function of Cycles of Loading . . . . .	67
28. Histogram of Crack Spacings for Measurements from $+45^\circ$ Laminae of a Type II Laminate . . . . .	70
29. Histogram of Crack Spacings for Measurements from $-45^\circ$ Laminae of a Type II Laminate . . . . .	71



FIGURE	PAGE
30. Histogram of Crack Spacings for Measurements from 90° Laminae of a Type II Laminate. . . . .	72
31. Schematic Diagram of Crack Patterns in a Type III Laminate . . . . .	75
32. Equilibrium Element Used for One-Dimensional Model of Characteristic Damage State Formation . . . . .	80
33. Normalized Stress as a Function of Distance from the Crack Face Predicted by the Analysis . . . . .	85
34. Observed (top) and Predicted (bottom) Characteristic Damage State for Type I Laminate . . . . .	89
35. Observed (top) and Predicted (bottom) Characteristic Damage State for Type II Laminate. . . . .	90
36. Schematic Diagram of the Cracked Laminate. . . . .	91
37. Through-the-thickness Variation of $\sigma_x$ for a Type I Laminate with a 90° Ply Crack. . . . .	96
38. Through-the-thickness Variation of $\sigma_x$ for a Type II Laminate with a 90° Ply Crack. . . . .	97
39. Through-the-thickness Variation of $\sigma_x$ for a Type I Laminate with 90° and -45° Ply Damage. . . . .	98
40. Through-the-thickness Variation of $\sigma_x$ for a Type II Laminate with 90° and 45° Ply Damage. . . . .	99
41. Contours of $\tau_{xz}$ (psi) for a Type I Laminate with 90° and -45° Ply Damage. . . . .	101
42. Contours of $\tau_{xz}$ (psi) for a Type II Laminate with 90° and 45° Ply Damage . . . . .	102
43. Variation of the Shear Stress $\tau_{xz}$ with $x$ Directly Above the Crack Tip for Damaged Type I Laminates . . . . .	103
44. Variation of the Shear Stress $\tau_{xz}$ with $x$ Directly Above the Crack Tip (in the 0° ply) for Damaged Type II Laminates. . . . .	104
45. Variation of the Shear Stress $\tau_{xz}$ with $x$ Above the First Node Ahead of the Crack Tip for Damaged Type I Laminates . . . . .	105

FIGURE	PAGE
46. Through-the-thickness Variation of the Interlaminar Normal Stress for a Type I Laminate with Cracked 90° Ply. . . . .	107
47. Through-the-thickness Variation of the Interlaminar Normal Stress for a Type II Laminate with Cracked 90° Plies. . . . .	108
48. Through-the-thickness Variation of the Interlaminar Normal Stress for a Type I Laminate with Cracked 90° and -45° Plies . . . . .	109
49. Through-the-thickness Variation of the Interlaminar Normal Stress for a Type II Laminate with 90° and 45° Ply Cracks . . . . .	110
50. Pre-fracture Crack Patterns Showing A Breakdown of the Characteristic Damage State By Crack Coupling and Longitudinal Cracking. . . . .	112
51. Through-the-thickness Variation of $\sigma_x$ Ahead of the Crack Tip for Complete Off-axis Ply Failure (crack tip in 0° ply) . . . . .	114
52. Contours of $\tau_{xz}$ (psi) for a Type I Laminate with Complete Off-axis Ply Failure. . . . .	115
53. Through-the-thickness Variation of $\sigma_z$ for a Type I Laminate with Complete Off-axis Ply Failure. . . . .	117
54. Contours of $\sigma_z$ (psi) for a Type I Laminate with Complete Off-axis Ply Failure. . . . .	118
55. Contours of Strain Energy (psi) for a Type I Laminate with Complete Off-axis Ply Failure . . . . .	120
56. Pre-fracture Crack Patterns for Two Laminates Showing Crack Coupling and Longitudinal Cracking . . . . .	121
57. Variation of $\sigma_x$ with Distance from the Crack Face for a Type I Laminate with 90° Plies Cracked . . . . .	123
A1. Transverse in-plane normal stress in a $[0, \pm 45, 90]_S$ laminate. The thermal residual stresses are shown by the solid lines while the stresses due to a 4.45 kN applied load are shown by the dotted lines. . . . .	130

FIGURE	PAGE
A2. Through-the-thickness " $\sigma_z$ " stress distribution for a $[0, \pm 45, 90]_S$ laminate . . . . .	131
A3. Transverse in-plane normal stress in a $[0, 90, \pm 45]_S$ laminate. Solid lines show thermal residual stresses while dotted lines show the stresses under a 4.45 kN applied load . . . . .	133
A4. Through-the-thickness " $\sigma_z$ " stress distribution for a $[0, 90, \pm 45]_S$ laminate . . . . .	134

# LIST OF TABLES

TABLE	PAGE
1 Room Temperature Material Property Data Type AS/3501 Graphite Epoxy. . . . .	8
2 Average Mechanical Properties of Graphite Epoxy Laminates. . . . .	8
3 Stress Level (MPa) at which Saturation Spacing First Attained by Type I Specimen. . . . .	41
4 Number of Cracks/Saturation Spacing Attained by Type I Specimens. . . . .	42
5 Stress Level (MPa) at which Saturation Spacing First Attained by Type II Specimens. . . . .	50
6 Number of Cracks/Saturation Spacing (mm) Attained by Type II Specimens. . . . .	51
7 Statistical Aspects of Crack Spacing Observations. . . . .	69
8 Predicted and Observed Crack Spacings for the Characteristic Damage State in Several Laminates . . . . .	87

## SECTION I

### INTRODUCTION

The entire discipline of solid mechanics was originally developed as a means to describe the response of "ideal" materials, materials that were generally homogeneous (i.e., only one material phase can be distinguished on a scale of length pertinent to engineering considerations), had uniform material properties from point to point, were continuous, and in some cases were also linear, elastic and isotropic. As notch-sensitive materials became more commonly used for structural applications, especially during World War II, treatments of behavior dominated by single notches, cracks or other defects appeared, and the subdiscipline called "fracture mechanics" was developed. Fracture mechanics was a significant departure from the phenomenological yield theories or failure theories that had been the only alternative earlier, in that it recognized the importance of a damage state, a characteristic condition that was common to notch sensitive materials, which controlled the state of stress and state of strength for a given geometry and loading, namely, a single crack. While fracture mechanics is not generally thought of as a mechanistic approach, especially not in the sense of dislocation theories of strength which were also developed during that time, it is based on what might be called a mechanistic characterization of the most important aspects of the damage state which controls response in many homogeneous notch-sensitive materials at the engineering level.

Composite materials are not homogeneous, and, using our earlier definition of that word, the individual material phases are large enough in characteristic dimension (volume, length, etc.) so that their individual

as well as combined response is of importance to engineering considerations. The single most important consequence of that fact is that when these materials are subjected to significant load histories a very complex combination of defects may develop in each phase as well as between phases. In fact, since fibrous composite materials are generally used in laminated form with certain layers oriented in one direction and other layers having different orientations, and since the strength and stiffness of each layer is highly anisotropic, when several layers are laminated together with different orientations they will develop very different types and degrees of damage during a specific loading. Hence, the resulting laminate damage state will be non-uniform through the thickness in a manner defined by the anisotropic material properties of each ply and the stacking sequence of the plies.

In the context of even these simple and obvious facts, the most common approaches to the description of damage development in composite laminates (as well as the resulting strength, life and stiffness) are at least incomplete; in some cases they are unreasonable. The most widely used approach is the "failure theory" concept whereby a phenomenological philosophy is adopted which results in a relationship which is imagined to represent the strength of the laminae in a laminate. Some systematic reduction of laminae properties may be effected for sequential application of the failure theory to successive ply failure and eventual laminate fracture. This approach is of great value to current engineering design considerations, but it is inherently limited by its phenomenological nature. Moreover, the stress states calculated to compare with such failure surfaces are calculated using the ideal undamaged condition



rather than some characteristic damage state as a basis for the determination. While it is true that some properties (usually stiffness) may be changed to simulate a damaged condition, the same boundary value problem (representing the ideal undamaged state) is generally solved. When stress concentrators are present, the so-called notched response must be treated differently, usually by some "adjusted" or "fitted" linear elastic fracture mechanics approach, or a closely related restatement of single-flaw analysis with additional parameters [1]. Neither of these approaches has any direct relationship to the mechanisms of damage development or fracture. Neither of these approaches is sensitive to stacking sequences, edge effects, interlaminar stresses, interlaminar constraint effects on strength, or microstructural detail of any kind. The successes and failures of these two approaches are not the object of this report; there are a considerable number of each.

A rational general approach to the mechanics of failure of laminated composite materials has not been established, primarily because a thorough and complete understanding of damage has not been established, a characteristic damage state or condition has not been identified, and the corresponding mechanics problem has not been set. Indeed, it may not be possible to identify a single characteristic damage state for all laminates, but it is certainly not possible to deal with every crack on an individual basis. Nor can much real progress be made by continued refining of empirical or phenomenological descriptions which have very limited sensitivity to the physical damage involved.

In the context of these remarks, the following are the objectives of the present investigation.

- 1) To identify the precise nature of damage development in quasi-isotropic graphite-epoxy laminates under various load histories,
- 2) to determine the physical parameters which lead to a loss of strength and/or life,
- 3) to establish the mechanics of the individual and combined action of these parameters as they influence mechanical response, and
- 4) to address the question of how these findings can best be described by analysis.

The purpose of undertaking these objectives is to attempt to develop an understanding of the precise nature of damage so that a rational approach to the mechanics of failure can be determined. The motivations for these activities are both practical and academic. The designer who uses composite laminates, as well as the academician, should be able to predict laminate response from lamina response, to estimate notched or unnotched strength accurately, to estimate life, to predict the change in stiffness of a component, and to design materials and material systems for specific service (including reliability) specifications.

## SECTION II

### APPROACH

The approach to attaining the objectives stated previously was largely experimental. Analytical treatments of some of the situations observed in the laboratory were introduced to enhance the learning process and to develop an understanding of the mechanics which applied to the observed behavior. The general approach was to attempt to determine completely and precisely, the nature of damage, that is, the initiation, growth and interaction of damage modes in composite laminates during various load histories. Secondly, a study was made to identify an underlying characteristic that related the many details of damage development to each other in order to properly and uniquely define a damage state for these materials. Finally, an attempt was made to develop analytical descriptions and models, based on the well defined damage state, which could be used to generalize the understandings and to anticipate behavioral response without recourse to excessive testing.

The experimental investigations were conducted using AS/3501 graphite epoxy composite laminates having the following stacking sequences:

- $(0, \pm 45, 90)_S$  , Type I
- $(0, 90, \pm 45)_S$  , Type II
- $(0, 90_2, \pm 45)_S$  , Type III
- $(90_2, 0, \pm 45)_S$  , Type IV .

All specimens were normally 178 mm (7.0 in.) long by 25.4 mm (1.0 in.) wide and had end taps. Type I and Type II specimens had a 76 mm (3.0 in.) test section, and Type III and Type IV specimens had a 70 mm (2.75 in.) test section. The same specimen geometry was used for static

tension and tension-tension fatigue tests. A number of investigative techniques were employed before, during, and after the mechanical tests to measure the response of the material and study the damage state in the specimens. The techniques include:

- microscopy
- ultrasonic c-scan
- ultrasonic attenuation
- acoustic emission
- replication
- x-radiography
- stiffness
- thermography
- sectioning.

The analytical work used to assist in the interpretation of data and representation of the damage process includes:

- a laminated plate theory stress analysis with thermal residual stress and interlaminar normal stress approximation
- a finite element stress analysis of the transverse plane of the specimens
- a one-dimensional model of a characteristic damage state
- a three-dimensional finite difference solution of the stress balance equations for a variety of cracked-ply problems.

Static tension tests were conducted in displacement control on an Instron testing machine and in load control on an MTS load frame. Strains were measured using strain gages (single element and rosettes) and a 25.4 mm (1.0 in.) extensometer. Tensile loads were applied using a slow rate

ramp function. At selected intervals in the loading, the tests were interrupted to observe edge damage using microscopy and replication techniques while the specimens were in the testing machine and under load. Some tests were terminated prior to fracture and the specimens were sectioned to determine the extent of damage growth through the width of the specimens. In other cases, the tests were run to fracture. Material and laminate properties are given in Tables 1 and 2, respectively.

Cyclic loading tests were performed in load control at 15 Hz with a stress ratio  $R = 0.1$ . Strains were measured by a 25.4 mm (1.0 in.) extensometer attached to the specimen and the load and strain signals were processed on-line by a Tektronix WP1100 data acquisition system. At intervals of 1650 cycles, the system provided data on maximum load, maximum strain, compliance, damping, and specific damping. At selected cyclic intervals, the fatigue tests were stopped and the specimens were held at mean load for a short period of time while making replicas of the damage on the free edges of the specimens. In some cases, the tests were terminated prior to one million cycles so that through-the-width sectioning studies could be made to examine the damage in interior regions. Specimens which survived one million cycles were either sectioned or loaded to fracture in tension to determine residual stress.

During the static and fatigue tests, attempts were made to follow the initiation and development of damage in a nondestructive manner. When possible, these investigations were carried out in real time or with only short interruptions in the loading history. Three techniques for the study of damage states in composites have been developed and

TABLE 1  
ROOM TEMPERATURE MATERIAL PROPERTY DATA  
TYPE AS/3501 GRAPHITE EPOXY

<u>Property</u>	<u>Type I</u>	<u>Type II</u>	<u>Type III</u>	<u>Type IV</u>
Average 0° Tensile Strength (KSI)	232	225	---	---
Average 0° Tensile Modulus (MSI)	20.0	19.4	---	---
Fiber Volume (%)	63.8	60.4	63.4	62.2
Resin Content (%)	28.87	31.95	29.0	30.0
Density (lb/in. <sup>3</sup> )	0.0577	0.0570	0.0578	0.0574
Void Content (%)	0.13	0.04	0.16	0.47
Ply Thickness (in.)	0.0054	0.0054	---	---

TABLE 2  
AVERAGE MECHANICAL PROPERTIES OF  
GRAPHITE EPOXY LAMINATES

<u>Property</u>	<u>Type I</u>	<u>Type II</u>	<u>Type III</u>	<u>Type IV</u>
Elastic Modulus (MSI)	6.2	6.5	5.5	5.0
Tensile Strength (KSI)	67.3	70.4	55.6	59.3
Fracture Strain ( $\mu$ in/in)	10,400	11,400	---	---



applied during this program. These techniques, namely the replication technique, a modified pulse-echo ultrasonic technique, and vibrothermography, are described in more detail later in this section.

A number of more common techniques have also been used in concert with each other and with the newly developed techniques. A brief description of each technique follows:

- 1) Microscopy - Light microscopy and scanning electron microscopy were used to observe the details of cracks and delaminations. Early in the program, a traveling light microscope was attached to the crosshead of the testing machine to observe the edges of the specimens during static tests. A major limitation of this form of microscopy was the localized field of view and the long time required to scan and photograph the entire length of the free edge of the specimen. In many cases, the damage events just prior to fracture occurred outside the field of view of the microscope. This form of light microscopy was replaced by the replication technique.
- 2) Ultrasonic c-scan - The c-scan is one of the more frequently used nondestructive methods for inspection of composite materials. It is particularly suited for detecting defects in the plane of a laminated plate, and mapping regions of relative good and bad quality in the plate. However, it is not possible to quantify the severity of a defective region on an absolute scale and the data is most accurately interpreted when it is compared to a c-scan of a calibrated test standard. In the present investigation, the c-scan was primarily used to

determine the extent of the through-the-width growth of edge delaminations.

- 3) Acoustic emission - During several static tension tests, acoustic emission was monitored to detect the initiation of damage in the laminates. Generally, the first acoustic emissions were recorded at stresses between 15 and 25 percent of the static tensile strength, and the acoustic emission count rate increased steadily until the applied stress reached approximately 70 percent of static strength. At higher stress, the count rate became constant or decreased slightly until just before fracture. Although the acoustic emission data is difficult to interpret in terms of discrete damage events (matrix cracks, fiber fracture, delamination, etc.), the trends in the data are consistent with observations made using other techniques.
- 4) Radiography - The acceptance of x-radiography as a common nondestructive evaluation technique for graphite epoxy composites has been impeded by the need to use an image enhancement agent, such as tetra-bromoethane (TBE), to make the damaged regions opaque to x-rays. However, it is possible in some instances to create a situation which permits "soft" x-radiography of graphite epoxy without the need for an image enhancement agent. Although all aspects of the technique are not completely understood at the present time, some success has been achieved in our laboratory in resolving the details of internal damage such as matrix cracks, delaminations, and flaws.

- 5) Stiffness - Unlike strength, stiffness decreases monotonically with damage and the change in stiffness can be monitored to follow the development of damage throughout the loading history. In some design situations, stiffness changes may be incorporated in the failure criterion. Change in stiffness data correlates very well with data from other techniques which measure damage in composite laminates. Specifically, a sharp change in ultrasonic attenuation and, in some cases, acoustic emission count rate occur at the same stress, at a knee or step in the static stress strain curve. During cyclic loading of Type II laminates, the static and dynamic stiffnesses may decrease by as much as 10 to 12 percent while strength decreases by only 2 to 3 percent over one million cycles. The strength of Type I laminates, for example, tested in fatigue at the same maximum stress (310 MPa) decreased by 15 percent after one million cycles, and the stiffnesses decreased by 8 to 11 percent.
- 6) Sectioning - In order to completely and precisely determine the nature and extent of damage in the composite laminates, a large number of specimens with monotonic and cyclic loading histories were sectioned parallel to the loading axis and examined using the replication method. Sectioning studies aid in the interpretation of the nondestructive investigation data and provide a detailed description of the damage state along the length and through the width of the specimen. The results of these studies are presented in this report.

#### Development of New Test Methods

The development of several experimental techniques that are distinctly advantageous for the study of the initiation and growth of damage in composite materials has been one of the major auxiliary contributions of this program. Replication, a modified pulse-echo ultrasonic technique, and vibrothermography have proven their versatility and importance as complementary, experimental methods for monitoring the mechanical behavior of graphite-epoxy laminates. The replication technique uses a cellulose-acetate tape to record the surface topography of a material and, as applied to composites, yields much information on the development of damage along free edges (and can also be used to infer interior damage). The modified pulse-echo method, on the other hand, yields real-time information about the development of damage in the interior of the composite. Finally, the vibrothermography technique indicates damaged regions throughout the entire volume of the specimen. The development of each of these techniques and their utility for obtaining data in the present program are discussed in the following section.

The replication method, as indicated above, uses a cellulose-acetate tape to record the surface topography of a material. The tape is applied to the desired surface partially dissolved or softened with acetone and allowed to set on the surface. Because of the good wettability of the plastic for graphite-epoxy materials, the softened tape will flow into the underlying surface and when set, create an exact duplicate record of that surface. Replication procedures have been employed for a long time for the study of metallographic micro-structures.

However, as far as the present authors are aware, the technique was first applied and adapted to composites during this program. For composite materials research, the technique has proven invaluable as a means of recording the state of damage at intermediate points during the load-time history applied to a specimen. The final failure site, for example, can be followed backward through the replicas to ascertain the pattern of damage development in this region. Furthermore, as discussed throughout this report and in earlier reports, the replication method has been directly and immediately responsible for obtaining the data required for the development of the characteristic damage state model. The development of the first transverse cracks in the weakest layers, the subsequent multiplication into an equilibrium set of uniformly spaced cracks, the additional development of transverse cracks in the adjacent layers, and the final development of damage in the region of final failure is easily followed and interpreted on the replicas.

Much work has also been done to develop the technique to the point that free edge information can be used to infer damage development in the interior, that is, across the width, of the composite specimens. A large number of sectioning and replication tests were performed to verify that, at least at the higher load levels, the information contained on the replicas taken from the free edges is quite consistently indicative of the damage state across the width of the material.

The ultrasonic pulse-echo method for measuring attenuation of stress waves in materials was modified as part of this project to measure the attenuation in thin, composite laminates with the use of a buffer, or delay, block. This procedure has been detailed in earlier reports



[2-3]. Careful analysis of the path followed by the echos in the specimen and buffer blocks led to the conclusion that measured attenuation changes had to be accounted for by diffraction or scattering effects caused by the developing damage state in the composite [4]. An analysis was developed that can account for every type of attenuation change that was observed experimentally, although at the present time, the predictions are only qualitative [5]. The attenuation measurements were consistent in every case, in that a small change in attenuation was always observed to occur at a load consistent with the first appearance of transverse cracks in the 90° laminae and a large change always occurred at the load corresponding to the knee in the bi-linear load-strain curve. In the large majority of runs, these changes corresponded to an increase in attenuation, but in a few cases, the attenuation decreased. Again, these effects can be accounted for by the diffraction model when one considers different crack spacings or crack openings.

The modified pulse-echo method has proven to be a very sensitive monitoring method for indicating the onset of damage in the interior of the composite laminates. It has now been used on a number of different laminate configurations and in a number of different projects. In every case, it yields a sharp indication of damage initiation that has been verified by other methods such as sectioning and X-radiography.

A third NDT technique that is both novel and unique was developed through the support of this project. Vibrothermography [6] employs low-amplitude mechanical vibrations to excite thermal patterns around damaged regions. The thermal patterns are detected and displayed by a real-time video-thermographic camera. The mechanical vibrations in the



specimen are preferentially transformed into thermal energy by either coulomb or hysteretic stress-strain effects in areas of internal damage. Stress concentrations around these regions generate greater hysteretic heating at those locations. The preferential heating develops thermal gradients that are easily detectable with a thermographic camera. There are two important aspects of this technique which should be noted; (1) the high frequency (~20 kHz) mechanical vibrations applied to the specimen are of such low amplitude that they do not cause additional mechanical damage and (2) since the developed heat patterns are directly related to the stress fields, they are also closely correlated with the actual mechanical state of damage. The last point should be considered in comparison to the more usual thermographic method used elsewhere whereby an external heat source is used to passively heat a material and the thermographic camera is used to detect thermal gradients established by regions of varying thermal conductivity. Such regions may be caused by any number of variations (heterogeneous materials, for example) that are not necessarily directly related to the mechanical damage state. Analysis [6] has shown that for graphite-epoxy laminates the surface heat patterns detected by the thermographic camera are nearly identical to the underlying damage zone.

The vibrothermography technique has recently attracted some attention in the aerospace industry and in a number of research laboratories as a possible method for detecting damage in composite structures. Further development and discussions are on-going between those organizations and our laboratory to help effect the technology transfer.

These three experimental techniques that have been developed under the support of this project in our laboratory are uniquely capable of

determining, with a high degree of accuracy and reproducibility, the damage state in a composite laminate. The three techniques are complementary in that each yields differing information about damage in different regions of the specimen. Taken together, they yield reasonably complete information about the degree of damage in the laminate.

### SECTION III

#### STATIC TEST RESULTS

As mentioned previously, from studies of replicas made at increasing load, we can observe progressive damage at the specimen edge. These studies have been made of specimens loaded quasi-statically to high stress levels and cyclically at lower stress levels. Results of observations indicate that two distinct damage patterns develop in the specimens depending on the stacking sequence, i.e., the damage states in Type I and Type II materials were reproducible from specimen to specimen and were distinctly different according to the specimen type. Furthermore, the reproducible "Characteristic Damage State" was identical for specimens loaded quasi-statically and cyclically.

In the case of both Type I and Type II specimens, damage in the form of transverse cracking appears first. In both cases, it appears first in  $90^\circ$  laminae, i.e., the lamina whose fibers are perpendicular to the load axis or the lamina with the lowest strength along the load axis. Initially, these transverse cracks are arrested at the lamina interfaces, and do not propagate to adjacent plies. With increasing load, cracks appear for a time almost solely in these  $90^\circ$  laminae. Stated differently, the general trend is for the damage pattern to develop along the entire length of the specimen rather than through the laminate thickness to adjacent lamina. From this point on, however, the sequence of events differs for the two stacking sequences. In Type I  $[0, \pm 45, 90]_s$  laminates, as load increases, the number of transverse cracks in the  $90^\circ$  lamina increases until a constant or saturation spacing is reached. These transverse cracks extend continuously across both  $90^\circ$  lamina and initially stop at the  $90^\circ/-45^\circ$  lamina interfaces (Fig. 1A, B, C).



A



B



C



D

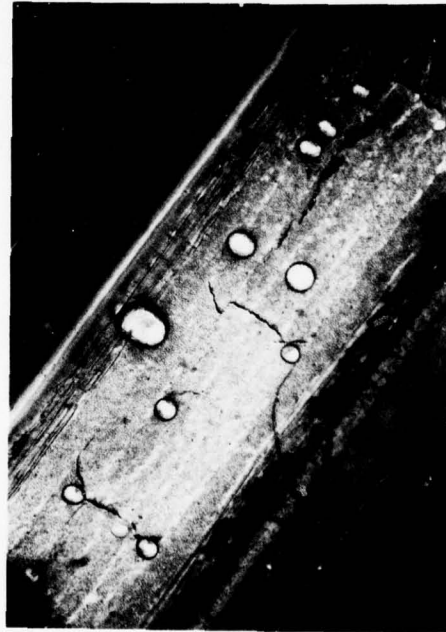
Figure 1. Crack Patterns in Type I Laminates



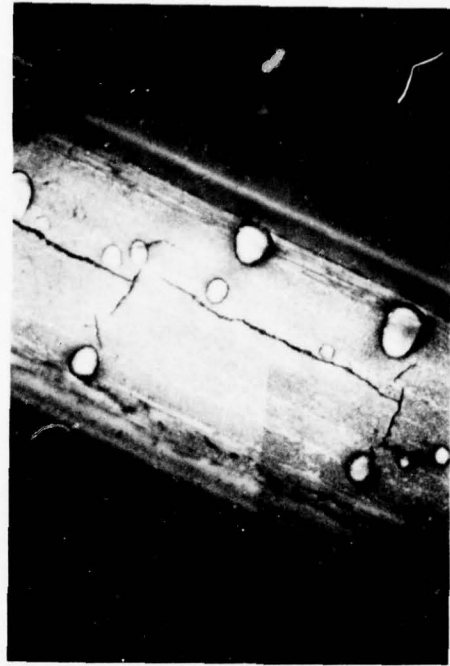
E



F



G

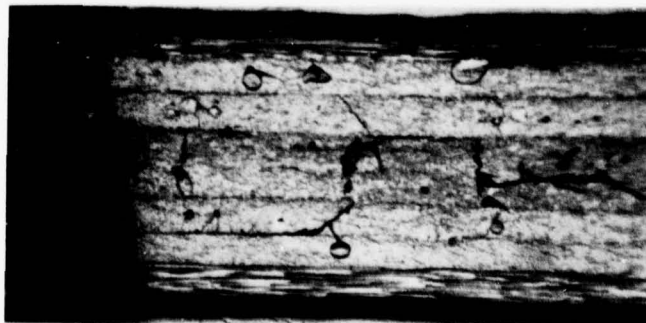


H

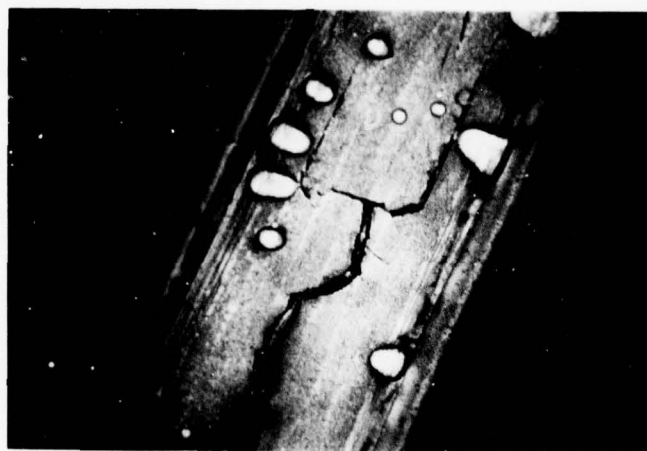
Figure 1. (cont'd) Crack Patterns in Type I Laminates



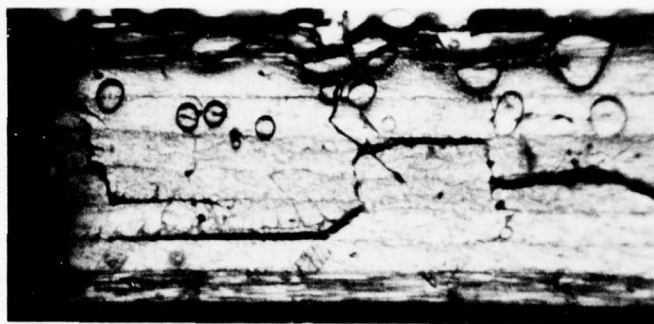
As the load increases, however, these cracks extend into the adjacent  $-45^\circ$  lamina and terminate at the  $-45^\circ/+45^\circ$  lamina interface. Hence, cracks in these  $-45^\circ$  lamina are frequently associated with transverse cracks in the  $90^\circ$  lamina. While all transverse cracks in the  $90^\circ$  lamina are flat, i.e., are perpendicular to the lamina interfaces, the cracks in the  $-45^\circ$  lamina are angular. They appear at angles approximately  $45^\circ$  from the horizontal as shown in Fig. 1D, E. All cracks along the length of a  $-45^\circ$  lamina have the same orientation and make approximately the same angle with the horizontal. Furthermore, as the figures show, cracks in the opposite  $-45^\circ$  lamina (on the other side of the  $90^\circ$  laminae) are mirror images of the aforementioned cracks. Again, all cracks within those laminae are consistent in orientation. Cracks in the  $-45^\circ$  lamina on the opposite specimen edge have a reverse orientation, in the sense that they extend in a direction which forms an angle with the through-the-thickness "z" direction which has an opposite sign compared to its counterpart on the opposite edge, if the origin of their rotation is taken to be the point at which they join the transverse cracks in the  $90^\circ$  plies. Again, cracks in the opposite  $-45^\circ$  laminae are mirror images. Examination of specimens sectioned lengthwise through the center of the width reveals that the transverse cracks in the  $-45^\circ$  lamina are colinear with those in the  $90^\circ$  plies. Coincident to the appearance of the transverse crack extension into the  $-45^\circ$  lamina, longitudinal cracks appear in the  $90^\circ$  laminae. These longitudinal cracks seem to grow from transverse cracks as indicated in Figs. 1E, F and G. Eventually all of these longitudinal cracks join also, linking all transverse cracks (Fig. 1H). Examination reveals that in extending over the specimen length, the longitudinal crack will at times "jog" to the  $90^\circ/-45^\circ$  interface (delamination) and then "jog" back to the interior



I



J



K

Figure 1. (cont'd) Crack Patterns in Type I Laminates

of a  $90^\circ$  lamina or to the central  $90^\circ/90^\circ$  lamina interface as shown in Fig. 1I. In other instances, central longitudinal cracks have been observed to intersect a transverse crack and "jog" simultaneously to both  $90^\circ/-45^\circ$  interfaces, forming a fork pattern such as that shown in Fig. 1J. In the case of static loading, once transverse crack saturation spacing has been reached, branching into the first adjacent  $45^\circ$  lamina has been completed and the longitudinal crack/delamination has extended over the specimen length, no new damage appears. Very few cracks were observed in the  $+45^\circ$  lamina for static loading, even when loading was carried to failure. When they did appear, however, they were horizontal in orientation and extended from the  $-45^\circ/+45^\circ$  interface to the  $+45^\circ/0^\circ$  interface (Fig. 1K). If loading continued, the central longitudinal crack opened further, extending from the edges toward the center of the specimen, until failure occurred. This can be demonstrated by comparing the longitudinal cracks in Figs. 1I and 1K.

Damage in the Type II  $[0,90,+45]_S$  specimens again begins in the form of transverse cracks in the  $90^\circ$  lamina. Again they initially span only the  $90^\circ$  lamina and do not cross the  $90^\circ/+45^\circ$  interfaces, as shown in Fig. 2A. These cracks become much more numerous than the transverse cracks in the Type I material, i.e., the saturation spacing is much smaller (0.332 mm average for 6 Type II specimens vs 0.735 mm average for 5 Type I specimens). The  $90^\circ$  lamina are not adjacent in this stacking sequence and constraint on the  $90^\circ$  lamina is also much greater (the adjacent lamina have  $0^\circ$  and  $+45^\circ$  orientations as opposed to  $-45^\circ$  and  $90^\circ$  orientations in the Type I material). The stiffer plies surrounding the  $90^\circ$  plies transfer the stress back into the  $90^\circ$  ply over a shorter distance above and below a crack than for the type I laminate causing the next crack



A



B



C



D

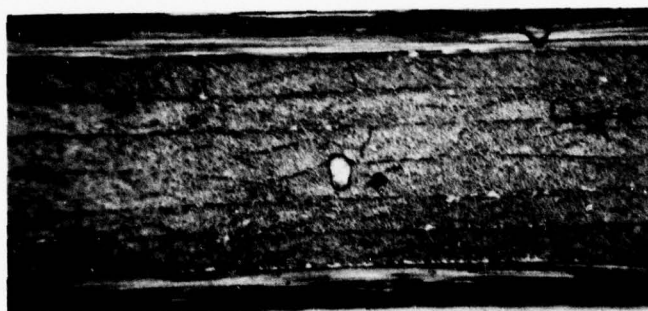
Figure 2. Crack Patterns in Type II Laminates

to form closer to a given preceding crack. Because the cracks are much smaller and more numerous, observation becomes much more difficult in the Type II material. This, in turn, makes fixing the exact chronology of damage events more difficult. As the load increases, transverse cracks appear in all the remaining off-axis laminae. These subsequent cracks are more numerous in the  $45^\circ$  laminae adjacent to the  $90^\circ$  lamina than in the interior  $45^\circ$  laminae. (The saturation spacing in the  $+45^\circ$  laminae was 0.693 mm for 6 specimens vs 1.712 mm for the  $-45^\circ$  lamina in the same statically loaded specimens.) As mentioned earlier, these different crack spacings are entirely a result of the rate at which stress builds back up from zero at the crack face in a broken ply. The stiffness of the broken ply and the stiffness of the surrounding plies determine this rate of build up and, therefore, the spacing of the cracks. The closest distance from an existing crack that a new one can form is the distance required to transfer stress back into the broken ply up to the undisturbed level that formed the first crack. Figures 2B, C illustrate these differences. Of the cracks in the  $45^\circ$  lamina adjacent to  $90^\circ$  lamina, nearly half of them appear to be linked to cracks in the  $90^\circ$  lamina. This is particularly evident at elevated load (Fig. 2G). This is similar to the observation that a large number of transverse cracks in the  $-45^\circ$  laminae in the Type I material appeared to develop from transverse cracks in the  $90^\circ$  laminae. However, in the case of the Type II material most of the transverse cracks were aligned at approximately  $45^\circ$  angles to the transverse plane at the outside edges. Figure 2G shows that some transverse cracks in the  $+45^\circ$  laminae are horizontal (in the transverse plane) and others form at some angle to the horizontal for this case. As was the case for Type I material,

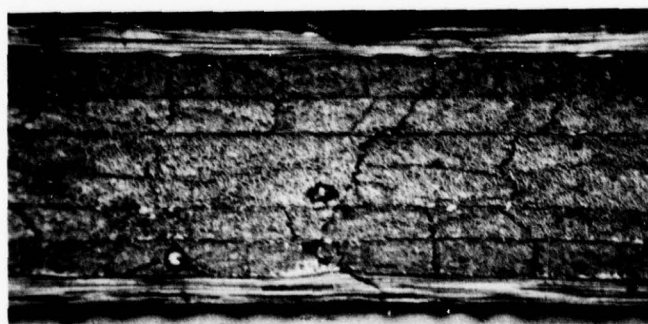




E



F



G

Figure 2. (cont'd) Crack Patterns in Type II Laminates

cracks in the double interior plies ( $-45^\circ$  laminae for Type II material,  $90^\circ$  laminae for the Type I material) extended across both interior plies as seen in Fig. 2D. Also similar to the Type I material was the appearance of longitudinal cracking, again in the  $90^\circ$  lamina or at the  $90^\circ/+45^\circ$  interface (Figs. 2E, F). In Type II material, however, this longitudinal cracking did not extend along the entire specimen length. It occurred only in short segments in one or two locations along the specimen length. The depth of penetration of the longitudinal edge cracks was also less than it was for the Type I material. In general, each off axis lamina seeks to achieve a saturation crack spacing before ultimate laminate failure. This can be demonstrated by comparing Figs. 2G and 2C which cover the same general specimen area.

At this point we introduce the concept of a characteristic damage state. While the precise and complete nature of this concept will be explained in subsequent sections, a statement of the concept will be useful at this point. We have discovered that the transverse cracks that form in the off-axis plies do not form in a random way, but form a regular pattern with a regular spacing of cracks in each layer of each laminate. The most important aspects of this regular crack spacing are that it is a laminate property (entirely determined by the material in each ply, the stacking sequence of the plies, and the laminate properties but independent of load history, geometry, residual stress, etc.) and that it is stable in the sense that when that pattern has formed no new transverse cracks form in that ply until quite close to fracture at which time cracks grow through the thickness from ply to ply. We have come to call this condition the "characteristic damage state" (CDS) of a laminate.

Having described the general sequence of events leading to failure and introduced the concepts of saturation spacing and a characteristic damage state (Figs. 1D, E and 2G), we will now look more closely at the details of the physical behavior. In the interest of presenting data in its most useful and meaningful context, information defining the observed characteristic damage states will be reported in terms of crack spacing. This can be interpreted, physically, as the average distance between transverse cracks when the whole length of the lamina is examined. These distances were determined by dividing the lamina length by the total number of transverse cracks observed in a given lamina. These values were obtained by scanning the replicas of specimen edges and counting the number of transverse cracks in each lamina. These numbers will, of course, be identical for the center two laminae ( $-45^\circ$  plies for Type II material and  $90^\circ$  plies for Type I material) since cracks in these lamina extend across both plies. However, values obtained for each  $+45^\circ$  and  $-45^\circ$  (Type I) lamina and each  $90^\circ$  and  $-45^\circ$  lamina will generally differ slightly. In those laminae we were monitoring damage in two "identical" plies symmetrically positioned about the laminate midplane. To simplify the data presentation, the average of those two values was used in subsequent calculations. The validity of this operation is seen when Figs. 3 and 4 are examined. Figures 3 and 4 show the total number of cracks over the 75 mm (3 in) gage length in each  $90^\circ$  lamina of specimen 2652-14 (edges I and II respectively) at low stress levels. These figures show the crack development in each  $90^\circ$  lamina to be quite constant; indeed, they coincide at several stress levels.

It can be shown that this procedure is equivalent to physically measuring the distance between each crack and taking the numerical

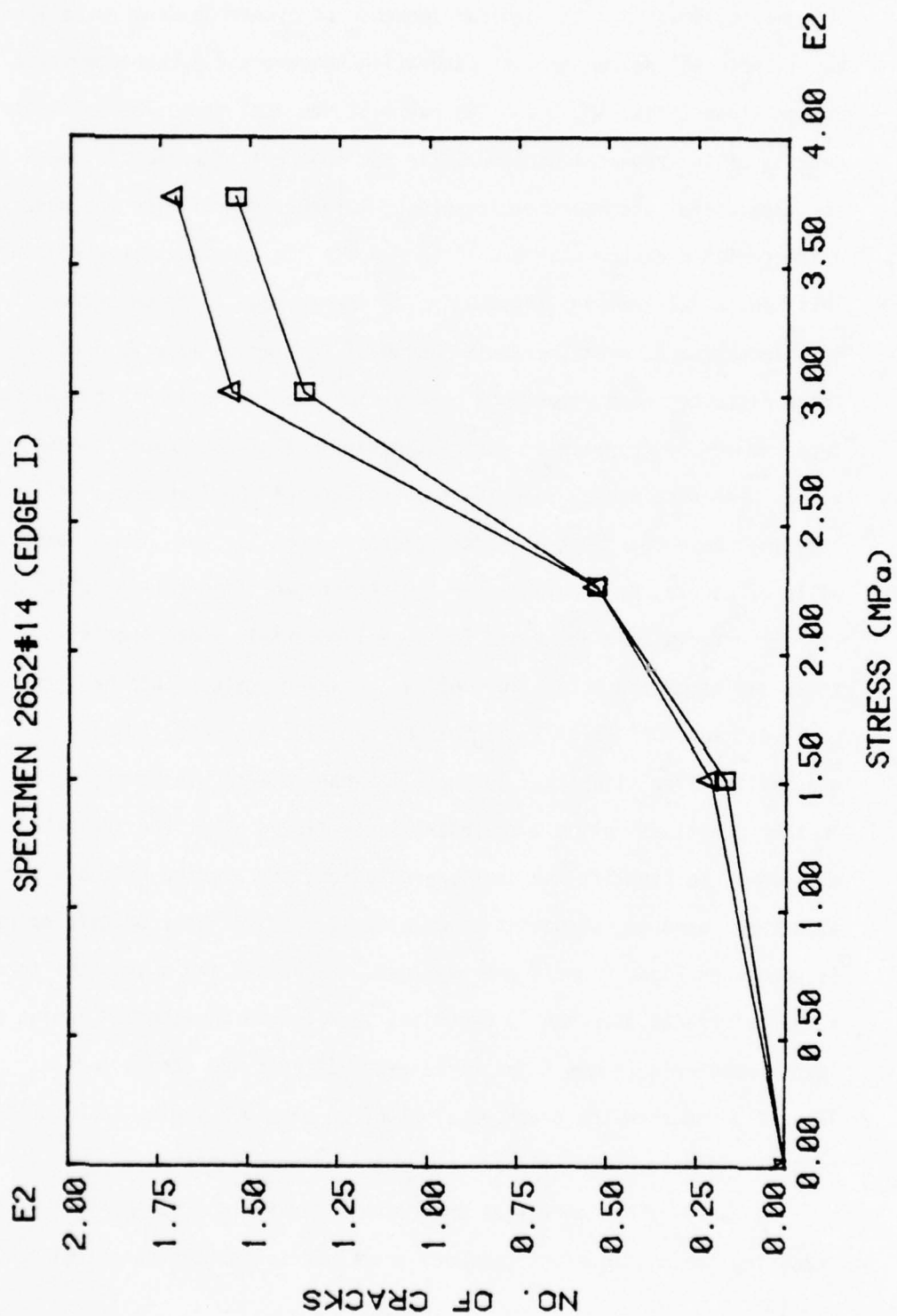


Figure 3. Number of Cracks Observed in each 90° Lamina at Edge I of Type II Specimen 2652#14

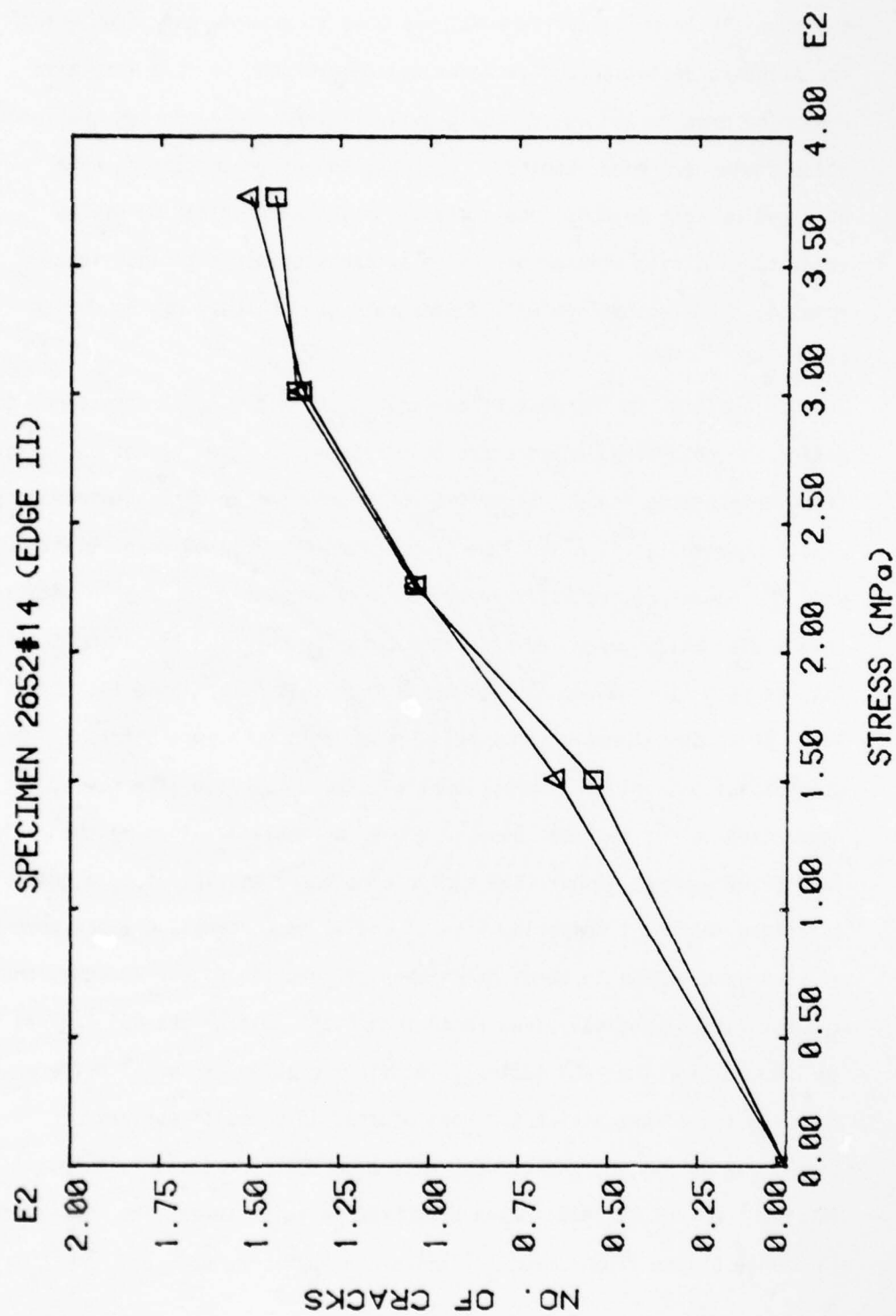


Figure 4. Number of Cracks Observed in each 90° Lamina at Edge II of Type II Specimen 2652#14



average. While this later process was used to provide data from which the standard deviation and variance was determined, it is a very time consuming process and would have greatly limited the number of specimens which could have been examined. A comparison of crack spacing data obtained by both methods, and a statistical characterization of the crack spacing data will be presented in the section on Fatigue Test Results. This comparison will demonstrate the validity of the chosen procedure.

In addition to the ease of operation, there are other advantages to making and reporting damage state observations in terms of the number of transverse cracks found. Figures 5 and 6 show the results obtained for Type I specimen No. I-6 and Type II specimen No. 2652-10 respectively. When the number of cracks is reported in this manner, the stable saturation levels are easily perceived as plateaus in the curves. Comparing these figures with Figs. 8 and 12, it can be seen that determining the stress level at which saturation spacing is reached is much more difficult when crack spacing is plotted versus applied stress. In the later case, the resolution is not as great because we are essentially plotting the inverse of a whole number (the number of cracks) multiplied by a constant (specimen length). Comparing Figs. 7 and 12 also reveals another advantage of recording damage in terms of numbers of cracks. Figure 12 shows that the saturation spacing values range from 0.385 mm (for the 90° lamina) to 1.65 mm (for the -45° lamina). At first glance, the small difference may seem to be insignificant. When plotted in terms of numbers of cracks, as in Fig. 6, the values range from 204 (for the 90° lamina) to 46 (for the -45° lamina). When presented in this manner, the differences in damage states from lamina to lamina are much more obvious.

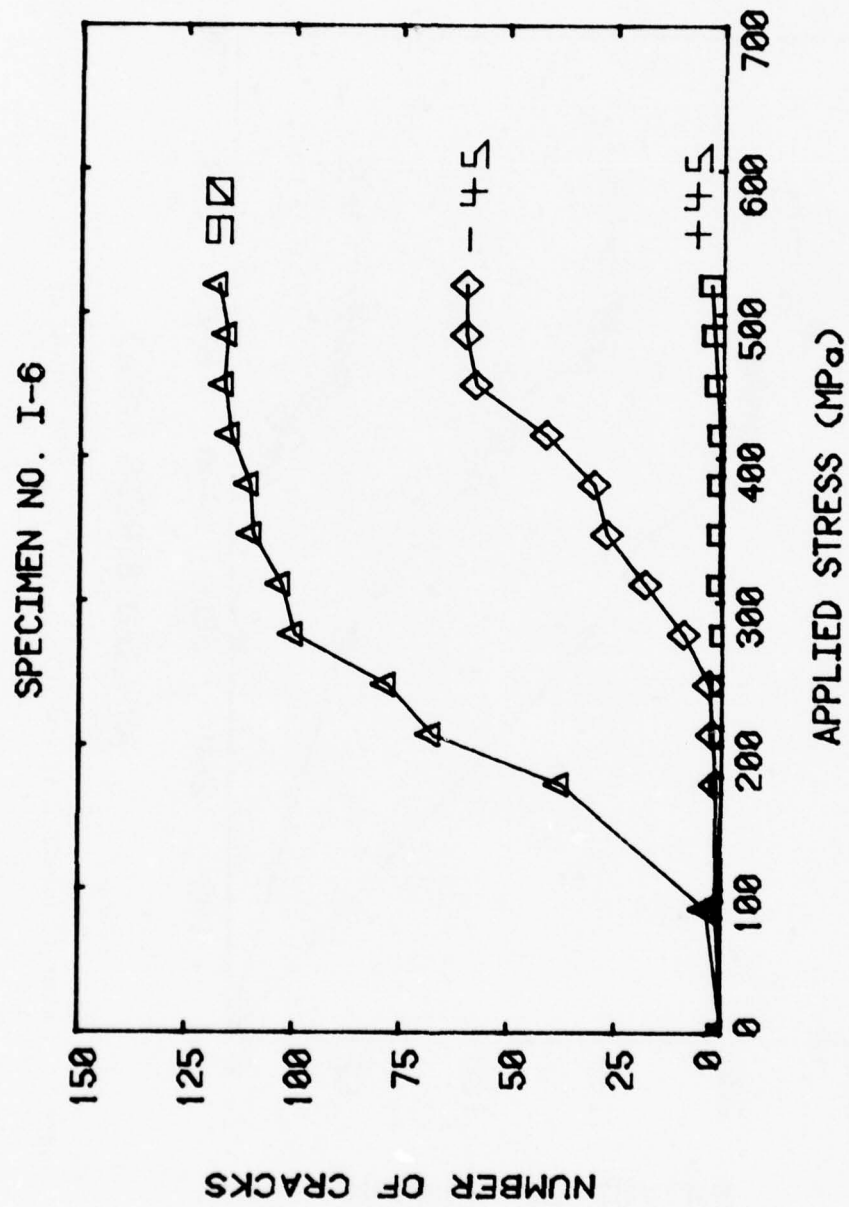


Figure 5. Number of Cracks Observed in 90°, +45° and -45° Lamina of Type I Specimen I-6

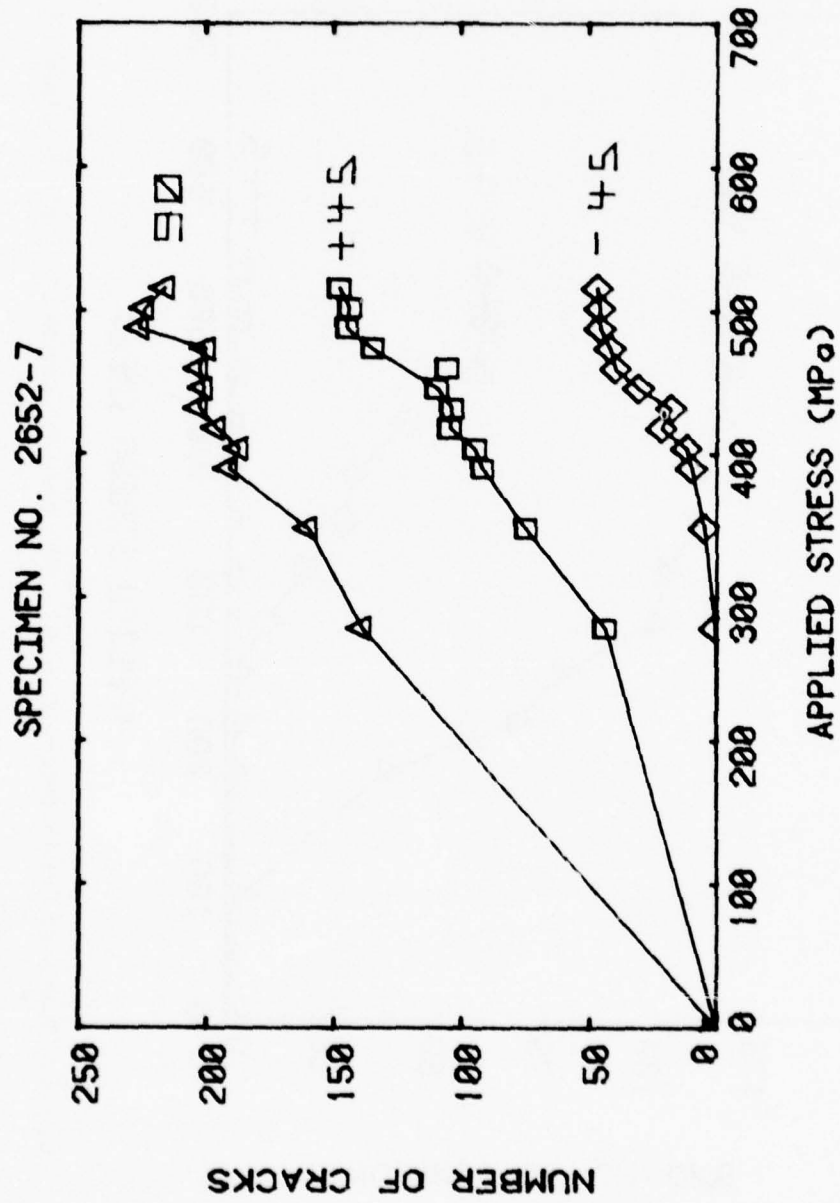


Figure 6. Number of Cracks Observed in 90°, +45° and -45° Lamina of Type II Specimen 2652-10

As stated earlier in the report, observations were made from replicas taken while the specimen was under load in the test machine grips. Since acoustic emission and ultrasonic transducers were often attached to the specimens, access to both specimen edges was not always possible. In these cases, replicas were made of only one edge. Much of the data presented here was gathered in this manner. Although only one specimen edge was examined, this information is representative of the specimen behavior. Figure 7 shows the crack spacing in the  $90^\circ$  and  $+45^\circ$  laminae at both edges of specimen No. 2652-14. It shows that while the average crack spacings on either edge differed at low stresses, the values did coalesce as the applied stress increased. This indicates that while it is desirable to monitor damage on both edges simultaneously, the validity of the characteristic damage state concept does not suffer when only one edge is examined.

Figures 8 and 9 illustrate the development of the characteristic damage state in two Type I specimens. Neither specimen was loaded to failure. (Both specimens were loaded to 3000 lbs.) Specimen I-6 was tested in load control; specimen I-9 was tested in stroke control. Several fundamental characteristics of damage development in statically loaded Type I material can be seen in these figures. First, there was no appreciable damage in the  $+45^\circ$  lamina. This was true of all specimens tested, even those loaded to failure. The figures also demonstrate that transverse cracks appear first in the  $90^\circ$  lamina, and crack spacing values near the final saturation spacing values are attained early in the loading. Saturation spacing is not attained in the  $-45^\circ$  lamina until much later in the loading history. For specimen No. I-6, the final saturation value of 0.664 mm was first reached at 415 MPa but at

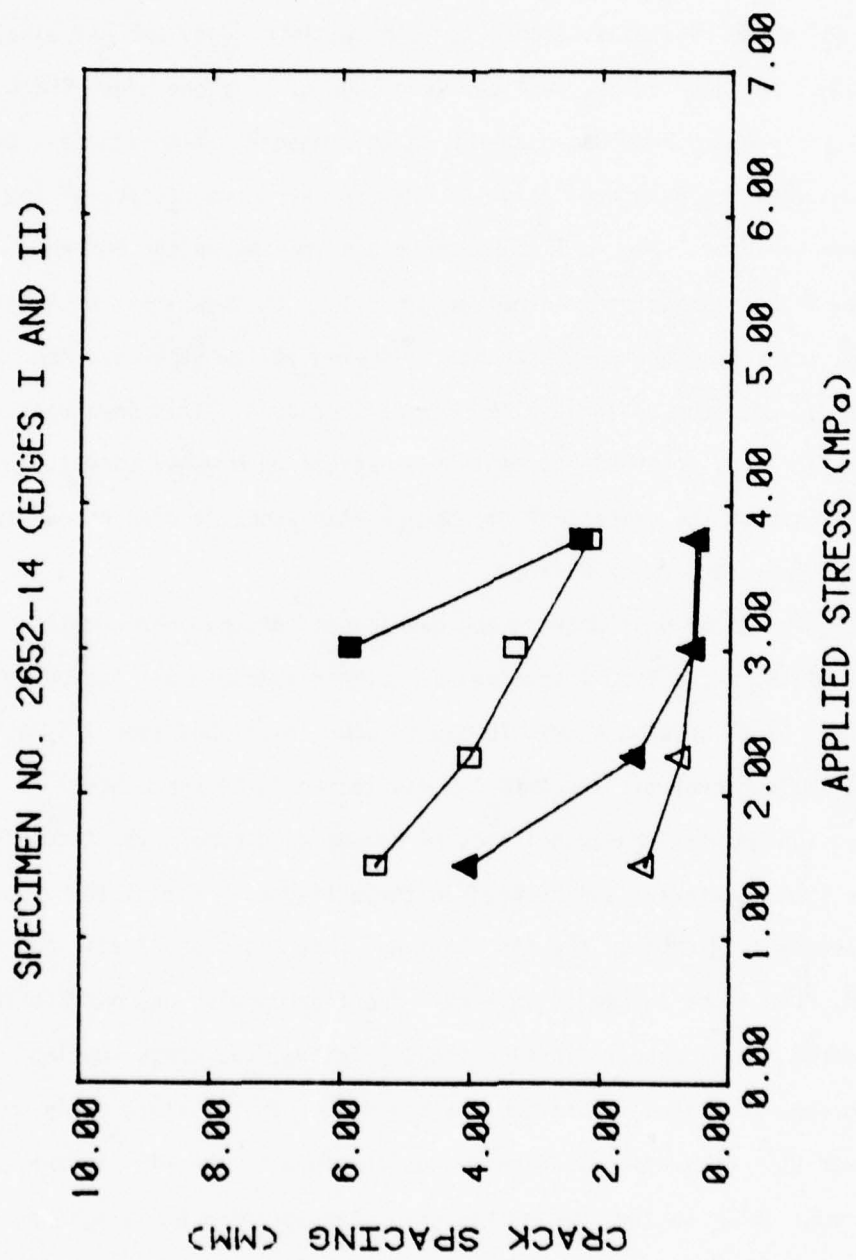


Figure 7. Average Crack Spacing in 90° and +45° Laminates for Edges I and II of Specimen 2652-14



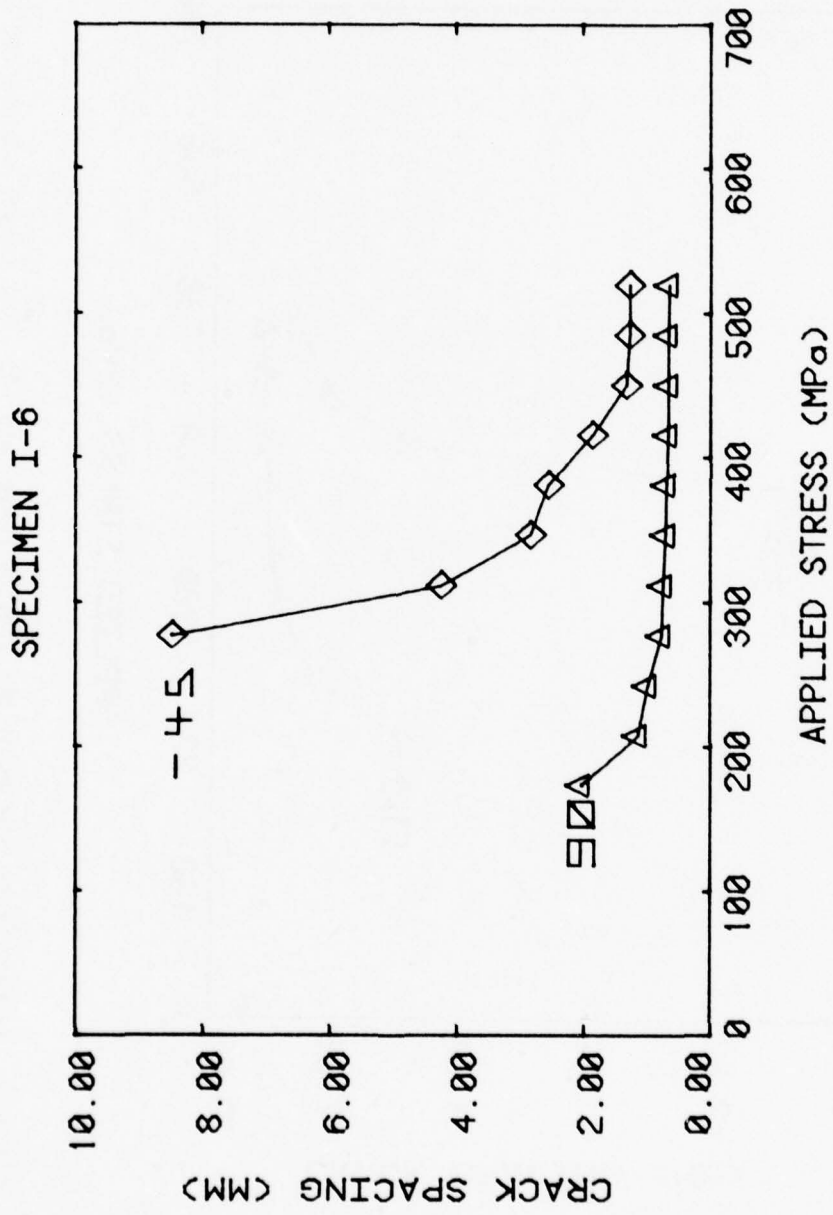


Figure 8. Average Crack Spacings in 90° (bottom curve) and -45° (top curve) Lamina for Specimen No. I-6

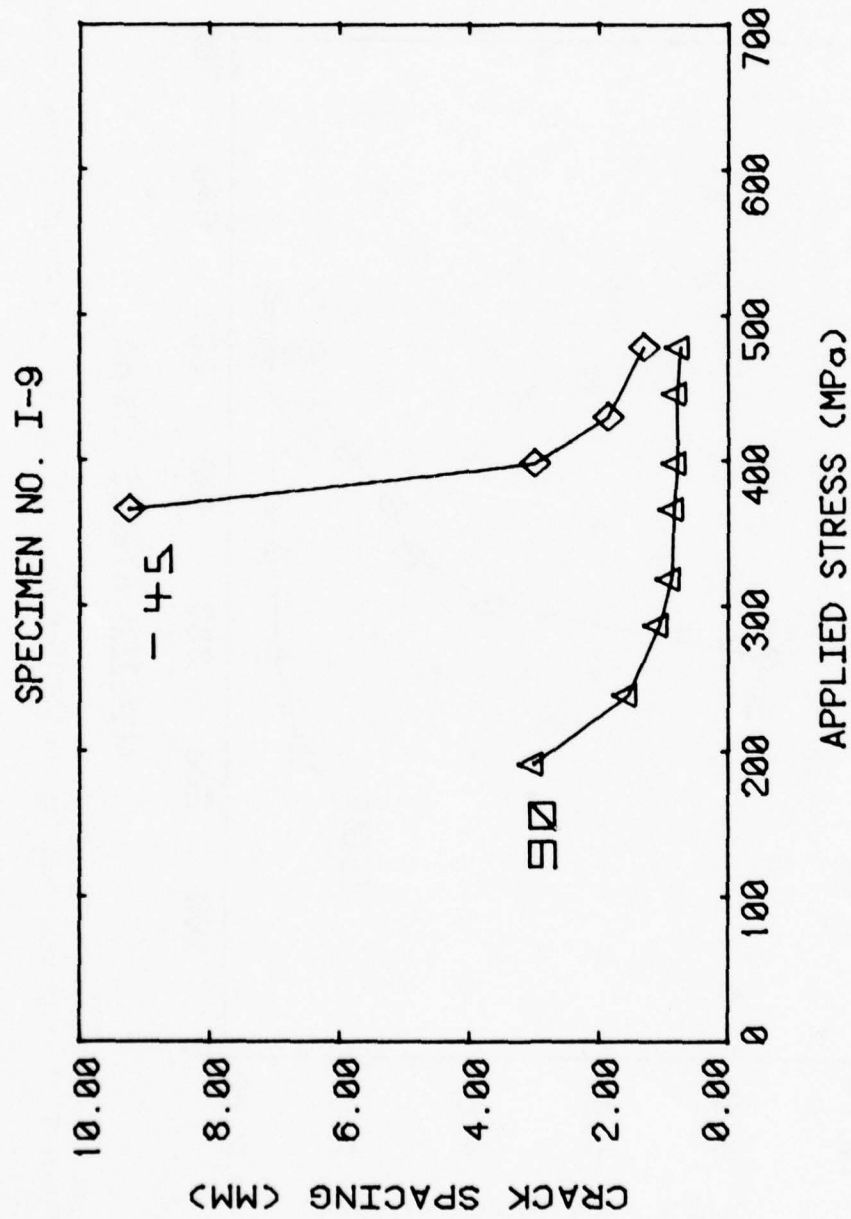


Figure 9. Average Crack Spacing in 90° (bottom curve) and -45° (top curve) Laminae for Specimen No. I-9

277 MPa, the crack spacing was at 90% of the saturation level (i.e., 0.764 mm). Saturation spacing in the  $-45^\circ$  lamina for I-6 was first attained at 450 MPa. Similarly, in specimen No. I-9, saturation spacing for the  $90^\circ$  laminae was first achieved at 400 MPa but it never was reached in the  $-45^\circ$  laminae. When the test was halted at 3000 lb load (520 MPa applied stress) a crack spacing of 1.30 mm was attained. This is approximately equal to the average value attained by several other specimens which were loaded to failure. It is believed that had loading continued, crack spacing would have remained at approximately this value.

To demonstrate the reproducibility of the characteristic damage state, the crack spacing vs applied stress histories of five Type I specimens have been plotted in Figs. 10 and 11. Two of the specimens were tested in load control, the remaining three in stroke control. The horizontal lines in each figure represent values predicted earlier by Reifsnider using a modified Shear-Lag analysis which we will discuss in a subsequent section. Figure 10 illustrates the results obtained for the  $90^\circ$  laminae. Saturation spacing was attained in all specimens. Although the initial portions of the curves may differ in slope, and values may differ at low stress levels, they all did coalesce to the same approximate crack spacing. Figure 11 shows the crack spacings in the  $-45^\circ$  laminae for the same five Type I specimens. Examination of the data (see Table 1) shows that saturation spacing was achieved in three of the specimens. It could not be stated conclusively that crack spacing values in the remaining two specimens, which were not loaded to failure, had stabilized. However, the values attained at maximum load were comparable to saturation spacing values reached in the other three specimens.

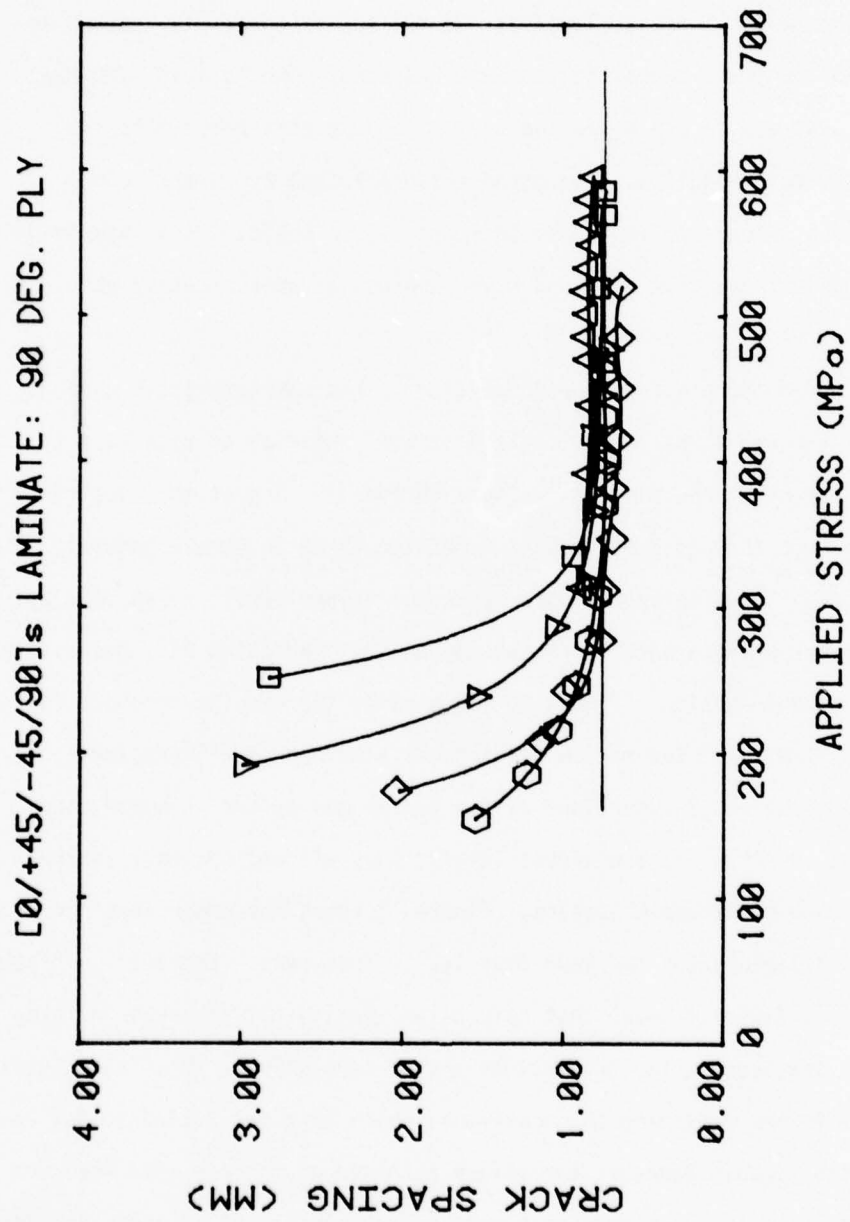


Figure 10. Average Crack Spacings in 90° Laminates for Five Type I Specimens

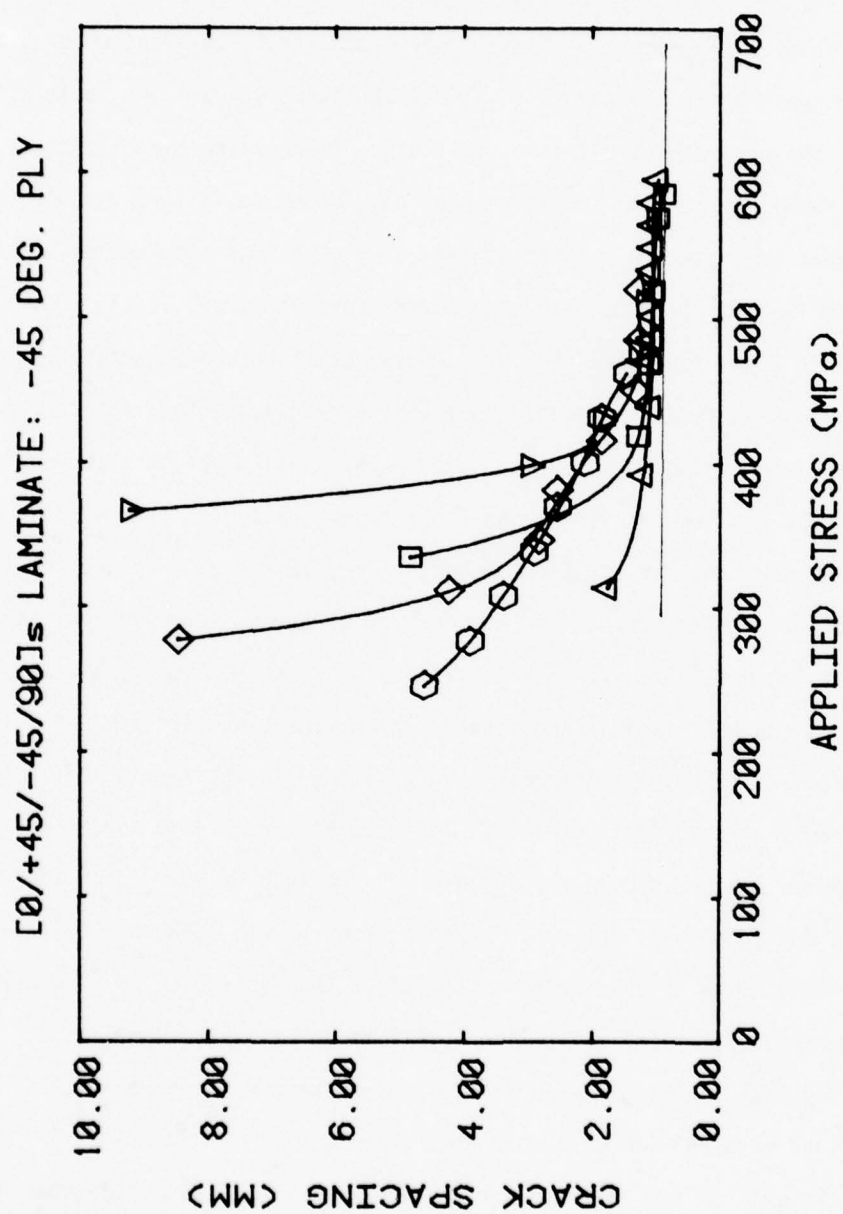


Figure 11. Average Crack Spacings in -45° Laminae for Five Type I Specimens



We can state from the figure that, as in the case of the  $90^\circ$  lamina, although we see a variance in the curves initially, consistent final values were achieved.

Tables 3 and 4 provide further information from the specimens described in the figures. Table 3 gives the stress level at which the crack spacing first attained its final, constant value. The table also lists the ultimate stress level of the specimen or the highest stress level applied when the specimens were not loaded to failure. Table 4 provides the number of cracks and the crack spacings attained at those stress levels. It should be emphasized that the stress levels reported in Table 3 for the  $90^\circ$  lamina are the values at which the constant crack spacings were first achieved. As the figures illustrated, not only does extensive cracking occur at low load in these plies but it also reaches crack spacings comparable to the final crack spacings at low load levels.

We now consider the Type II  $[0,90,+45]_S$  laminates. Unlike the Type I specimens, extensive damage in the form of transverse cracking, appeared in all laminae. Transverse cracks appeared first in the  $90^\circ$  laminae, then in the  $+45^\circ$  laminae and finally in the interior  $-45^\circ$  laminae. In general, the appearance of cracks in a lamina did not seem to be linked to cracking in adjacent laminae. That is, the cracks did not appear to be linked as they did in the  $90^\circ$  and  $-45^\circ$  laminae of Type I specimens. There does, however, appear to be some crack growth between the  $90^\circ$  and the  $+45^\circ$  lamina if loading continues after the saturation spacing has been achieved. Also, unlike the Type I material, there was little longitudinal cracking. When it did appear, it was in short lengths confined to a  $90^\circ$  lamina or a nearby interface.

Figures 12 and 13 trace the development of the saturation spacings for the  $90^\circ$ ,  $+45^\circ$  and  $-45^\circ$  laminae of two Type II specimens. Both

TABLE 3  
STRESS LEVEL (MPA) AT WHICH SATURATION SPACING FIRST ATTAINED  
TYPE I SPECIMEN

Specimen No.	Lamina			Ultimate Stress
	90°	+45°	-45°	
I-3	392	---	438	611
I-4	468	---	569	594
I-6	415	---	450	520 <sup>1</sup>
I-7	338	---	--- <sup>3</sup>	520 <sup>2</sup>
I-9	398	---	--- <sup>5</sup>	477 <sup>4</sup>
Average Stress Level:	402.2	---	485.6	
Standard Deviation:	46.7	---	72.4	

Note: Specimen Nos. I-3, I-4 and I-9 tested in stroke control  
Specimen Nos. I-6 and I-7 tested in Load control

<sup>1</sup>Specimen not loaded to failure (3000 lb max load)

<sup>2</sup>Specimen not loaded to Failure (3000 lb max load)

<sup>3</sup>Saturation spacing not attained

<sup>4</sup>Specimen not loaded to failure (3000 lb max load)

<sup>5</sup>Saturation spacing not attained

TABLE 4  
NUMBER OF CRACKS/SATURATION SPACING  
ATTAINED BY TYPE I SPECIMENS

Specimen No.	Lamina		
	90°	+45	-45°
I-3	120/.846mm	---	95/1.07mm
I-4	135/.753mm	---	104/.977mm
I-6	153/.664mm	---	77/1.32mm
I-7	138/.736mm	---	70/1.45mm
I-9	130/.781mm	---	78/1.30mm
Average Number of Cracks:	135	---	92 <sup>1</sup>
Standard Deviation:	12		13
Average Saturation Spacing (mm);	.756	---	1.12 <sup>1</sup>
Standard Deviation:	.06		.17
Predicted Saturation Spacing (mm):	.760	.755	.879

Note: Cracks were Counted over 4 in. length

<sup>1</sup>Averages Based on Results Obtained from Specimens I-3, I-4, I-6.

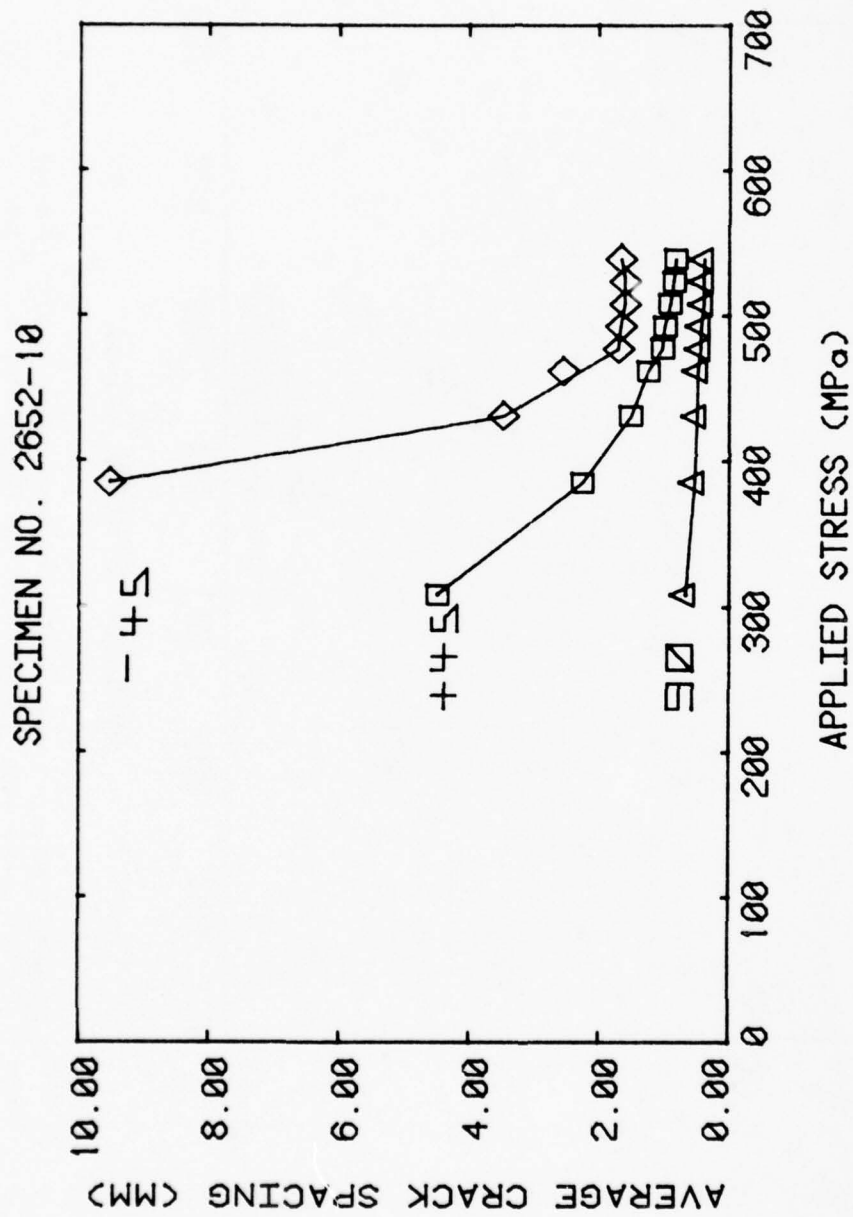


Figure 12. Average Crack Spacings in 90° (bottom), +45° (middle) and -45° (top) Laminæ for Type II Specimen No. 2652-10

SPECIMEN NO. 2652-8

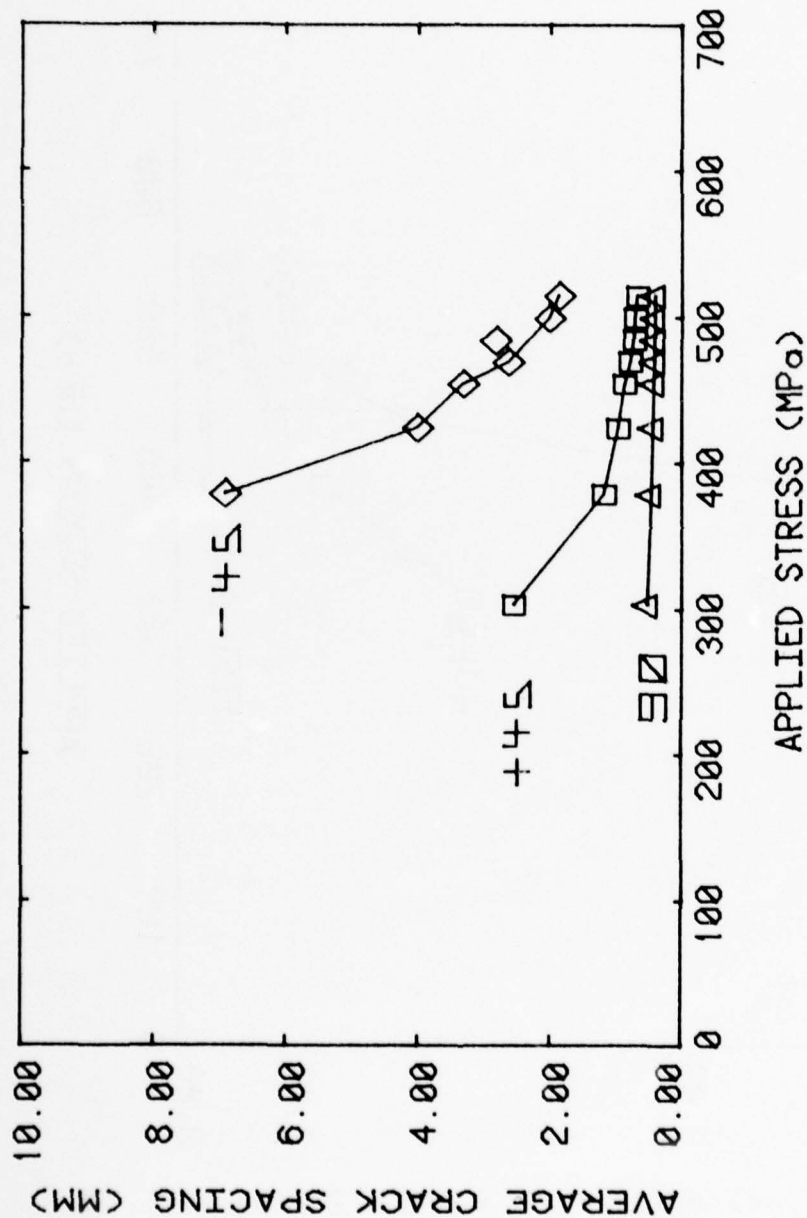


Figure 13. Average Crack Spacings for 90° (bottom), +45° (middle) and -45° (top) Laminæ for Type II Specimen No. 2652-8



specimens were loaded to failure in stroke control. Saturation spacing was achieved for all three orientations in specimen No. 2652-10 and for the 90° and +45° lamina of specimen No. 2652-8. The final crack spacing recorded before failure in the -45° lamina was 2.00 mm and the average saturation spacing for this lamina was 1.64 mm, suggesting that the spacing may have been approaching a comparable value when failure occurred. The figures again demonstrate that transverse cracking appears first in the 90° lamina. The 90° lamina curves are also flat indicating that crack spacings comparable to saturation values were attained quite early in the loading. The curves for the other two ply orientations demonstrate that although cracking appears at higher loads, it rapidly achieves saturation.

Considering Fig. 12 again, we can see that although saturation spacing was apparently achieved for all three fiber orientations, the +45° lamina values decline slightly near the end of the test. In Fig. 6, a corresponding increase in the number of cracks is quite evident as is a slight increase in the number of 90° lamina cracks. This phenomenon has also been observed in other Type II specimens and is believed to be due to crack growth between the 90° and +45° laminae.

Six Type II specimens were tested to failure. The results of four of these tests were plotted in Figs. 14, 15 and 16. These figures show the crack spacing in the 90°, +45° and -45° laminae respectively. The results of only four of the tests were displayed to simplify the figures. The horizontal lines in each figure represent the predicted values. The figures also demonstrate the consistency of the characteristic saturation spacing values from specimen to specimen. Saturation spacing was achieved by the 90° and +45° laminae in all specimens. It was reached in the -45° laminae of all specimens except 2652-8. Although some variance is

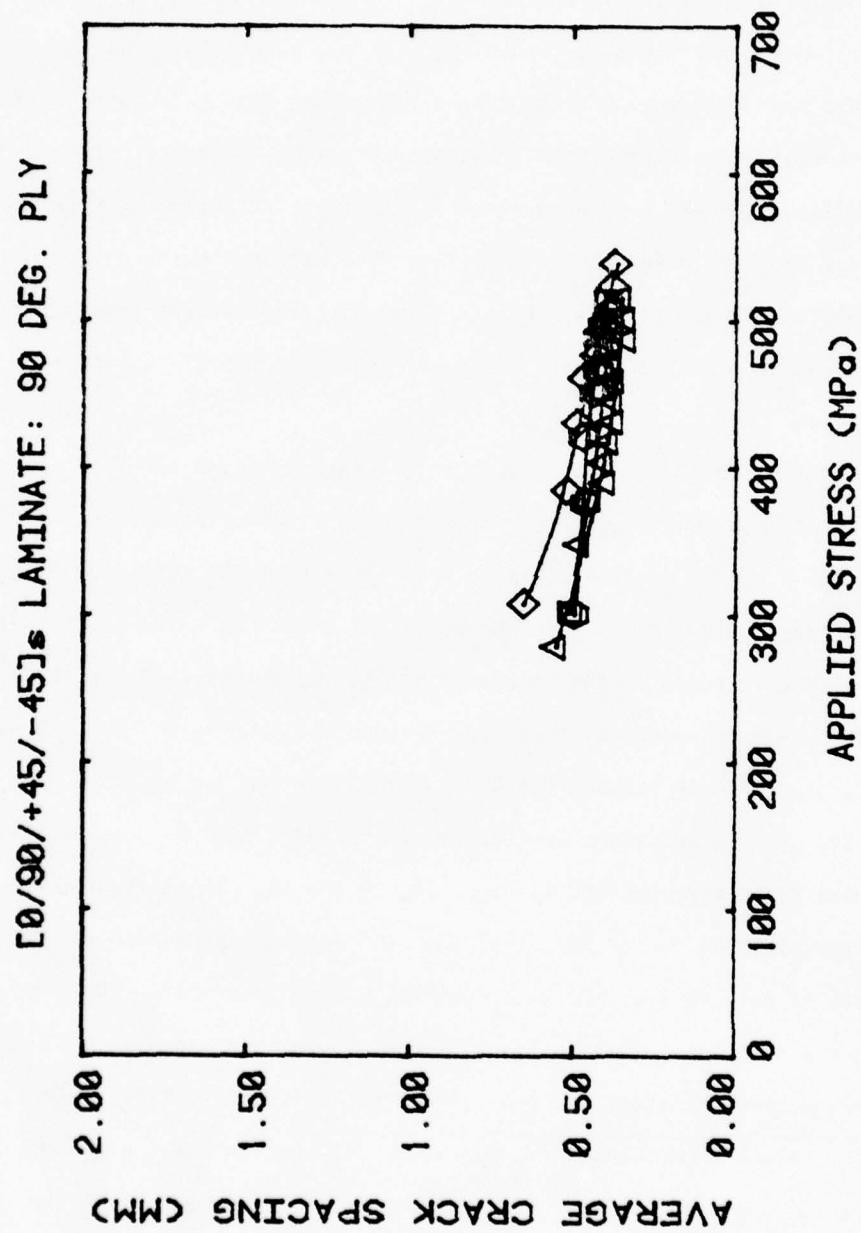


Figure 14. Average Crack Spacing in 90° Laminae for Four Type II Specimens

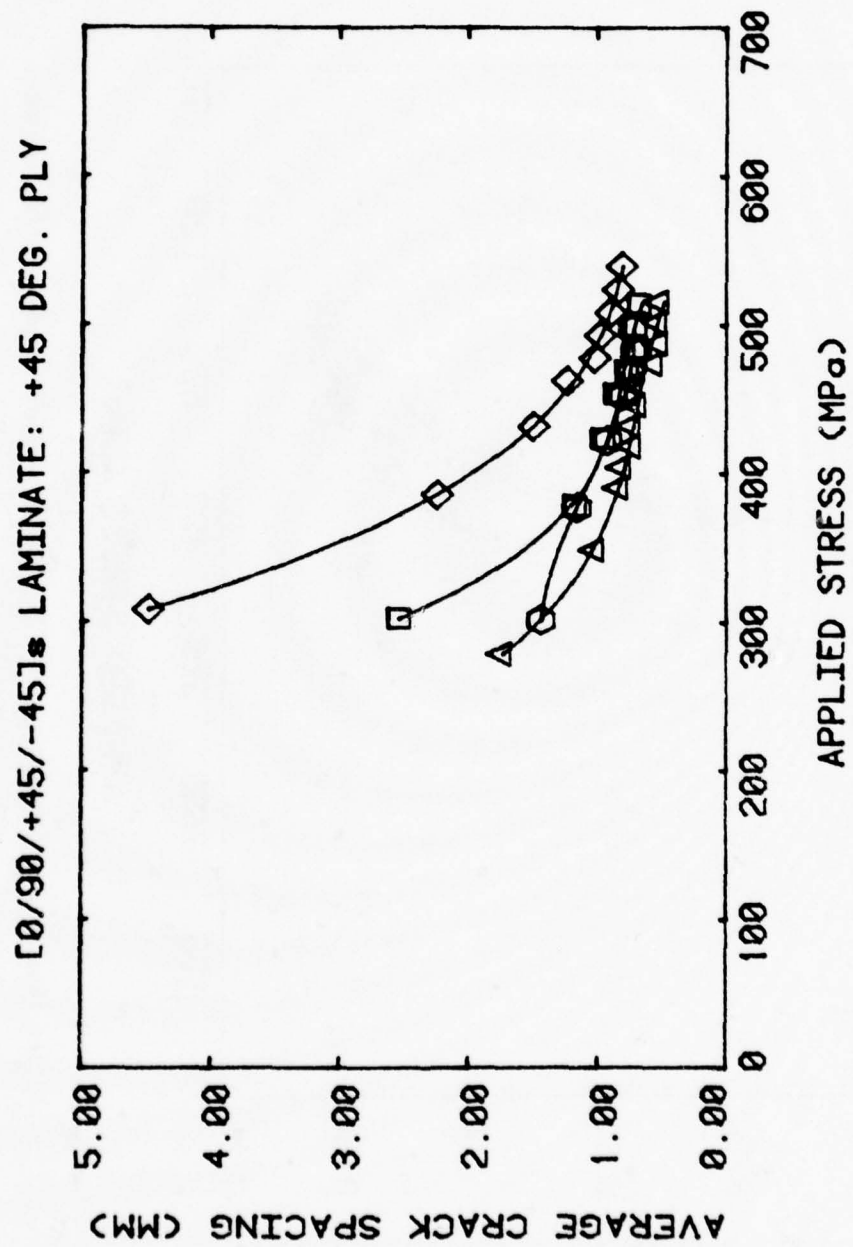


Figure 15. Average Crack Spacings in +45° Laminates for Four Type II Specimens

[0/90/+45/-45]<sub>s</sub> LAMINATE: -45 DEG. PLY

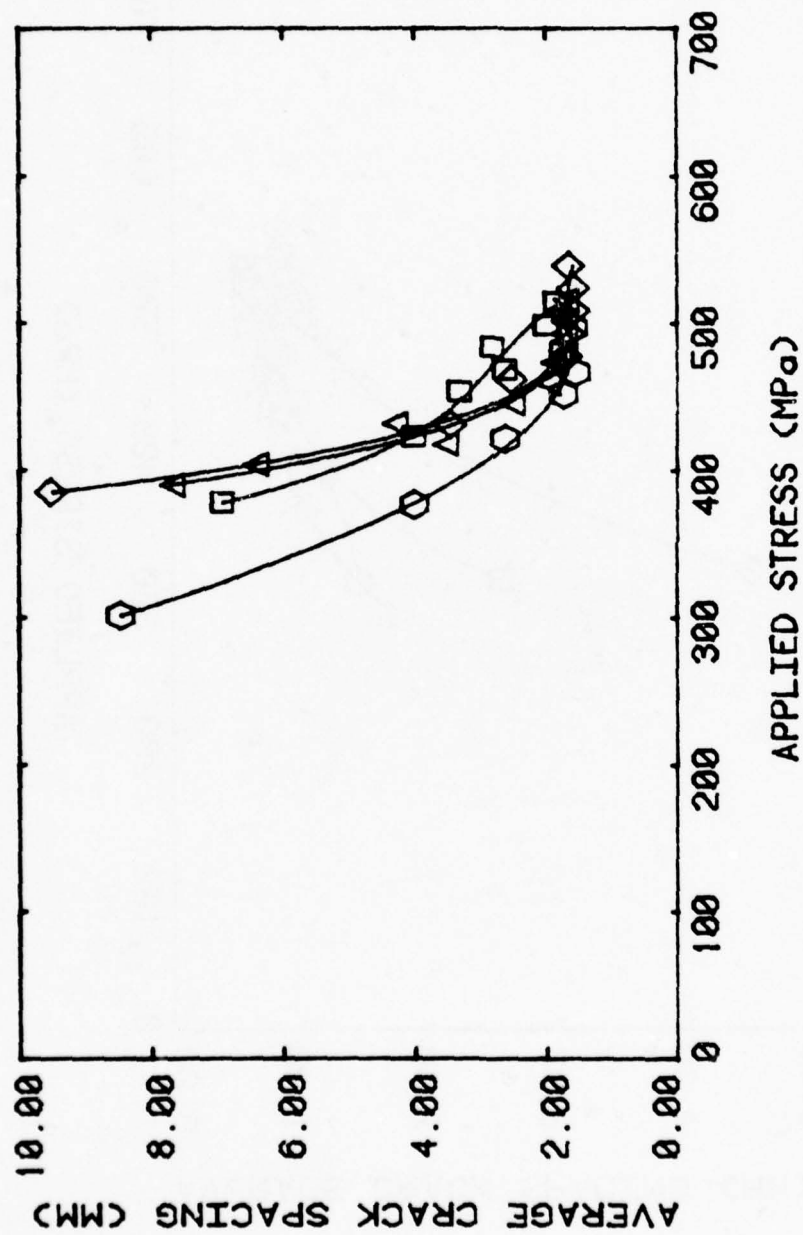


Figure 16. Average Crack Spacings in -45° Laminae for Four Type II Specimens

seen in the initial portions of the curves, crack spacing values coalesce to the characteristic crack spacing values for each fiber orientation. The figures also demonstrate that these characteristic values are unique for each lamina.

Tables 5 and 6 provide further information on the test specimens. Table 5 gives the stress level at which a constant crack spacing was first attained in each of the specimen laminae. It also lists the ultimate stress level of each specimen. Table 6 provides the number of cracks and the crack spacings at saturation. Although Figs. 12 and 13 demonstrate that cracking occurs first in the  $90^\circ$  lamina, then in the  $+45^\circ$  and finally in the  $-45^\circ$  lamina, Table 5 shows that they all achieve saturation spacing at approximately the same stress level. The average stress levels at which saturation was attained was 471.5 MPa, 473.4 MPa and 473 MPa for the  $90^\circ$ ,  $+45^\circ$  and  $-45^\circ$  lamina respectively. In the Type I specimens, saturation was achieved much later in the  $-45^\circ$  lamina than in the  $90^\circ$  lamina. The average values for those specimens were 402.2 MPa for the  $90^\circ$  lamina and 485.6 MPa for the  $-45^\circ$  lamina. As in the case of the Type I specimens, it must be emphasized that in the Type II  $90^\circ$  laminae, crack spacing values near to saturation values were attained at relatively low loads. Although cracking first appears in the  $90^\circ$  lamina of both specimen types, a comparison of these average stress levels also reveals that damage occurs at a much lower stress level in the Type I  $90^\circ$  laminae than in the Type II  $90^\circ$  laminae. The average threshold saturation stress level was 471.5 MPa for Type II specimens versus 402.2 MPa for Type I specimens. The average threshold saturation stress levels for the  $-45^\circ$  lamina were similar however, 485.6 MPa for Type I and 473 MPa for Type II specimens. While these stress levels are not important or precise, they indicate a significant difference in behavior.



TABLE 5  
STRESS LEVEL (MPA) AT WHICH SATURATION SPACING FIRST ATTAINED  
TYPE II SPECIMENS

Specimen No.	Lamina			Ultimate Stress
	90°	+45°	-45°	
2652-7	432	417	487	543
2652-8	468	483	--- <sup>1</sup>	514
2652-10	508	523	477	570
2652-11	477	477	477	523
2652-12 <sup>2</sup>	477	---	---	477
2652-13	467	467	451	512
Average Stress Level:	471.5	473.4	473.0	532.4
Standard Deviation:	24.4	38.0	15.4	24.3

<sup>1</sup>Saturation Spacing not Attained

<sup>2</sup>Specimen Failed During Loading at Time of Failure Load Was Jumping in 50 lb. Increments due to Electronic Control Problems. Saturation Spacing not Attained in +45° or -45° Lamina.

TABLE 6  
NUMBER OF CRACKS/SATURATION SPACING (MM)  
ATTAINED BY TYPE II SPECIMENS

Specimen No.	Lamina		
	90°	+45°	-45°
2652-7	202/.377 <sup>1</sup>	106/.719 <sup>2</sup>	46/1.66
2652-8	193/.395	107/.712	38/---
2652-10	198/.385 <sup>3</sup>	91/.837 <sup>4</sup>	45/1.69
2652-11	198/.385	112/.680	51/1.49
2652-12	193/.395	83/---	33/---
2652-13	180/.423 <sup>5</sup>	103/.739	44/1.73
Average Number of Cracks:	194	103.8	46.5
Standard Deviation:	7.6	7.8	3.1
Average Saturation Spacing:	.393	.737	1.64
Standard Deviation:	.016	.059	.10
Predicted Saturation Spacing:	.363	.875	1.21

<sup>1</sup>Rapid Increase @3500 lbs Load from 200-226

<sup>2</sup>Rapid Increase @3400 lbs Load from 106-135

<sup>3</sup>Number Increased Slightly @3400 lbs Load and Again @3500 lbs.

<sup>4</sup>Number Increased Slightly @3500 lbs Load

<sup>5</sup>Number Increased Slightly @3300 lbs Load

### Test Results: Fatigue Loading

Cyclic tensile loading of the specimens was conducted under load control on a servohydraulic testing machine with  $R=0.1$ . About half of the tests were interrupted at several intervals for the purpose of making replicas of the edges to obtain a record of the damage development. The dynamic stiffness as well as the specific energy dissipation (hysteresis loss) was recorded in real time during testing by an on-line computer aided data acquisition system. Static stiffness and residual strength was measured at the end of the cyclic loading history in about half of the tests. Other specimens were not fractured so that damage patterns could be studied. Some specimens were sectioned so that the damage state in the interior of the specimens could be assessed and compared with the observations made on the specimen edge. No significant difference in those observations beyond the obvious absence of delamination (ply separation) and longitudinal cracking (longitudinal cracks within a lamina) in the interior was observed. Figure 17 illustrates how the damage state information was gathered.

The sequence of development of damage under fatigue loading in the laminates examined is similar to the description given earlier for quasi-static loading. However, cycling at a given stress level causes additional cracks to form as a function of additional cycles of loading. The type of cracks that form (i.e., the type of laminae that develop cracks) is controlled by the load level, but the number of cracks increases for successive cycles of loading at that level until a saturation number of cracks is reached in each respective ply, forming a "characteristic damage state," as we have seen for the static loading case. Cyclic loading does not appear to change the stress threshold at which cracks

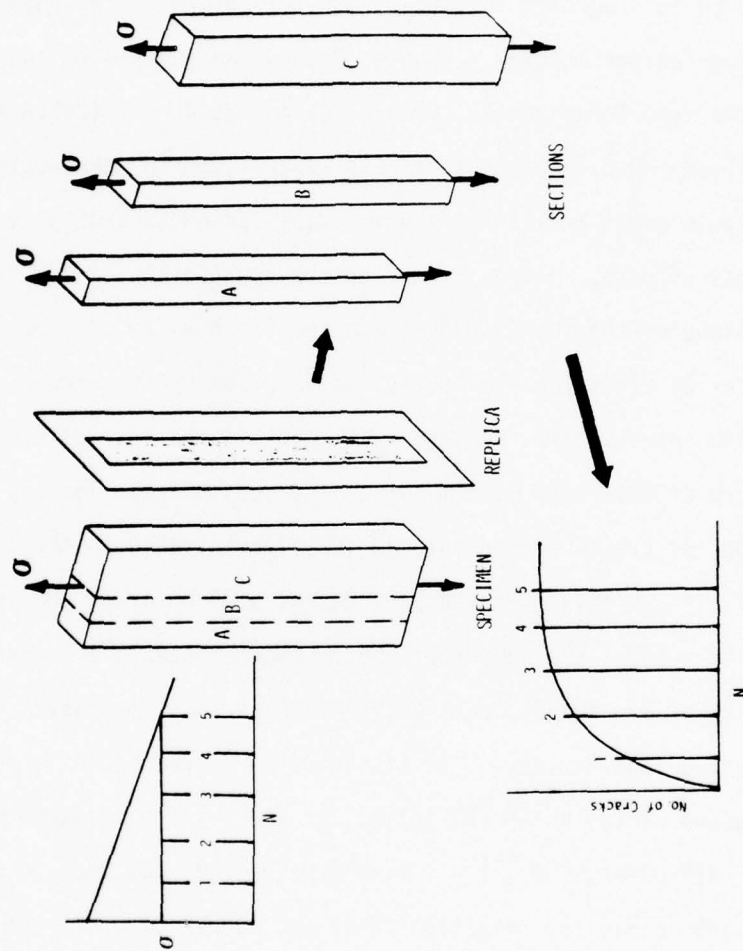


Figure 17. Schematic Diagram of Sectioning and Data Collecting Scheme for Cyclic Testing

form in an off-axis ply, but it will alter the number of cracks that occur for a given stress level if a stable number of cracks has not yet formed.

The Type I and Type II laminates discussed earlier will also be used in this section to demonstrate the nature of the physical behavior during fatigue loading. Figure 18 shows an example of crack development in the Type I laminates. Cyclic loading at 40 ksi (275.6 Mpa) stress amplitude ( $R=0.1$ ) was interrupted long enough to make replicas of the specimen edges at intervals which were chosen according to the rate of change of data. The number of cracks counted in the  $90^\circ$  plies (on the midplane of the  $[0, \pm 45, 90]_s$  laminate) is shown by the top curve, the number of cracks in the  $-45^\circ$  plies is given by the middle curve and the bottom curve is the running crack count in the  $+45^\circ$  plies. The general nature of this data is similar to the quasi-static loading case. The number of cracks becomes stable (or almost stable in the case of the  $+45^\circ$  ply at this stress amplitude) at some point in the load history. For this case, the number of cracks becomes stable after some number of cycles at a constant load, rather than at some load level in an increasing load history. The stable value is reached at about twenty thousand cycles in the  $90^\circ$  plies, at about fifty thousand cycles for the  $-45^\circ$  plies, and a truly stable value does not seem to be attained in the  $+45^\circ$  plies for this load level and number of cycles of loading. The straight lines shown on Fig. 18 are the stable values predicted (for the two cases where stable values are reached) by an analysis to be discussed in a latter section.

Since a more universal representation of the data is had by using crack spacings instead of crack counts, the data in Fig. 18 is converted



# SPECIMEN NO. I-15

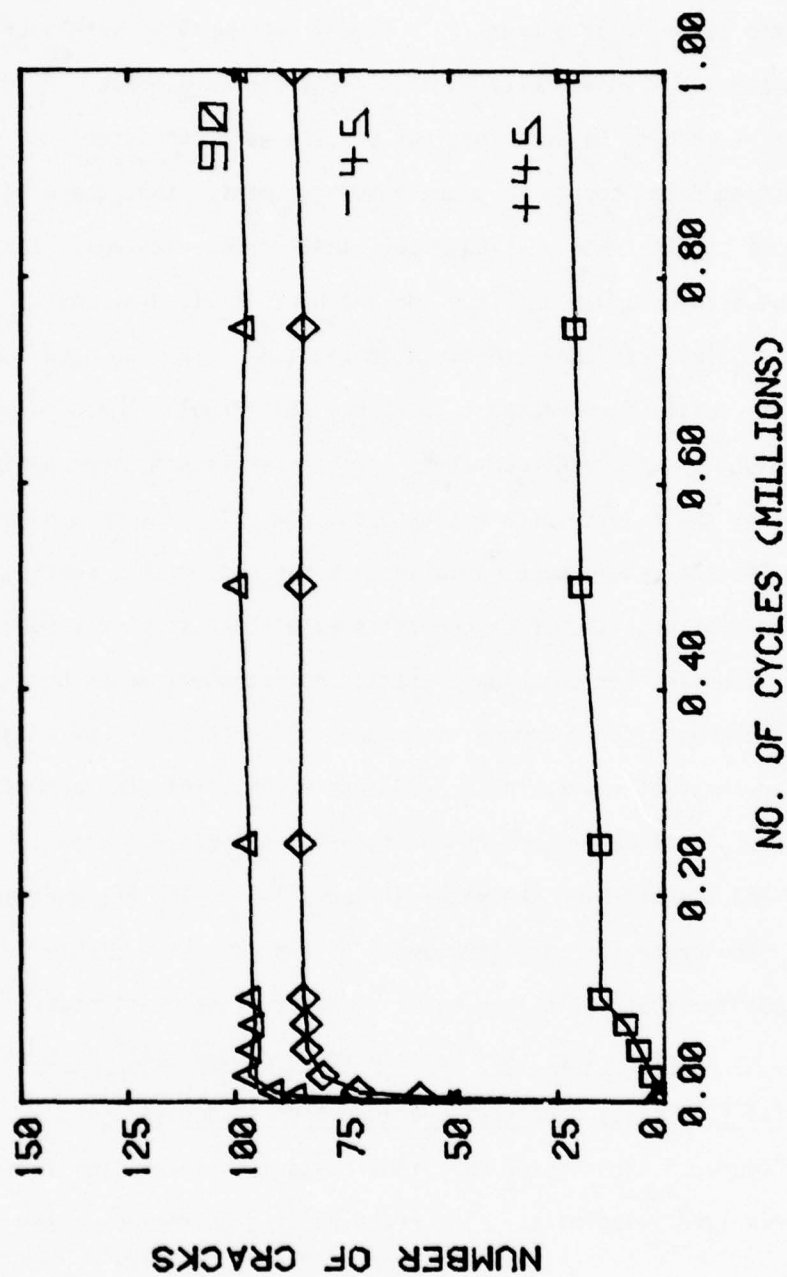


Figure 18. Number of Observed Cracks as a Function of Cycles of Loading at 40 Ksi (275.6 MPa) for Specimen I-15, in the 90° Plies (top curve), -45° Plies (middle curve) and +45° Plies (bottom curve)

to crack spacings in Fig. 19. (The ordering of the curves reverses of course.) However, much greater accuracy can be obtained by taking the data as crack counts because of the large number of cracks and the fact that the counting of a crack is a binary judgement while measuring a crack spacing involves experimental error for each crack. We did do enough of each to be sure that our results were consistent. Of course, converting crack counts to crack spacings implies that there is only one value of stable crack spacing, i.e., that cracks eventually form in a regular array equidistant from one another. It is precisely this tendency which creates the "characteristic damage state" that we have mentioned; but, of course, the spacing is not precisely regular there being local variations in strength, geometric irregularities and other perturbations caused by the reality of the situation. We will provide a quantitative characterization of these variations at the end of this section. The fact remains that the crack counts level off and the crack spacings become constant for both quasi-static and fatigue loading because a stable characteristic damage state does form consisting of a unique regular array of cracks in the off-axis plies. This characteristic damage state is determined by the material properties, the ply orientations and the stacking sequence. Figures 18 and 19 show another important fact. The crack spacings (or number of cracks at the stable level) are the same for the cyclic loading as it was for the quasi-static loading. Hence, we conclude that the characteristic damage state is a well defined material (laminate) property independent of load history.

Figure 20 shows three individual data sets taken from fatigue tests of three Type I laminates. The crack spacing in the  $90^\circ$  plies is plotted.

# SPECIMEN NO. I-15

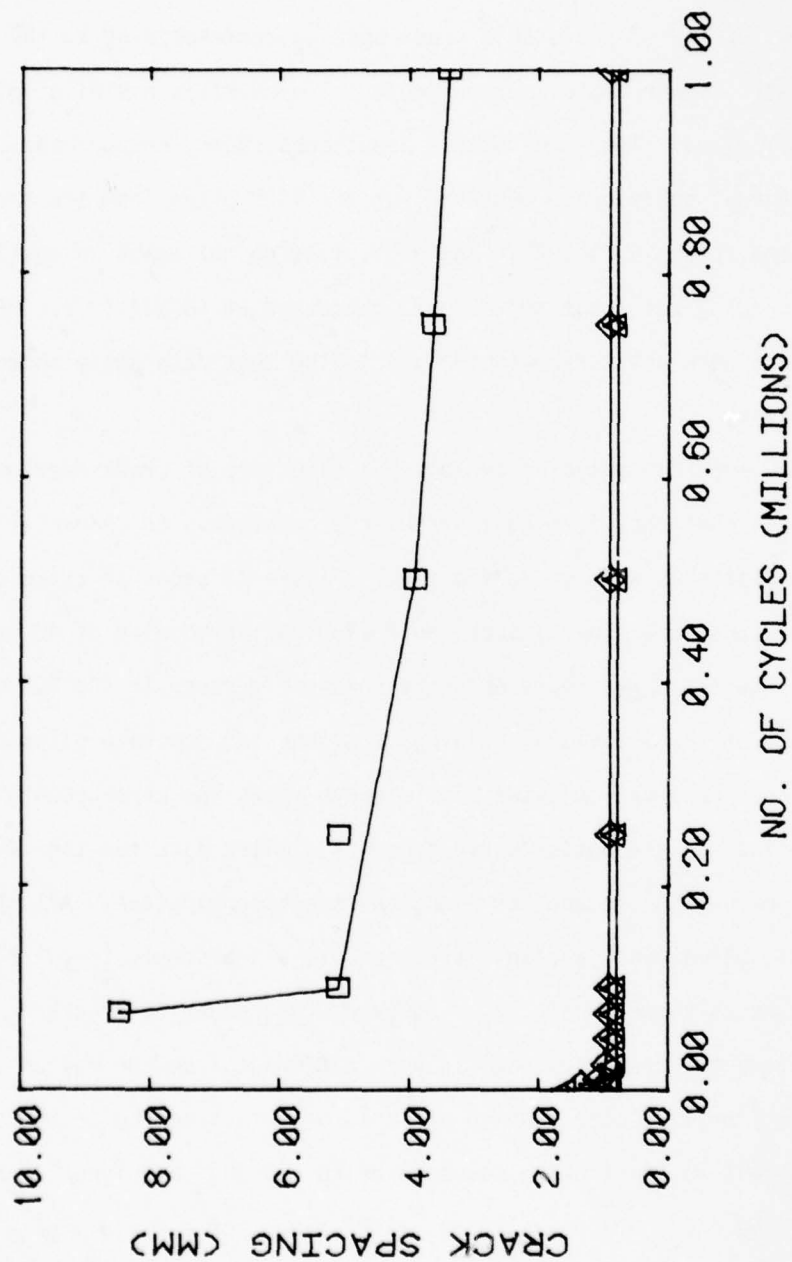


Figure 19. Spacing of Cracks as a Function of Cycles of Loading for Specimen I-15, in the +45° (top), -45° (middle) and 90° (bottom) Plies

The ordinate has been expanded compared to Fig. 19 so that a better perception of the consistency of the data can be obtained. While some small variability is seen in the data in the early part of the tests, the consistency of the stable crack spacing corresponding to the characteristic damage state is remarkable. Figure 21 is a similar plot for the  $-45^\circ$  plies. The same remarks about consistency can be made. The same general behavior is observed for the  $+45^\circ$  plies from the same three specimens shown in Fig. 22. The  $+45^\circ$  plies do not reach an equilibrium crack spacing for these three tests conducted at 40 ksi (275.6 MPa). (The specimens were not tested to failure.) The test data again shows good consistency.

The Type II laminates exhibit the same type of crack development in the sense that they form equilibrium crack patterns or characteristic damage states as we have called them. Figure 23 shows an example of the observations on a Type II specimen during cyclic loading at 40 ksi (275.6 MPa). The top curve represents the number of cracks in the  $90^\circ$  plies (average of the individual readings from the two separate plies on the edge under observation), the middle curve shows the crack counts for the  $+45^\circ$  plies and the bottom curve presents similar data for the  $-45^\circ$  plies which now adjoin one another along the specimen midplane. All three off-axis plies reach a stable crack count, and a stable (regular) spacing of cracks as shown in Fig. 24. However, the number of cracks in each layer (and the crack spacing) is very different from the values observed for the Type I specimens which differed only in stacking sequence (recall that Type I has a stacking sequence of  $[0, +45, 90]_S$  and Type II is arranged in a  $[0, 90, +45]_S$  order). Figures 18-22 show, for example, that the number of cracks in the  $90^\circ$  plies nearly doubles when we go from a Type

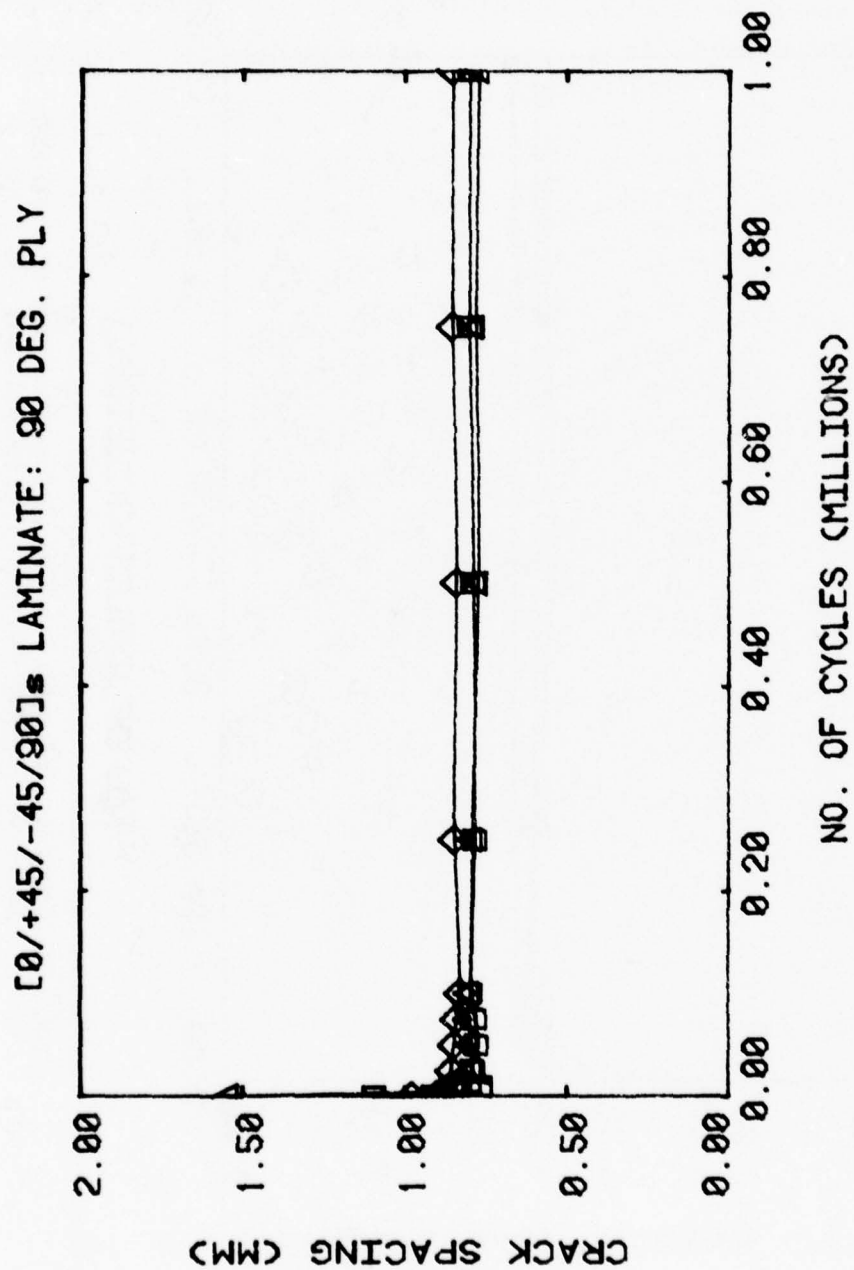


Figure 20. Crack Spacings as a Function of Cycles of Loading at 40 ksi (275.6 MPa) in the 90° Plies of Several Type I Laminates



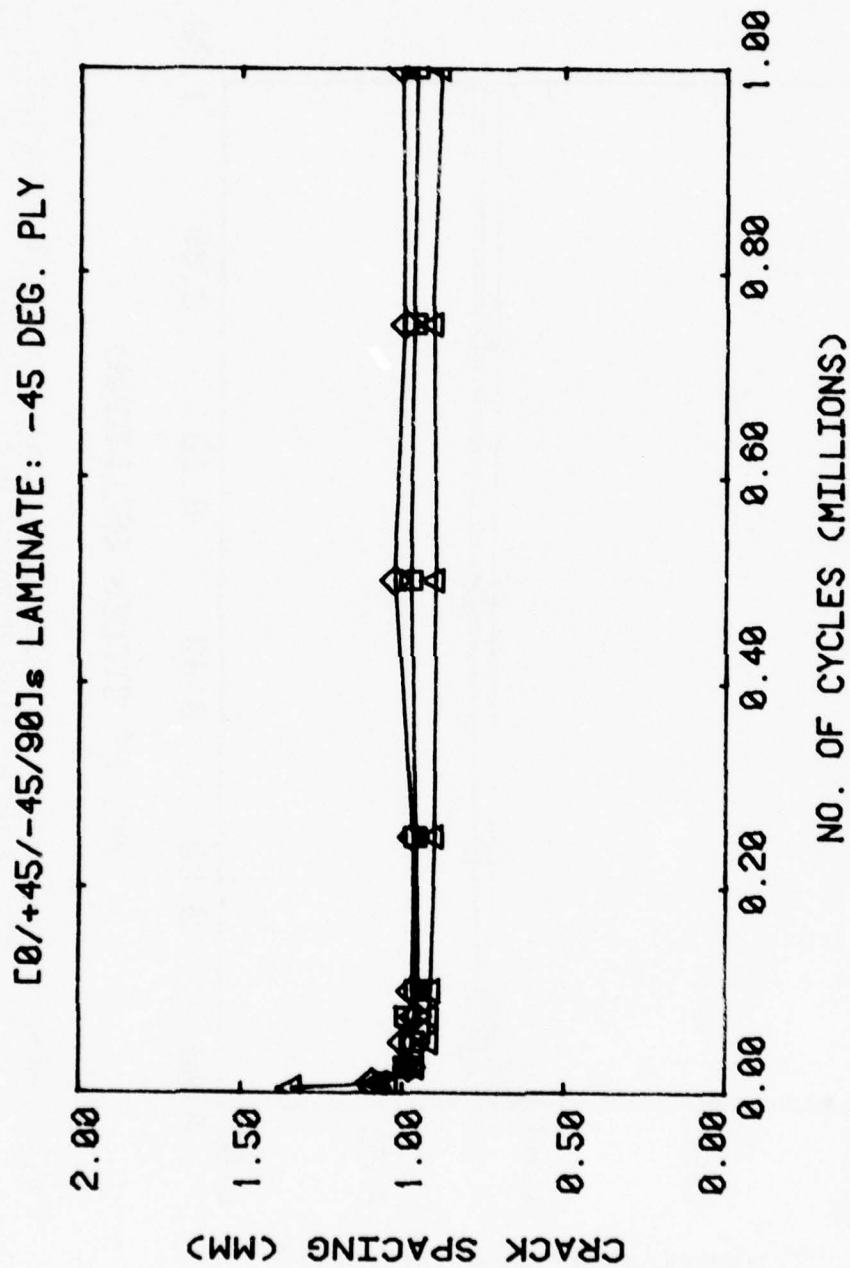


Figure 21. Crack Spacings as a Function of Cycles of Loading at 40 ksi (275.6 MPa) in the -45° Plies of Several Type I Laminates

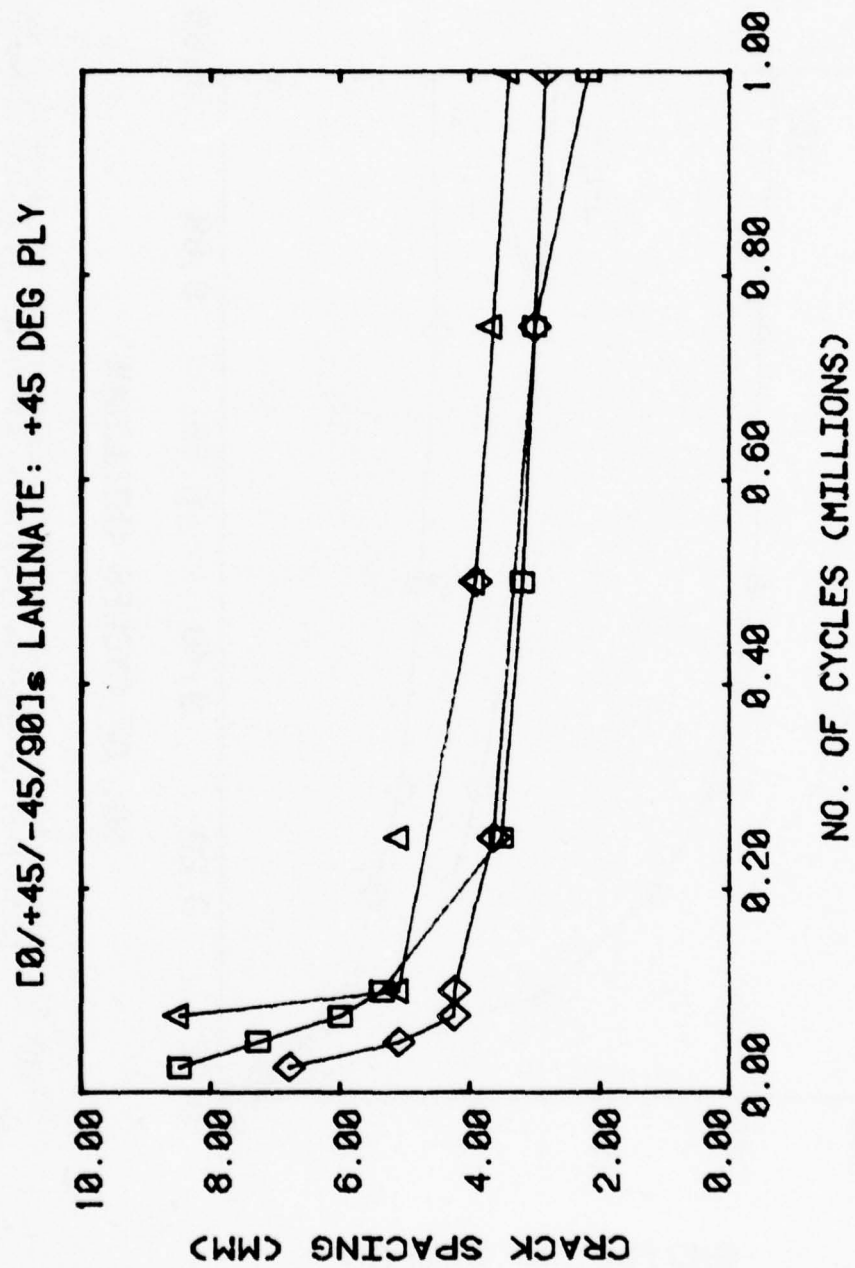


Figure 22. Crack Spacings as a Function of Cycles of Loading at 40 ksi (275.6 MPa) in the +45° Plies of Several Type I Laminates

# SPECIMEN NO. II-20

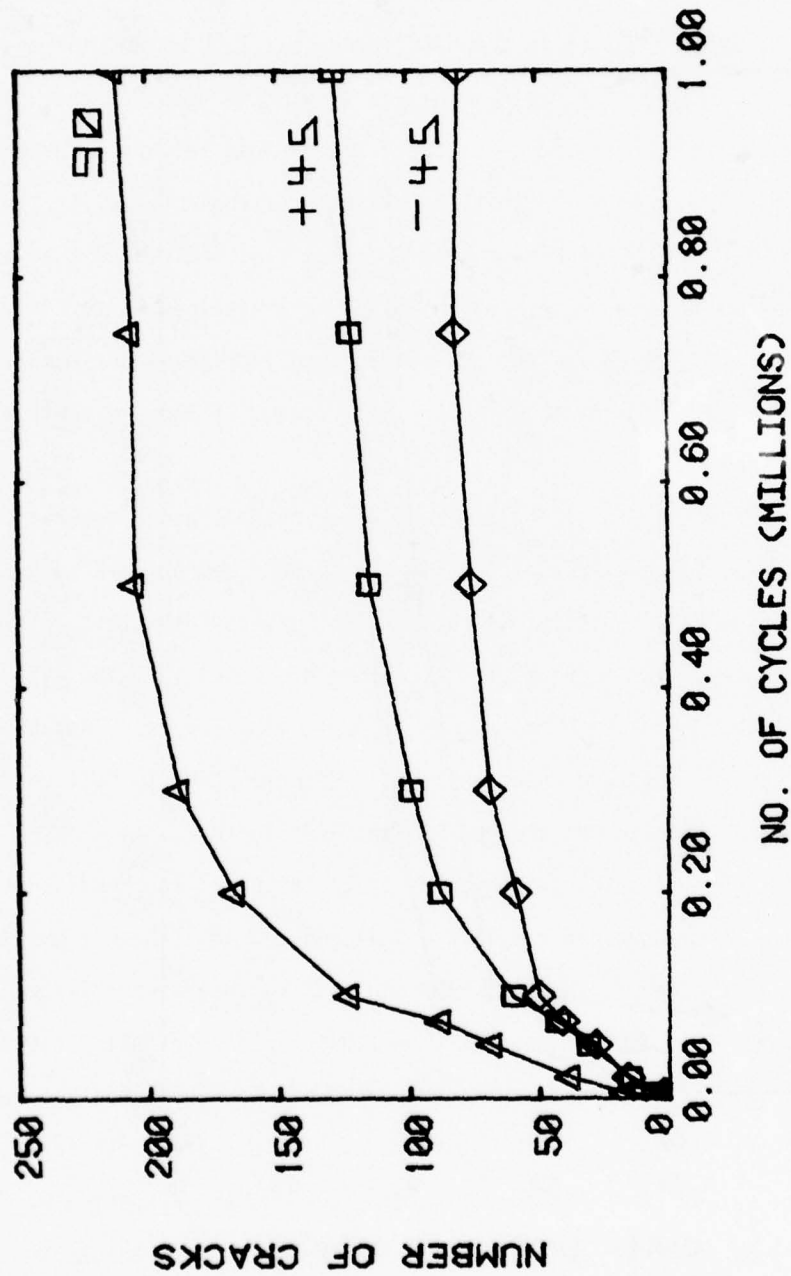


Figure 23. Number of Observed Cracks as a Function of Cycles of Loading at 40 ksi (275.6 MPa) for Specimen II-20 in the 90° plies (top curve), +45° plies (middle curve) and -45° plies (bottom curve).

# SPECIMEN NO. II-20

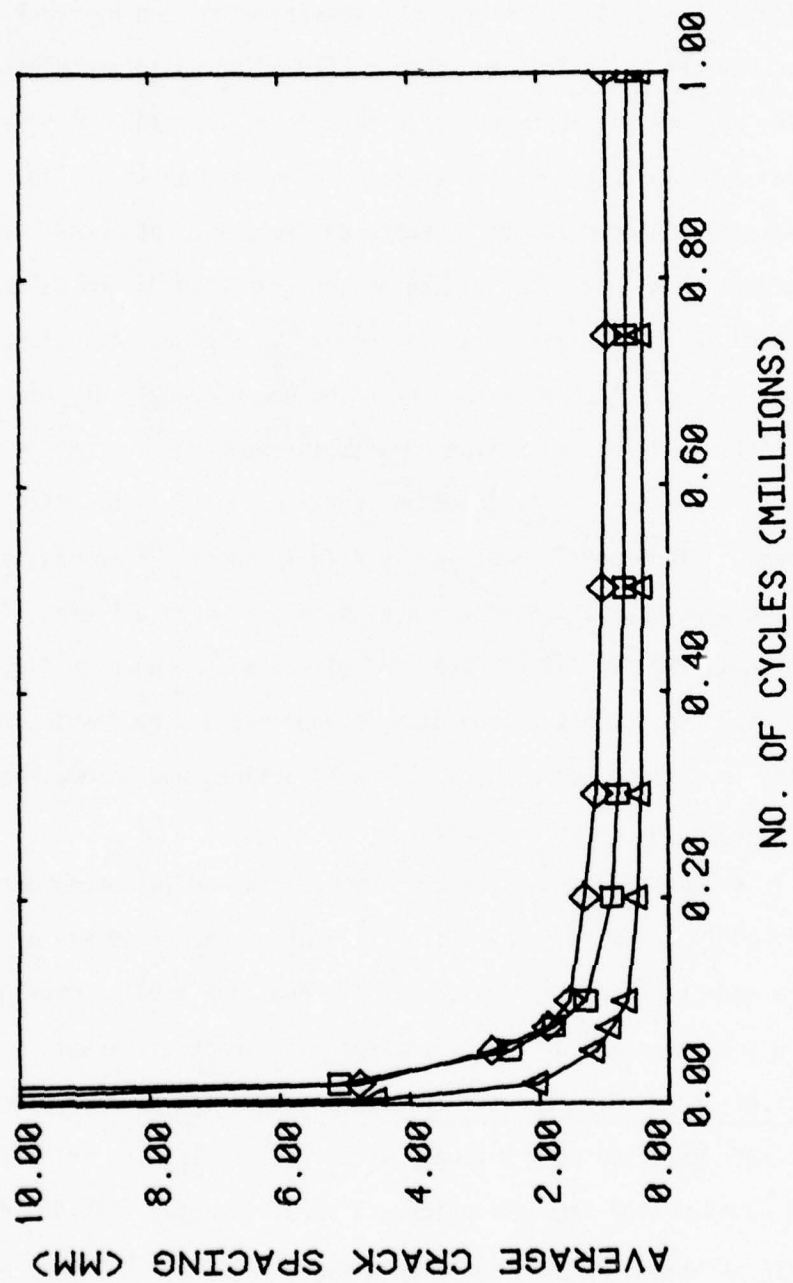


Figure 24. Spacing of Cracks as a Function of Cycles of Loading for Specimen II-20 in the 90° (bottom), +45° (middle) and -45° (top) Plies

I to a Type II stacking sequence. (The straight lines correspond to predictions of crack counts from our analysis, discussed in a latter section.) The differences are most sensitively shown by crack count plots, but crack spacings are more easily compared to other data so, as before, we use that representation hereafter. For the  $90^\circ$  plies in several Type II specimens the crack spacings are shown in Fig. 25. The ordinate is expanded for the purpose of assessing data consistency. It is evident that the crack spacing at the stable condition is extremely reproducible. The variability in the early developmental stages of the damage is simply further evidence of the nonuniqueness of that part of the phenomenon. The same type of data is shown in Fig. 26 for the  $+45^\circ$  plies of the same Type II specimens reported in Fig. 25. The nature of the damage state development is essentially identical to that in the  $90^\circ$  plies, except that the stable crack spacing is very different from that observed in the  $90^\circ$  plies. The  $-45^\circ$  ply data are shown in Fig. 27. Again, the consistency of the data is good and a very stable crack spacing is reached, creating a very well defined and unique characteristic damage state for these laminates.

It was mentioned earlier that damage state development data were generated in two ways. The most efficient and accurate way of obtaining an average crack spacing was to simply count the total number of cracks in a given layer and divide by the specimen length. Because a large number of cracks were counted from each layer in a given specimen and each crack involved only a binary decision (is it there or not), the crack count method was very quick and very effective. It did not, however, provide any information regarding the distribution of crack



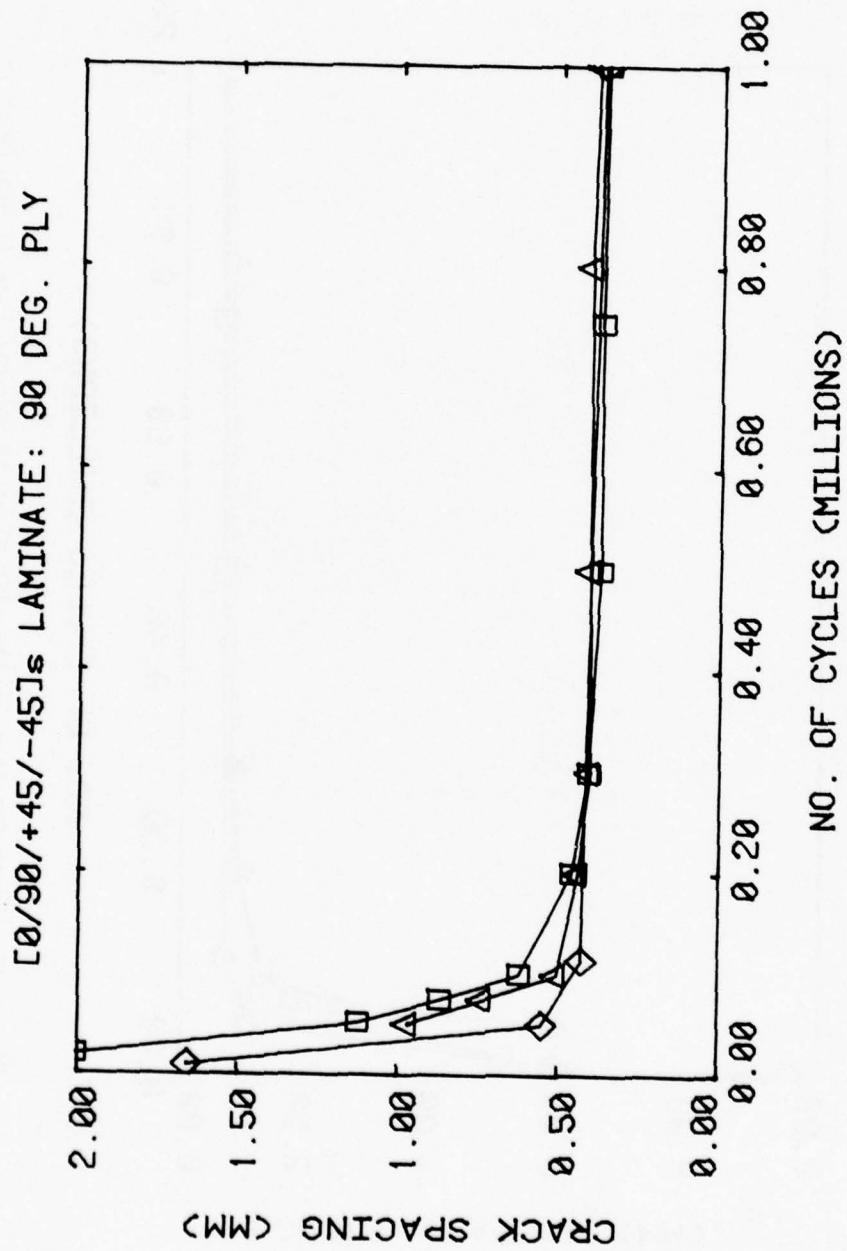


Figure 25. Crack Spacings in the 90° Plies of Several Type II Specimens as a Function of Cycles of Loading

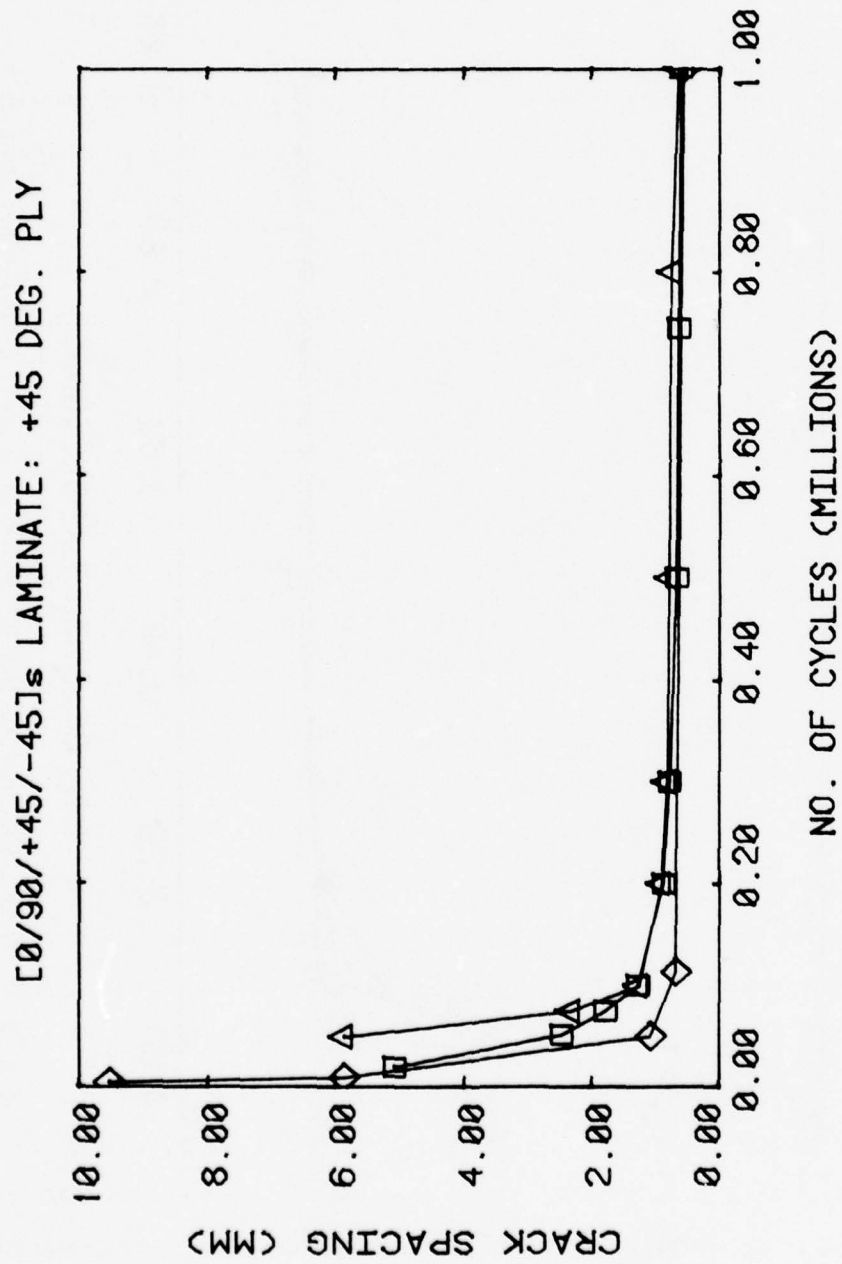


Figure 26. Crack Spacings in the +45° Plies of Several Type II Specimens as a Function of Cycles of Loading

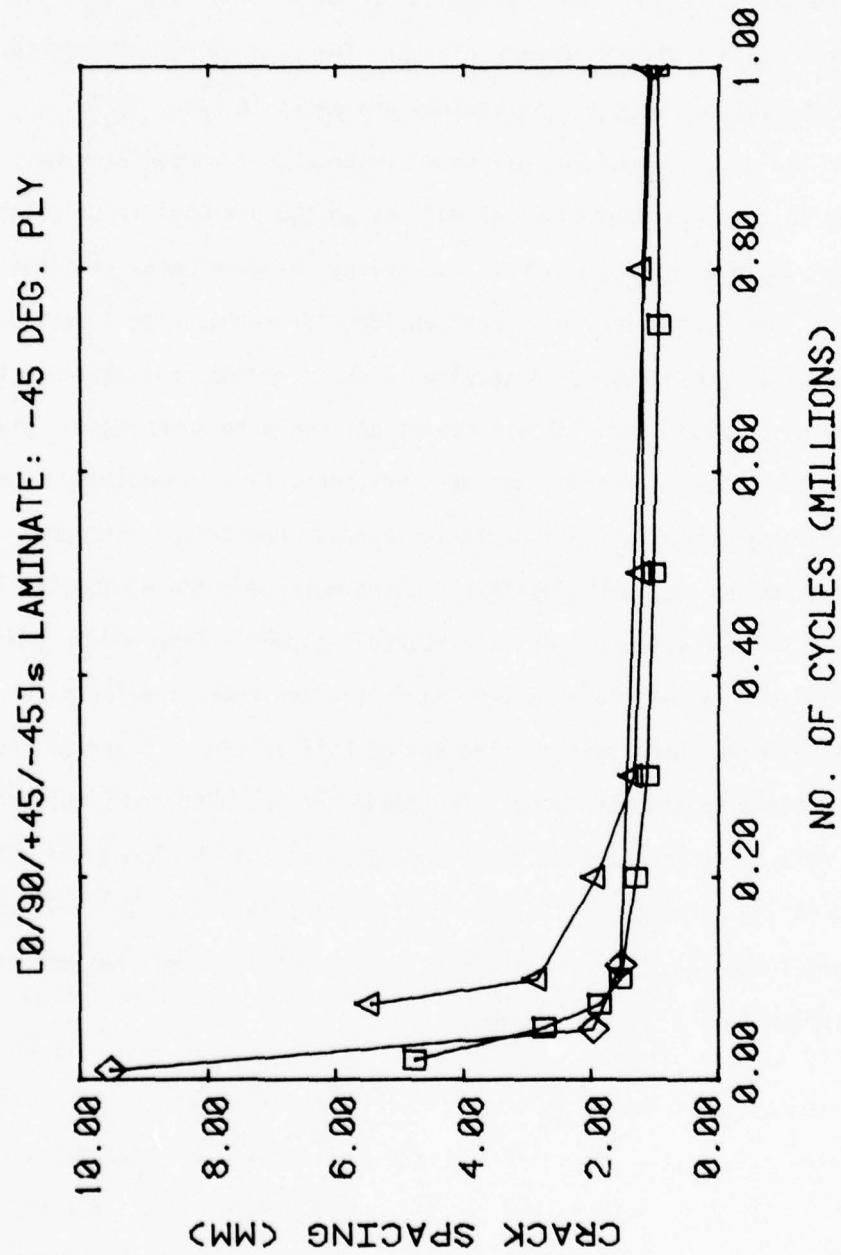


Figure 27. Crack Spacings in the -45° Plies of Several Type II Specimens as a Function of Cycles of Loading

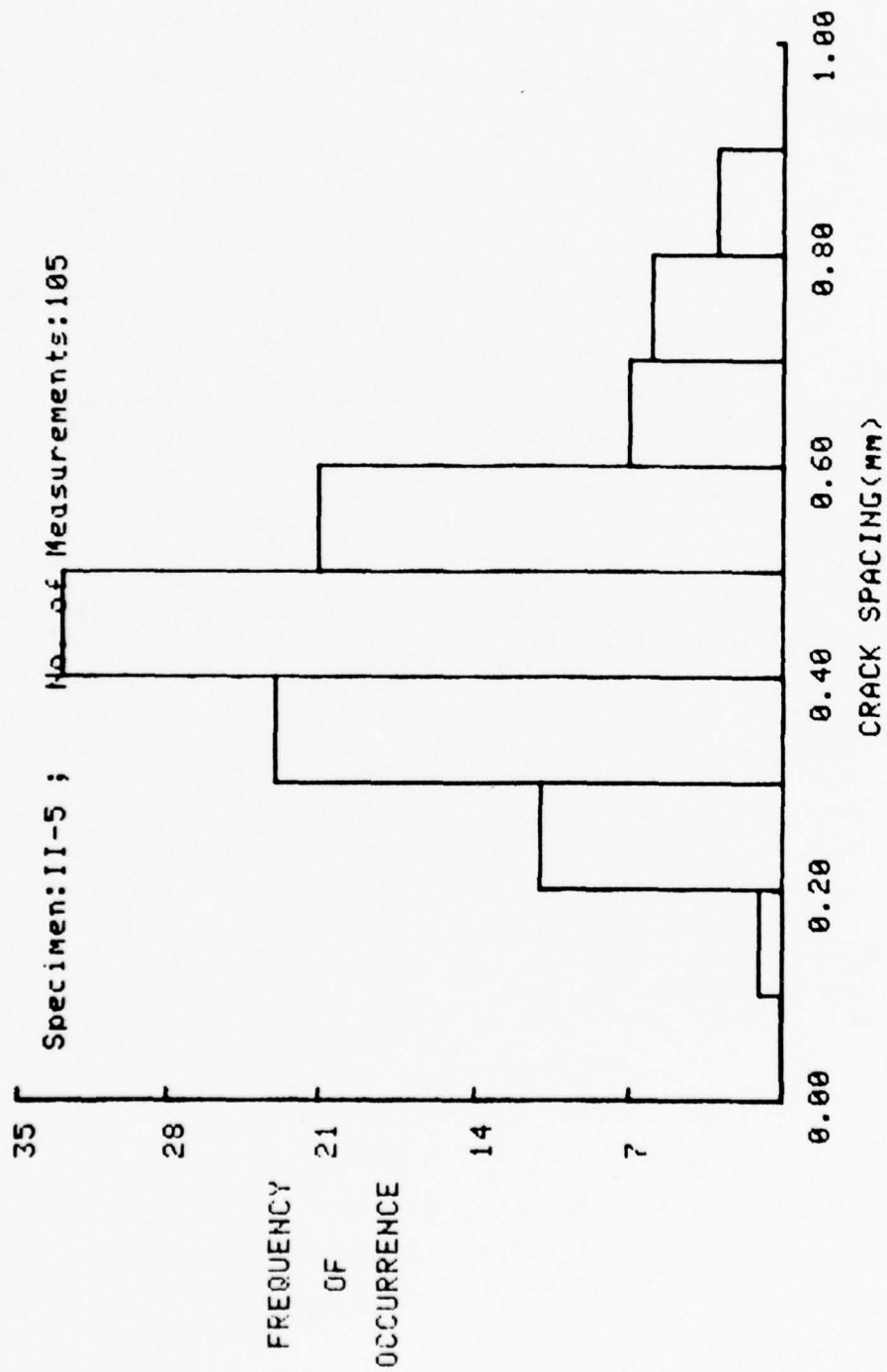
spacings and, therefore, did not reveal whether the stable crack counts actually corresponded to a well defined crack spacing or not. To obtain such information we took measurements of crack spacings directly, one by one from a large number of damage states. The data are summarized in Table 7; histograms of the observations are shown in Figs. 28-30. Data for individual specimens are shown to provide a perspective on specimen to specimen variations as well as on the variability of crack spacings within a given specimen. The values in parentheses are data which have been corrected for crack coupling by disregarding a crack which results from growth of a coupled crack in an adjacent layer in the crack counts. While the standard deviations for data taken from a given specimen are sometimes large, the data are consistent, especially from specimen to specimen in the Type II laminates. Comparison with the figures shown earlier verifies that the two methods produce essentially identical average values. The distributions shown in Figs. 28-30 indicate a more or less normal shape; a skewing to the low crack spacing side with tails on the high spacing side can be seen in Figs. 29 and 30, but the displacements are not large. The ranges of the data are significantly large, reflecting the complexity of the material and the local variations in such things as strength, volume fraction of fibers and geometry, but the central tendency of the distributions is certainly well defined and the distributions are well behaved.

TABLE 7  
STATISTICAL ASPECTS OF CRACK SPACING OBSERVATIONS

Specimen No.	Average 90° Ply	Crack +45° Ply	Spacing -45° Ply
TYPE I MATERIAL			
I-10	$\bar{x} = .665 (.764)$ S.D. = .207 N = 78	$\bar{x} = 1.485 (2.20)$ S.D. = .900 N = 34	$\bar{x} = .722 (.789)$ S.D. = .300 N = 71
I-11	$\bar{x} = .819 (.819)$ S.D. = .229 N = 62	$\bar{x} = 2.96 (2.71)$ S.D. = 1.33 N = 17	$\bar{x} = .868 (.946)$ S.D. = .347 N = 58
I-15	$\bar{x} = .722 (.738)$ S.D. = .199 N = 71	$\bar{x} = 2.24 (2.86)$ S.D. = 1.15 N = 22	$\bar{x} = .802 (.847)$ S.D. = .274 N = 64
TYPE II MATERIAL			
II- 5	$\bar{x} = .363 (.365)$ S.D. = .123 N = 137	$\bar{x} = .469 (.552)$ S.D. = .146 N = 105	$\bar{x} = .894 (1.03)$ S.D. = .299 N = 57
II- 9	$\bar{x} = .32 (.380)$ S.D. = .10 N = 162	$\bar{x} = .53 (.624)$ S.D. = .21 N = 96	$\bar{x} = .93 (1.07)$ S.D. = .38 N = 53
II-20	$\bar{x} = .363 (.343)$ S.D. = .142 N = 141	$\bar{x} = .594 (.567)$ S.D. = .231 N = 86	$\bar{x} = .873 (.908)$ S.D. = .358 N = 58

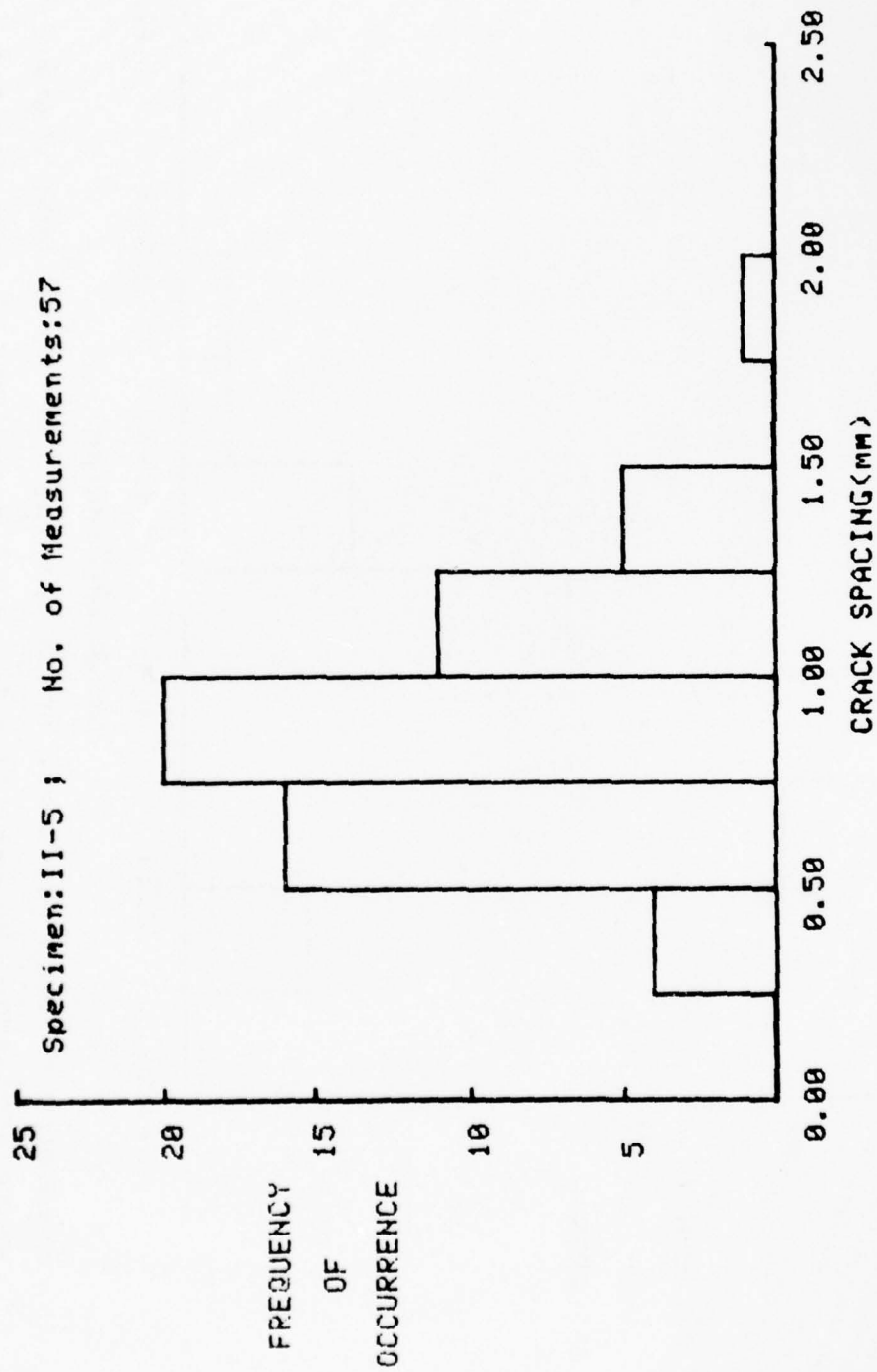
$\bar{x}$  = average value of crack spacing  
S.D. = standard deviation of data  
N = number of observations





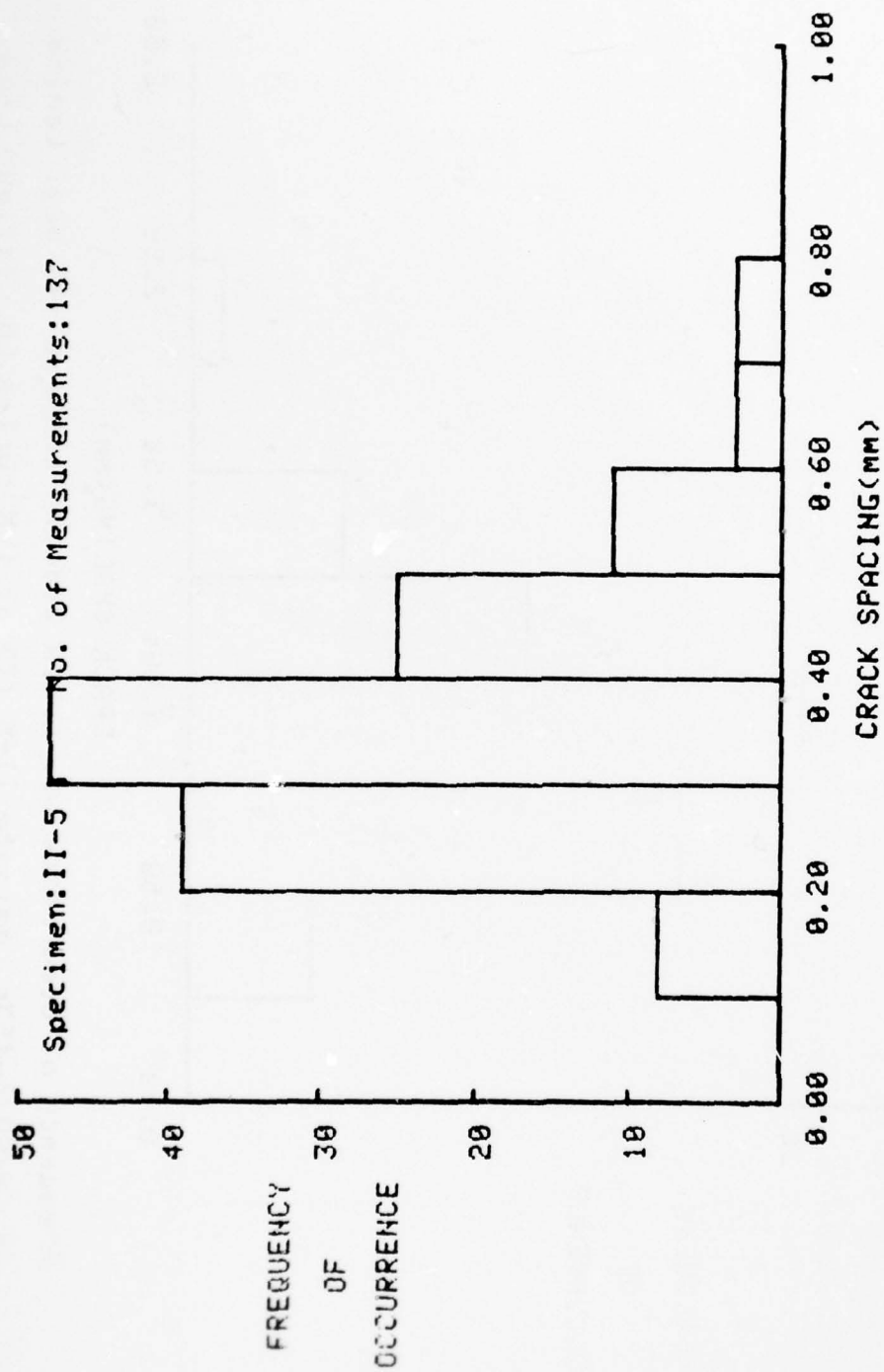
Frequency of Occurrence vs. Crack Spacing (mm) in +45 deg. Lamina of [0/90/+45]s Laminate II-5 (I) at 1 M cycles Lb. fatigue Load.

Figure 28. Histogram of Crack Spacings for Measurements from +45° Laminae of a Type II Laminate



Frequency of Occurrence vs. Crack Spacing (mm) in -45 deg. Lamina  
of [0/90/+45]s Laminate II-5 (I) at 1 M cycles Lb. fatigue Load.

Figure 29. Histogram of Crack Spacings for Measurements from -45° Laminae of a Type II Laminate



Frequency of Occurrence vs. Crack Spacing (mm) in 90 deg. Laminae of [0/90/+45]<sub>s</sub> Laminate II-5 (I) at 1 M cycles Lb. fatigue Load.

Figure 30. Histogram of Crack Spacings for Measurements from 90° Laminae of a Type II Laminate

### Survey Tests on Comparison Laminates

Two additional laminates were studied in order to establish the effect of parameters such as the influence of having two  $90^\circ$  plies next to one another, and the behavior of laminates having (double)  $90^\circ$  plies on the outside surfaces. The in-plane stress fields and interlaminar stresses were different from the type I and II laminates, and the plies used to make up the laminates were different. The material system was maintained constant. A  $[0,90_2,+45]_S$  (hereafter called Type III) and a  $[90_2,0,+45]_S$  laminate (hereafter called Type IV) were chosen for these studies. The number of tests of various types run on these two laminates was smaller than the number run on the Type I and II laminates. (About ten specimens each of the Type III and IV were tested.) The survey tests were intended to establish trends and present comparisons with earlier results. Some interesting contrasts did emerge.

The Type III laminate might be expected to compare with the Type II laminate since it differs only in that there are two  $90^\circ$  plies just below the outside  $0^\circ$  plies rather than just one. However, there is considerable contrast in the damage states that develop. The predicted and observed crack spacings in the two laminates are listed in Table 8 for the characteristic damage state in both cases. The crack spacing in the Type III laminate for the double  $90^\circ$  plies is much greater than for the Type II case, i.e., there are many more cracks per unit length in the laminate which has a single  $90^\circ$  ply between the  $0^\circ$  and  $45^\circ$  plies than there are in the double  $90^\circ$  plies of the Type III laminate. Since the  $90^\circ$  plies are in quite similar surroundings in both cases, the fact that the crack length is twice as long in one case would appear to be the most influential factor, i.e., a longer crack relaxes the stress

over a longer perpendicular distance from the crack tip, other things being equal. Such a result and conclusion might have been anticipated. A somewhat less expected result was the substantial increase in crack coupling and delamination in the Type III laminates compared to the Type II's. For example, at 40 ksi (275.6 MPa) amplitude cyclic loading ( $R = 0.1$ ), there was complete and stable characteristic damage state formation in the Type II laminate. For the Type III laminate the regular arrays of cracks in each ply that we identify with the CDS had begun to be disrupted by crack growth at about 800,000 cycles at that stress level, at least in the sense that many cracks in the  $+45^\circ$  plies were coupled to cracks in the double  $90^\circ$  plies. A schematic diagram of that situation is shown in Fig. 31. The observed crack spacing is smaller in the  $90^\circ$  plies than is predicted by our analysis. It appears from the analysis and from our observations, that cracks in the  $+45^\circ$  plies grow into the  $90^\circ$  plies, although it may be that some other coupling process occurs. If cracks in the double  $90^\circ$  plies grew into the  $45^\circ$  plies, the observed spacing in the  $45^\circ$  plies would be expected to be lower than the analysis prediction. The fact that such a discrepancy exists in the  $90^\circ$  plies, along with the facts that the cracks in the  $90^\circ$ 's become rather irregularly spaced in the case cited above and the cracks appear (from our replication studies) to have grown from the  $+45^\circ$  plies into the  $90^\circ$  plies leads us to suspect that growth may be occurring that way, at least in some cases.

Another interesting comparison is the strength of Type II and III laminates. Although we have relatively inconclusive data (due to only a limited number of ultimate strength tests) it would appear that the ultimate strength of the Type III laminates is low, especially in comparison to the Type II laminates. Figure 31 shows another aspect of growth in



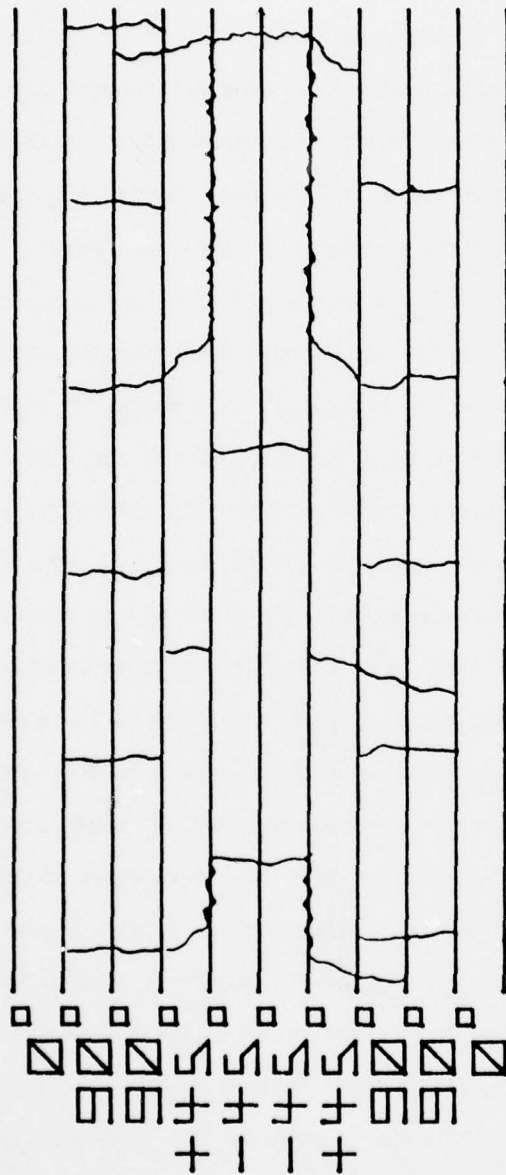


Figure 31. Schematic Diagram of Crack Patterns in a Type III Laminate

the Type III laminates that is peculiar to them. There is a considerable amount of interfacial or interlaminar crack growth and crack coupling, especially for this rather low stress level. A significant percentage of the  $\pm 45^\circ$  interface is cracked due to cracks in those two layers coupling together by that mechanism.

Perhaps the most unusual new type of behavior observed in the damage development in the Type III specimens is crack formation in only one of the double  $90^\circ$  pair at some early point in the load history. This type of behavior was only very rarely observed in the other laminate types. When a crack forms in one ply of an adjacent identical pair it virtually always extends across both plies for the other laminate types studied. However, for the Type III case cracks in one of the two  $90^\circ$  plies were observed to form independently of the other ply in a significant number of cases, usually at some discontinuity in the ply such as a matrix rich region or irregular ply boundary. Of course as loading continued the crack spread into the other ply to form a crack through both  $90^\circ$  plies in that location. However, this behavior contributed to irregularity of the crack spacing and acted to increase the number of cracks since it was found that when a crack in a single  $90^\circ$  ply formed alone, often a crack in the adjacent  $90^\circ$  ply would also form alone some short distance away. Rather than couple together those two cracks usually spread across both plies forming a pair of parallel cracks quite close together which disrupted the otherwise regular array of cracks that formed through both plies essentially instantaneously. These parallel pairs and the cracks coupling with cracks in the  $\pm 45^\circ$  plies are thought to be the principal reason for the observed CDS spacing being smaller than the predicted value in Table 8. Further data gathering is

needed to resolve this point. In summary, the Type III laminates appear to have a higher degree of crack coupling and growth through the laminate thickness and a correspondingly lower strength.

The Type IV laminates are also very different. The  $[90_2, 0, \pm 45]_s$  stacking sequence of these laminates isolates the cracks in the double  $90^\circ$  plies. No growth of cracks from the  $90^\circ$  plies to the  $45^\circ$  plies, or the reverse, can occur. As a result, the crack spacing in the  $90^\circ$  plies is very stable and very regular with variations usually being clearly traceable to surface irregularities or other local causes. The analytical prediction of the CDS spacing in Table 8 is quite satisfactory, even though the spacing is a very unusual value, the second largest value observed in any laminate tested. Another result of the constraint on crack growth appears to be an increase in strength, based on our limited sample size. It is also interesting to note that for quasi-static loading the  $\pm 45^\circ$  plies form very few cracks. In fact in some cases it is difficult to find any. This is further evidence of the influence of crack formation in one ply on that in another.

#### SECTION IV

##### MECHANICS OF THE "CHARACTERISTIC DAMAGE STATE"

As we noted in the earlier sections, during the course of our investigations we have made a very startling discovery regarding the transverse crack formation process. We have discovered that each laminate (i.e., each material and stacking sequence) has a completely unique characteristic damage state (CDS) that it creates by forming cracks with an essentially regular spacing in each off-axis layer of the laminate. The crack spacing in each off-axis ply is determined by the properties of the cracked ply and the properties of the neighboring plies, as well as the properties of the laminate. The same plies stacked differently will have a different spacing of cracks. We have come to call this situation the "characteristic damage state" of a given laminate. It has the following properties and attributes.

- 1) The characteristic damage state (CDS) depends only on the laminate properties, including the stacking sequence, and is independent of extensive variables such as tensile load history or geometry.
- 2) The CDS is a unique, distinct, well defined physical situation which can, therefore, be described and modeled analytically.
- 3) The CDS is the stable damage state that forms prior to failure and has the same significance, in that sense, as the single crack in a homogeneous material.

We noted earlier that the number of cracks seems to reach a common maximum as quasi-static loading occurs. As we also noted above, the same stable maximum is reached under cyclic (fatigue) loading. The CDS

is stable in that once it has formed no new transverse cracks form independently in the off-axis plies. Quite close to failure of the specimen cracks do couple up and spread from ply to ply as we will discuss below, but the damage state from which final fracture develops, the CDS, is stable up to that point.

The discovery of the CDS is a recent finding; the generality of the concept has not been established. However, the local mechanics of CDS formation has been examined and some apparent progress has been made in understanding and representing the physical situation. Reifsnider has postulated a simple model which can be used to predict the CDS for any laminate. Comparisons of those predictions with twelve cases for which experimental data is available shows very good agreement (see Table 8). The success of the simple model suggests that the principles it is based on are valid. The model utilizes an equilibrium element approach. The cracked ply (or plies) is represented as one element in a plane containing the thickness and longitudinal directions of the laminate as shown in Fig. 32. Neighboring (uncracked) plies are represented as elements, and the remainder of the laminate is represented by an element. Each element has one dependent variable, the average displacement. Axial and shear forces are summed up for each element and boundary conditions are set, resulting in a system of coupled equations to solve. Solution of these equations yields a rough estimate of the stresses in the neighborhood of the crack in the thickness-length ( $x,z$ ) plane. There is one parameter in the model, the length over which a gradient of shear stress exists between layers, which must be estimated based on experimental observations of deformation fields. The basic premise that



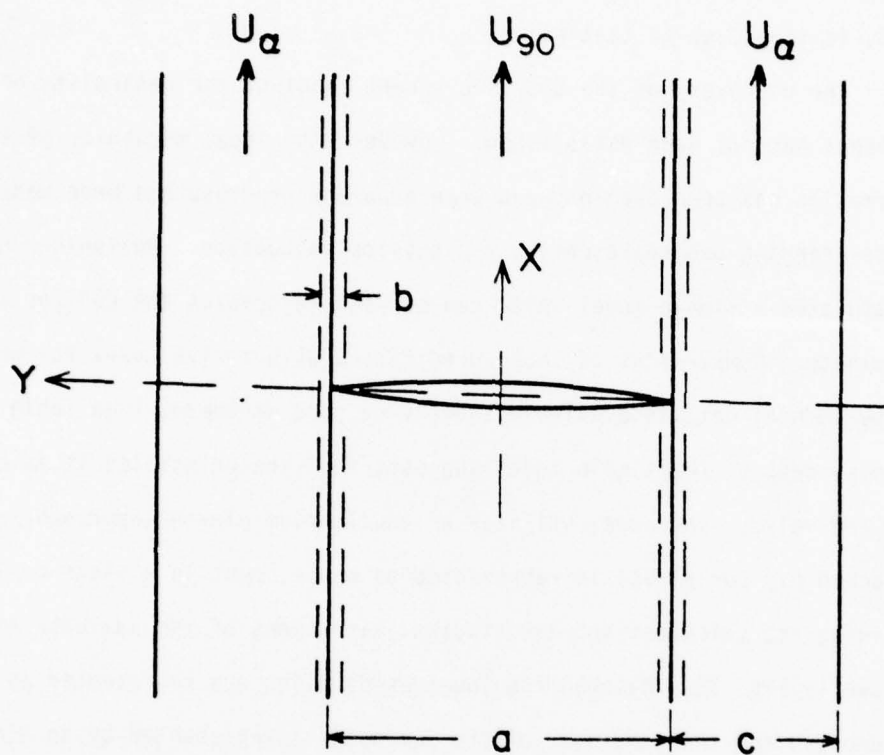


Figure 32. Equilibrium element used for one-dimensional model of characteristic damage state formation

is used to predict the CDS from the analysis is that the closest distance at which a new crack can form is determined by that distance from an existing crack at which the stress in the cracked ply reaches the undisturbed value which caused the first crack. Hence, that distance represents lower bound on crack spacing. When that spacing is reached a stable CDS is formed. The manner in which the stress is transferred into the cracked ply by the shear stresses exerted by the neighboring uncracked plies determines this characteristic distance. A brief example of these calculations is given below.

We imagine a schematic representation of the  $[0, \pm 45, 90]_s$  laminate situation shown in our earlier figures wherein two  $90^\circ$  plies are cracked, but no further damage propagation has occurred (see Fig. 32). We assume that the constraint layers next to the crack have an orientation of  $\alpha$  degrees to the load axis. We further assume that the disturbance caused by the broken layer does not extend beyond the first constraining (unbroken) ply on either side of the broken ply. Finally, on the basis of experimental observations we estimate that any gradients in response from ply to ply occur over a distance,  $b$ , which extends one twentieth of the ply width into each ply, or about the thickness or one tow or bundle on either side of the ply interface in the case of graphite epoxy for example.

To consummate the analysis, we invoke an equilibrium element approach, a method which is as old as the discipline of mechanics, and which has been applied to other problems in composite materials by other investigators [7,8]. Referring to Fig. 32, we consider the equilibrium of an element  $dx$  long, two ply thicknesses wide, and of unit thickness repre-

senting the region immediately above or below a crack in two  $90^\circ$  plies. A simple force balance can then be written including only stress components thought to be important, two shear stress components on either side of the element representing the action of the constraint layers and an axial normal stress component within the element in this case. The resulting equation is

$$aE_{x90} \frac{d^2 U_{90}}{dx^2} + 2G \left( \frac{U_{45} - U_{90}}{b} \right) = 0 \quad (1)$$

where  $E_{x90}$  is the uniaxial engineering stiffness of the  $90^\circ$  ply in the  $x$  direction,  $G$  is the engineering shear stiffness of the matrix material,  $U_{90}$  is the average  $x$  displacement of the  $90^\circ$  ply at a given point, and the stress transfer region dimension  $b$  has been used to write the constraining forces in difference form. For the constraint layers, an equilibrium element can also be constructed having width  $c$  and axial displacement  $U_2$  as shown in Fig. 32. The resulting equilibrium equation is

$$cE_{x\alpha} \frac{d^2 U_\alpha}{dx^2} + \frac{G}{b} (U_{90} + U^\circ - 2U_\alpha) = 0 \quad (2)$$

where  $E_{x\alpha}$  is the uniaxial engineering stiffness of the constraint layer,  $U^\circ$  is the undisturbed laminate displacement and  $U_\alpha$  is the average displacement in the constraint layer. We choose to normalize these equations by the definitions

$$U = \sigma_a \left( \frac{1}{E_x G} \right)^{\frac{1}{2}} au \quad X = \left( \frac{E_x}{G} \right)^{\frac{1}{2}} ax \quad (3)$$

where  $E_x$  is the laminate uniaxial stiffness and  $\sigma_a$  is the laminate applied

stress. Equations (1) and (2) then take the form

$$A \frac{d^2 u_{g0}}{dx^2} + u_{\alpha} - u_{g0} = 0 \quad \text{and} \quad B \frac{d^2 u_{\alpha}}{dx^2} + u_{g0} + x - 2u_{\alpha} = 0 \quad (4)$$

where

$$A = \frac{b}{2a} \quad \text{and} \quad B = \frac{bc}{a^2}$$

for this case. The boundary conditions require that the disturbance die out at large distances from the crack and that all stresses with normal components vanish at the crack face. We also require that displacement components vanish along the Y axis in all unbroken plies. The analytical statement of those conditions follows.

$$\frac{du_{g0}}{dx} (x \rightarrow \infty) = 1 \quad \frac{du_{\alpha}}{dx} (x \rightarrow \infty) = 1 \quad (5)$$

$$\frac{du_{g0}}{dx} (x = 0) = 0 \quad u_{\alpha} (x = 0) = 0 \quad (6)$$

Solutions to equations (4), as well as a large class of similar equations are easily obtained and are available from such familiar situations as the coupled oscillator problem. For our purpose we choose solutions of the form

$$u_{g0} = x + C_1 e^{-\alpha x} + C_2 e^{-\beta x} \quad (7)$$

$$u_{\alpha} = x + D_1 C_1 e^{-\alpha x} + D_2 C_2 e^{-\beta x}$$

as found in reference [8]. These are solutions if the auxiliary conditions

$$\begin{aligned}
D_1 &= 1 - A\alpha^2 \\
D_2 &= 1 - A\beta^2 \\
\alpha, \beta &= \frac{B+2A}{2AB} \pm \frac{1}{2AB} [B^2 + 4A^2]^{\frac{1}{2}} \quad (8)
\end{aligned}$$

are satisfied. Boundary conditions (6) also require that

$$C_1 = \frac{-D_2}{D_1 - D_2} \quad C_2 = \frac{D_2}{D_1 - D_2} \quad (9)$$

It can be seen that boundary conditions (5) are automatically satisfied by equations (7). The system of equations (7-9) then provide the complete solution to the problem.

Each ply in each laminate requires a new solution of coupled equations. When the plies on either side of the ply being analyzed are different from each other three coupled equations rather than two must be solved and new auxiliary equations will develop. Also, the equations take on somewhat different forms when a free surface is encountered. Laminates of arbitrary type can be easily analyzed, however, and characteristic damage states can be predicted for all cases.

To calculate this spacing we need only solve for the stress in the 90° plies, in the present case, and determine the distance required for our normalized stress to reach the value of approximately 1. For the present material we use  $a = 0.30$  mm,  $b = 0.015$  mm,  $c = 0.15$  mm,

$E_{x90} = 9.17$  GPA,  $E_{x0} = 142.7$  GPA in the analysis. A plot of normalized stress verses normalized distance from the crack face is shown in Fig. 33 for this case. In order to establish a value of  $x$  at which the stress reaches the undisturbed value one must either pick a discretionary value off of the plot or return to the equations and set a specific



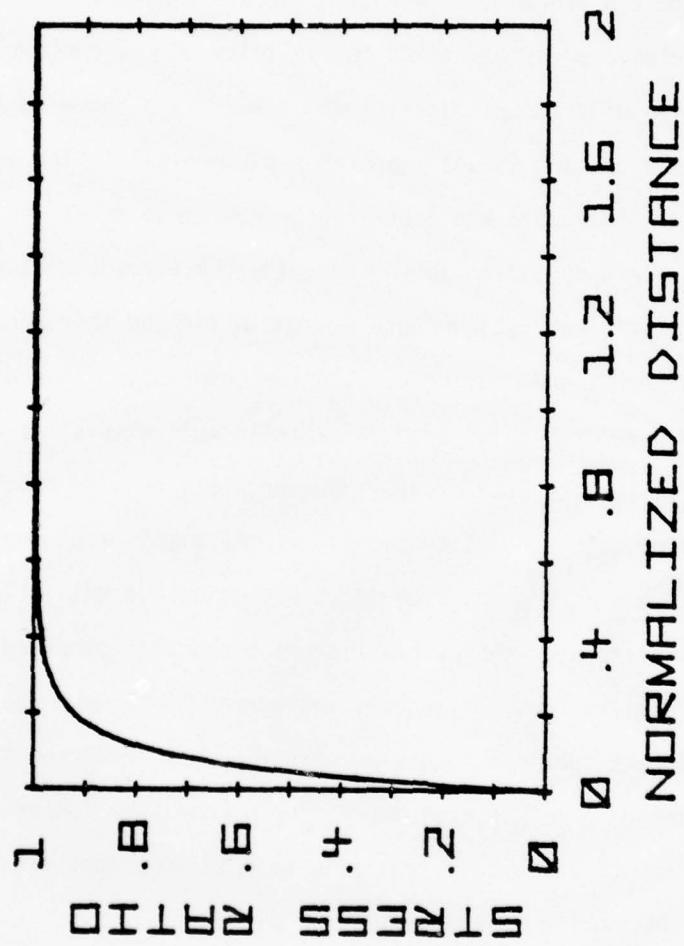


Figure 33. Normalized Stress as a Function of Distance from the Crack Face Predicted by the Analysis.

AD-A076 497

VIRGINIA POLYTECHNIC INST AND STATE UNIV BLACKSBURG  
DEFECT-PROPERTY RELATIONSHIPS IN COMPOSITE MATERIALS. PART IV.(U)  
JUN 79 K L REIFSNIDER , E G HENNEKE

F33615-77-C-5044

F/G 11/4

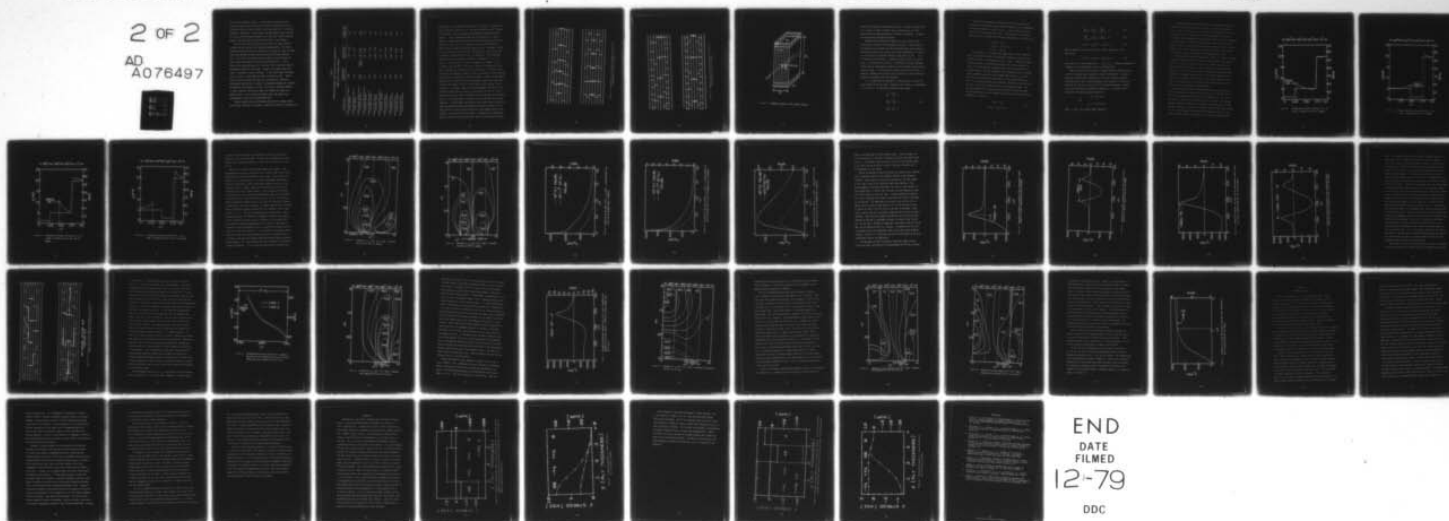
UNCLASSIFIED

AFML-TR-76-81-PT-4

NL

2 OF 2

AD  
A076497



value of the normalized stress. In the interest of precision, the latter was done for the data below; a value of 0.999 was used as the normalized value of stress at which a new crack would form. (Since the function is asymptotic it was reasoned that the material would not wait for the miniscule difference between, say, 0.999 and 1 before breaking. However, the choice does not affect the validity of the concept.)

The results of this calculation, and others, are shown in Table 8 along with the spacing values measured experimentally. The experimentally determined values are expressed as the range of values included within one standard deviation above and below the average measured value. Both static and fatigue data are shown for the third entry in Table 8 which corresponds to the calculation described. It can be seen that the predicted value of 0.76 mm falls well within the range of experimental values for both cases. However, this regular spacing of cracks is observed in other situations. If the simple model postulated above is valid, it should describe those situations as well. Table 8 shows several calculated characteristic crack spacings compared to experimental observations. In general the agreement between the predicted and observed crack spacings is close. The range of predicted spacings is large, covering a multiple of about four between the lowest and highest values. Of all predictions made to date none appear to be unreasonable in light of our experimental data.

Figures 34 and 35 show the predicted characteristic damage states for the Type I and Type II laminates, along with a tracing of the observed

TABLE 8

## PREDICTED AND OBSERVED CRACK SPACINGS FOR THE CHARACTERISTIC

## DAMAGE STATE IN SEVERAL LAMINATES

Specimen Type	Predicted Crack Spacing (mm)	Observed Crack Spacing (mm)	Average Crack Spacing (mm)
Cracks in two center 90° plies of [0,90] <sub>s</sub> laminate	0.882	1.087 - 0.532	0.81
Cracks in outside 90° plies of [90,0] <sub>s</sub> laminate	1.66	1.73 - 0.775	1.25
Cracks in center two 90° plies of [0,±45,90] <sub>s</sub> laminate	0.76 0.76	Static 1.51 - 0.62 Fatigue 1.44 - 0.47	1.07 0.96
Cracks in two center 45° plies of [0,90,±45] <sub>s</sub> laminate	1.21	1.25 - 0.995	1.12
Cracks in single 90° plies of [0,90,±45] <sub>s</sub> laminate	0.411	0.423 - 0.241	0.33
Cracks in +45° plies of [0,90,±45] <sub>s</sub> laminate	0.875	0.909 - 0.524	0.72
Cracks in outside 90° plies of [90 <sub>2</sub> ,0,±45] <sub>s</sub> laminate	1.12	1.40 - 1.07	1.24
Cracks in -45° plies of [0,±45,90] <sub>s</sub> laminate	0.879	0.960 - 0.889	0.92
Cracks in 90° plies of [0,90 <sub>2</sub> ,±45] <sub>s</sub> laminate	0.701	0.600 - 0.460	0.53
Cracks in +45° plies of [0,90 <sub>2</sub> ,±45] <sub>s</sub> laminate	0.890	1.05 - 0.650	0.85
Cracks in -45° plies of [0,90 <sub>2</sub> ,±45] <sub>s</sub> laminate	1.223	1.38 - 0.963	1.17

damage states. The observed state for Type I laminates is shown by the typical pattern on the top of Fig. 34 and the predicted state is shown on the bottom. The basic features are faithfully reproduced by the analysis. Figure 35 shows the same type of comparison for a Type II laminate. Aside from the fact that the analysis appears to predict the CDS well in both cases, it is important to notice how different the damage states are when the stacking sequence, only, is changed. The  $90^\circ$  plies for example, have nearly twice the density of cracks in the Type II laminate as they do in the Type I configuration. This difference might be expected to produce a difference in properties. It is, in fact, so. The strength of the Type I laminate, for example, is consistently lower than that of the Type II material (delamination of the Type I laminates may contribute to this difference). Transverse cracks also reduce the laminate stiffness so that a difference in crack densities will also mean a difference in stiffness change. Finally, during fatigue loading at stress levels of half the ultimate strength up to about two thirds of that value, the CDS of the laminate usually develops fairly completely. It becomes, then, a well defined damage state which can be modelled carefully and accurately, a state which controls the state of strength and state of stress from which the final fracture event develops. Hence, it is very desirable to be able to predict the CDS for arbitrary laminates. It would appear that even the very simple analysis discussed above can capture the essential features of the CDS, at least raising the possibility that we can anticipate the fatigue damage state for any laminate. The generality of the method is suggested by the comparisons shown in Table 8 and by the predictions shown by the straight horizontal



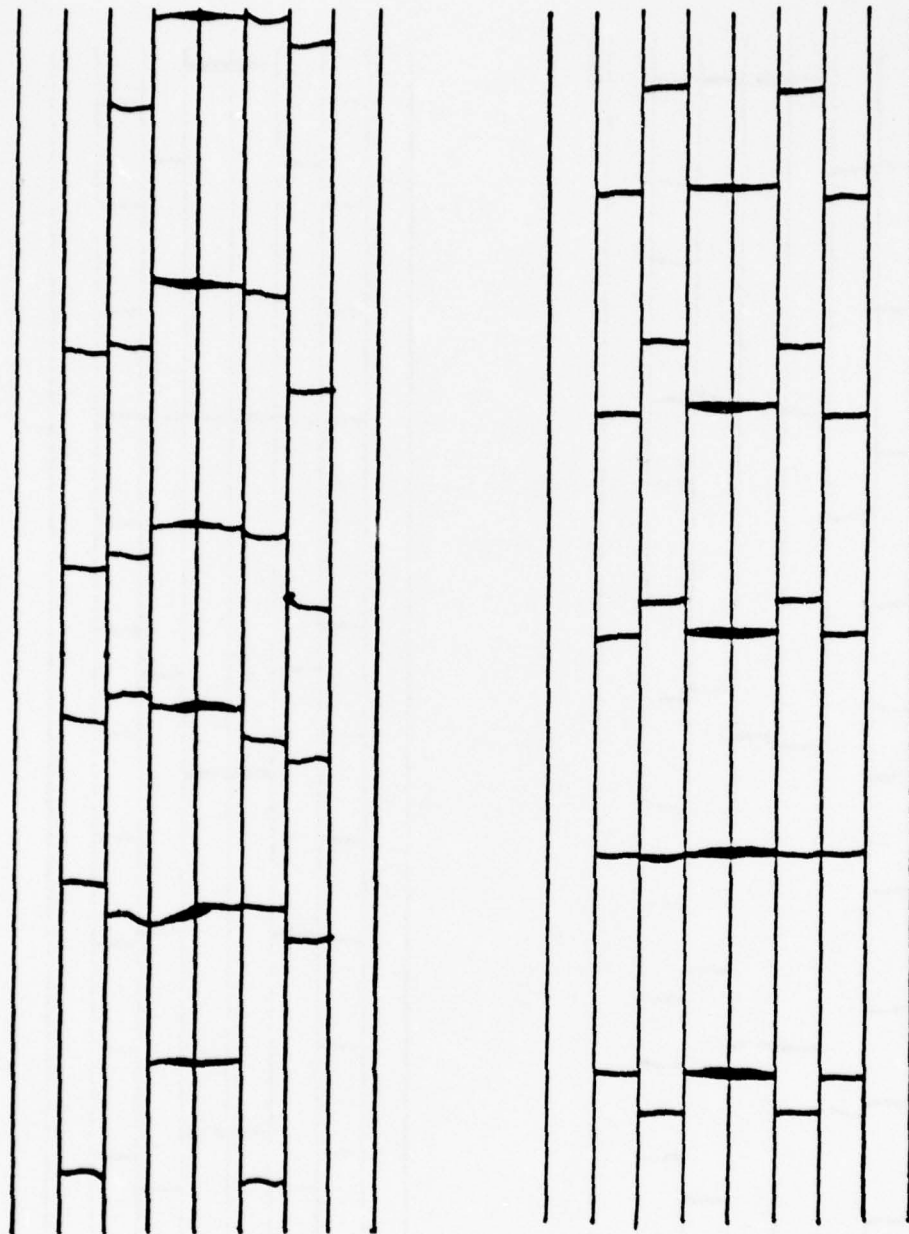


Figure 34. Observed (top) and Predicted (bottom) Characteristic  
Damage State for Type I Laminate

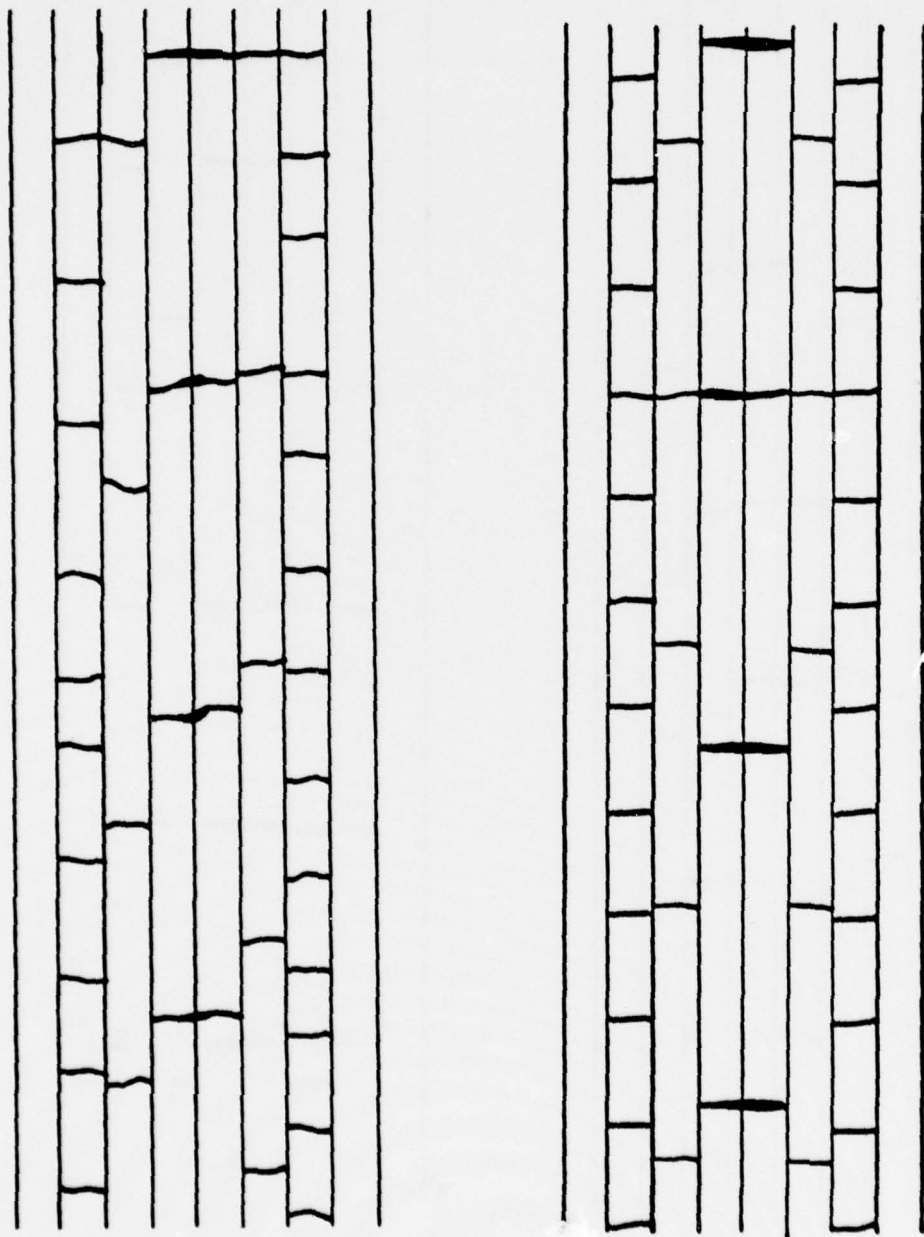


Figure 35. Observed (top) and Predicted (bottom) Characteristic  
Damage State for Type II Laminate

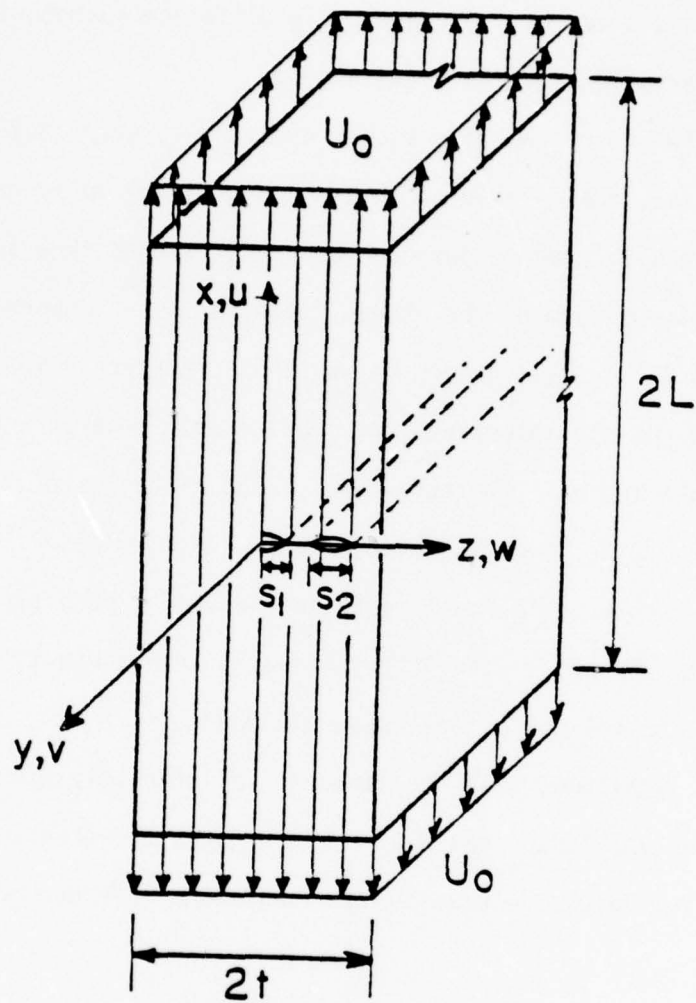


Figure 36. Schematic diagram of the cracked laminate

lines in the figures of the previous section. The model has been tried for a variety of widely different cases including plies on a free surface and plies having drastically different surroundings. Agreement with observations has been quite good.

Although the one dimensional analysis is very convenient and instructive, the details of the mechanics involved in crack formation and especially crack growth can not be extracted from such an analysis. The precise nature of the stress field in the neighborhood of a crack in an off-axis ply will determine how that crack grows into the next ply, or along the ply interfaces, or couples with other cracks, or participates in a laminate fracture event. The mechanics of these important aspects must be investigated by means of a more general and more precise analysis scheme. To investigate the nature of such stress fields in composite laminates with internal cracks transverse to the direction of loading the following model was developed.

It is assumed that the laminate is infinitely wide, and that the cracks extend across the width. Therefore, the stresses are independent of  $y$  (Fig. 36). The equilibrium conditions then become:

$$\begin{aligned}\frac{\partial \sigma_x}{\partial x} + \frac{\partial \tau_{xz}}{\partial z} &= 0 \\ \frac{\partial \tau_{xy}}{\partial x} + \frac{\partial \tau_{yz}}{\partial z} &= 0 \\ \frac{\partial \tau_{xz}}{\partial x} + \frac{\partial \sigma_z}{\partial z} &= 0 .\end{aligned}\tag{10}$$

Based on this assumption, and with the aid of the constitutive relations for the material system under consideration, the  $y$  dependence of the displacements  $u$ ,  $v$  and  $w$  (in the  $x$ ,  $y$  and  $z$  directions respectively) can be determined analytically. Accounting for the symmetry conditions, the functional forms of these displacements are found to be:

$$\begin{aligned} u(x,y,z) &= U(x,z) \\ v(x,y,z) &= V(x,z) + Cy \\ w(x,y,z) &= W(x,z) \end{aligned} \tag{11}$$

The constraint,  $C$ , represents the normal strain in the  $y$  direction. Due to the symmetric nature of the problem, Equations 10 need only be solved within the first quadrant of the  $x$ - $z$  plane. A numerical solution to these equations is obtained by expressing the stress components in terms of the displacements, and employing a finite difference discretization scheme. This way, Equations 10 are reduced to a set of coupled linear algebraic equations in the unknown nodal values of  $U$ ,  $V$  and  $W$  that must be satisfied at all nodal points of the finite difference grid. For improved accuracy near boundaries, Equations 10 are satisfied not only at all interior nodes, but also at the boundary nodes. The resulting unknown fictitious nodal values outside the physical domain are evaluated with the aid of boundary conditions discretized by central differences. These are:

$$\begin{aligned} U(L,z) &= U_0 \\ V(L,z) &= W(L,z) = 0 \end{aligned} \tag{12}$$



$$\left. \frac{\partial U}{\partial z} \right|_{z=0} = \left. \frac{\partial V}{\partial z} \right|_{z=0} = \left. \frac{\partial^2 W}{\partial z^2} \right|_{z=0} = 0 \quad (13)$$

$$\left. \frac{\partial^2 U}{\partial x^2} \right|_{x=0} = \left. \frac{\partial V}{\partial x} \right|_{x=0} = \left. \frac{\partial W}{\partial x} \right|_{x=0} = 0 \quad (14)$$

$$\sigma_z(x,t) = \tau_{zy}(x,t) = \tau_{zx}(x,t) = 0 \quad (15)$$

When a transverse crack exists in the y-z plane, conditions 14 are replaced by

$$\sigma_x(0,z) = \tau_{xy}(0,z) = \tau_{xz}(0,z) = 0 \quad (16)$$

over that part of the boundary where  $z$  ( $S_1$  or  $S_2$ ). A complete mathematical treatment of this formulation is given in Reference [9].

Some of the stress distributions in damaged laminates obtained by the use of this analysis are presented in Figures 37 through 57. Two quasi-isotropic, graphite-epoxy laminates with the same constituent laminae, differing only in their stacking sequences, are considered. These laminates have  $[0^\circ, \pm 45^\circ, 90^\circ]_S$  and  $[0^\circ, 90^\circ, \pm 45^\circ]_S$  stacking sequences, referred to as Type I and Type II laminates, respectively. The applied strain values for all examples discussed here are:

$$\bar{\epsilon}_x = 10^{-3} \text{ in/in}$$

and

$$\bar{\epsilon}_y = -2 \times 10^{-4} \text{ in/in}$$

where  $\bar{\epsilon}_x$  and  $\bar{\epsilon}_y$  are average global quantities.

Through-the-thickness distributions of the axial normal stress in the plane of the crack for Type I and Type II laminates are shown in Figs. 37 and 38 respectively. A transverse crack extending across the thickness of the  $90^\circ$  layer results in the disturbances in the stress field which can be compared to the undisturbed laminate stresses indicated in these figures. In the Type I laminate the crack extends across the two  $90^\circ$  layers on each side of the mid-plane, whereas, the two  $90^\circ$  layer cracks in the Type II laminate have a length equivalent to one lamina thickness each, and are separated by four undamaged  $\pm 45^\circ$  layers.

The disturbance created by these cracks results in a greater increase in the axial normal stress over the undisturbed laminate value (at the crack tip) in the  $-45^\circ$  layers of the Type I laminate than in the  $45^\circ$  layers of the Type II laminate. On the other hand, the axial normal stresses in the  $0^\circ$  layers of the Type I laminate are essentially undisturbed while a maximum increase over the undisturbed laminate value of about 8% is observed in the  $0^\circ$  layers of the Type II laminate. These stress concentrations aid in the through-the-thickness growth of the transverse cracks observed in these laminates.

Figures 39 and 40 show the through-the-thickness distribution of the longitudinal normal stress for Type I and Type II laminates after the  $90^\circ$  ply damage has spread into the next weakest ply, i.e., the  $-45^\circ$  ply for Type I and the  $+45^\circ$  ply for the Type II laminate. The damaged laminate stresses increase with increasing crack length under constant strain as expected. In the Type I laminate, extending the crack through the  $-45^\circ$  ply is observed to cause not only a greater increase in the crack tip stress within the adjacent  $45^\circ$  ply, but also more than an 8%

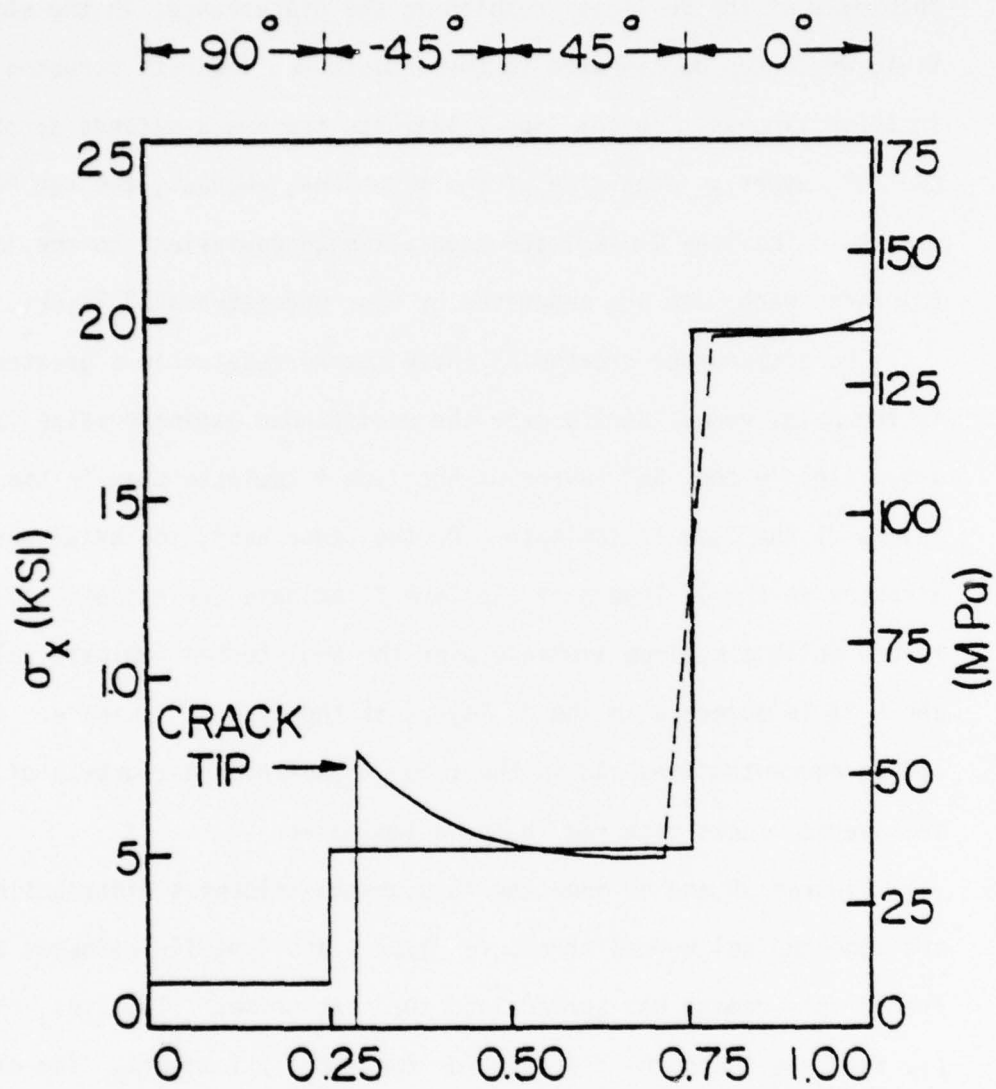


Figure 37. Through-the-thickness variation of  $\sigma_x$  for a type I laminate with  $90^\circ$  ply damage

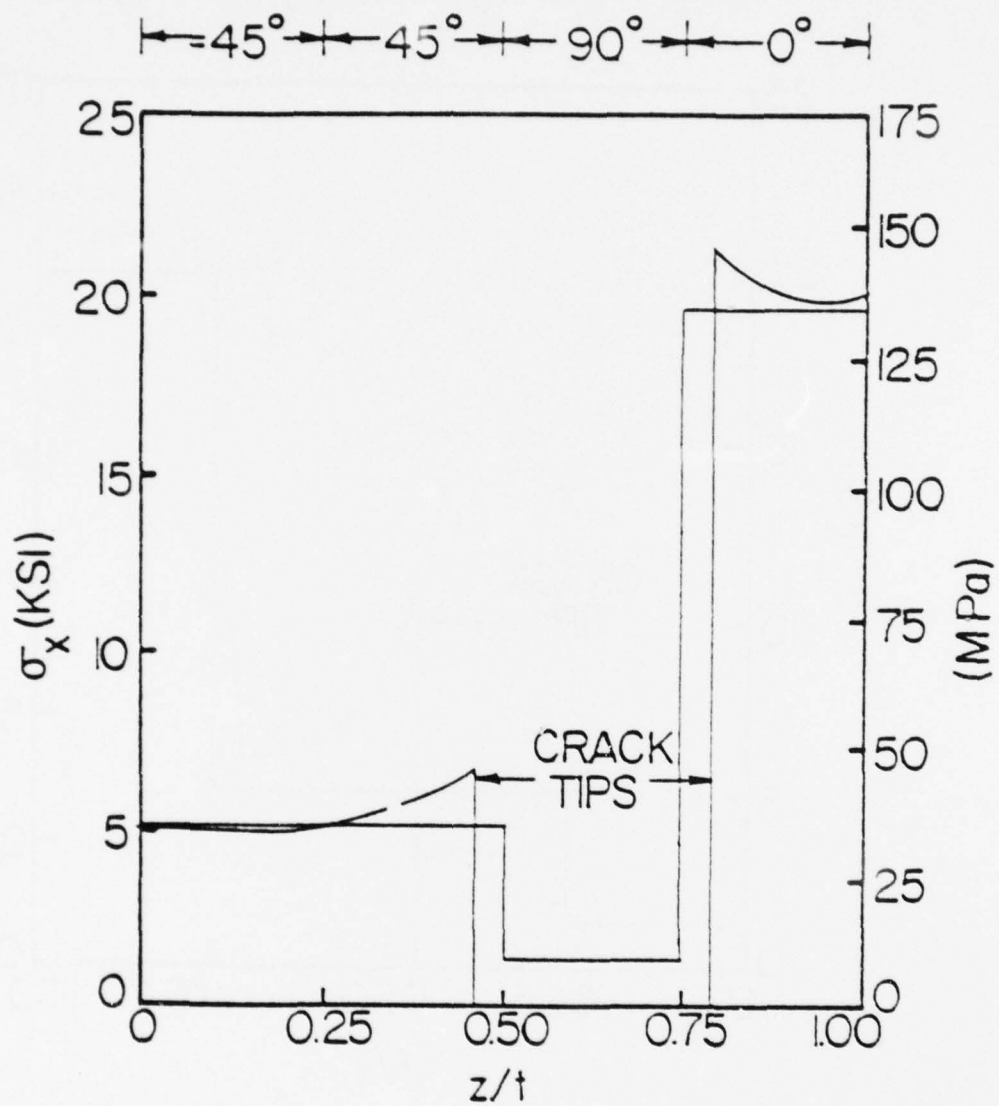


Figure 38. Through-the-thickness variation of  $\sigma_x$  for a type II laminate with 90° ply damage

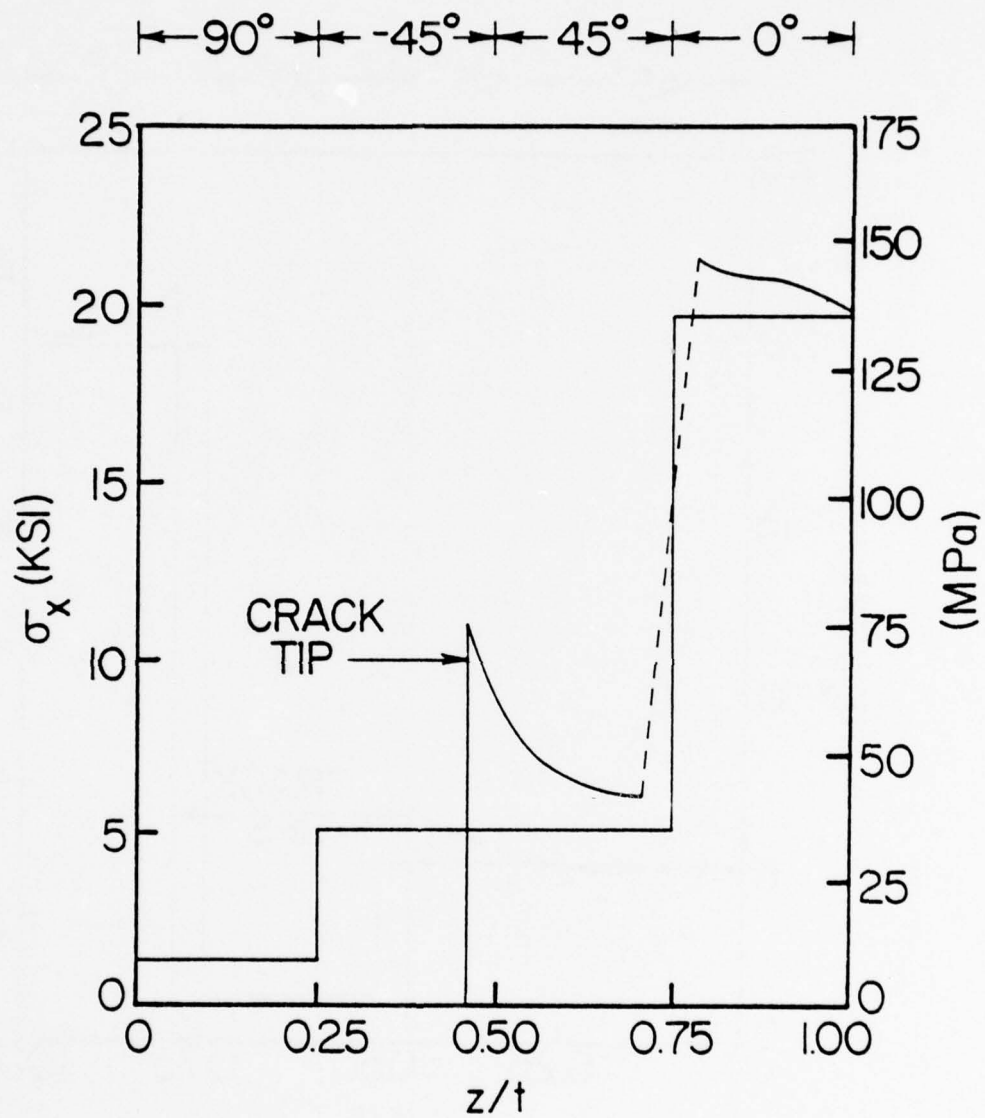


Figure 39. Through-the-thickness variation of  $\sigma_x$  for a type I laminate with 90° and -45° ply damage



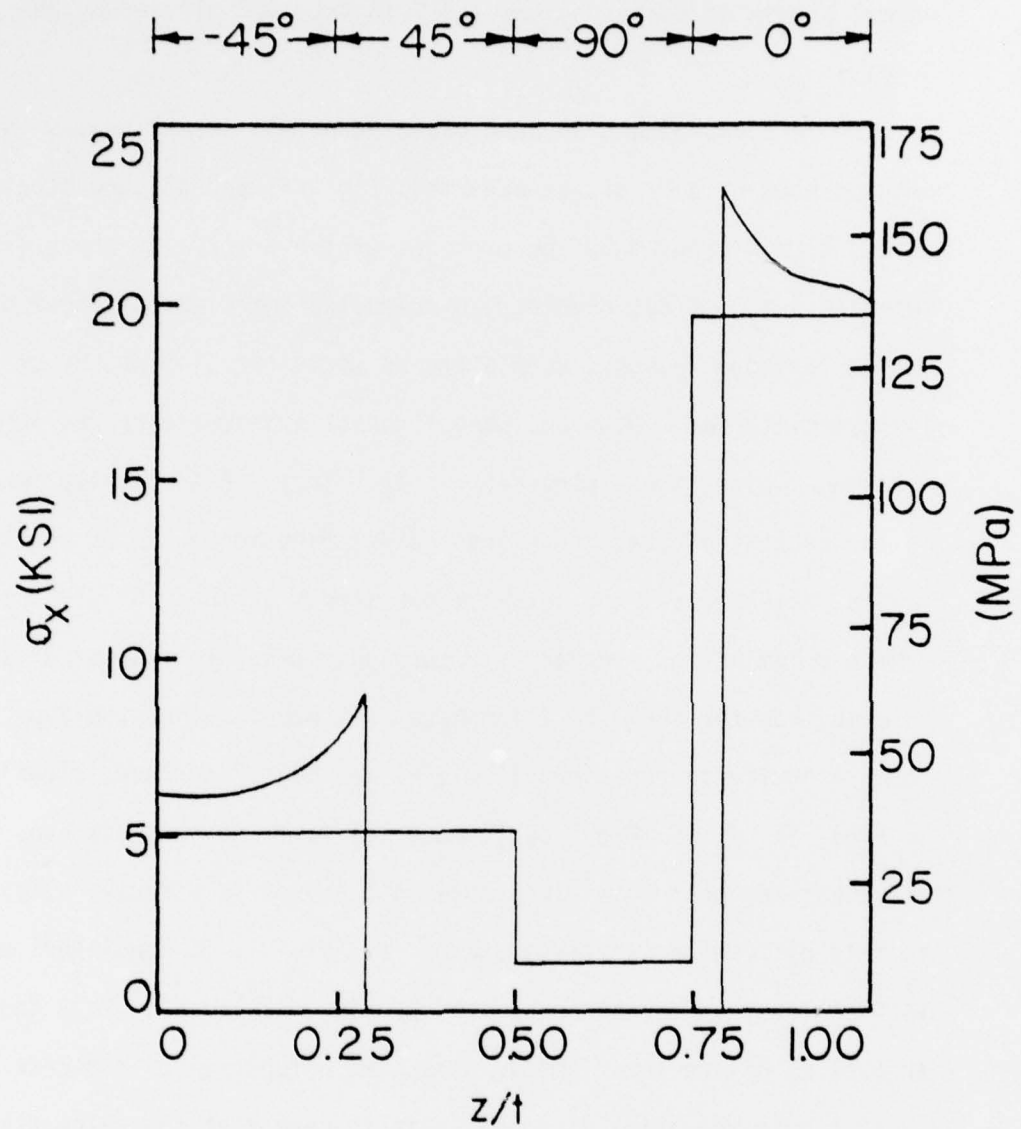


Figure 40. Through-the-thickness variation of  $\sigma_x$  for a type II laminate with 90° and 45° ply damage

increase in the axial normal stress which was seen to be almost undisturbed by a  $90^\circ$  ply failure alone. For the Type II laminate, the axial normal stress increases by about 78% in the  $-45^\circ$  ply and by 19% in the  $0^\circ$  ply.

While Figs. 39 and 40 show elevated normal stress values in the neighborhood of a crack, as expected, Figs. 41 and 42 show stresses that were entirely created by the presence of the crack. As the crack faces separate a  $\tau_{xz}$  stress develops, a so-called interlaminar shear stress. Except for edge regions, such a stress would normally not occur in the laminate interior. However, when internal transverse cracks form in individual plies these stresses appear. They are especially important in the context of crack coupling and delamination modes of crack growth. In the present case, the interlaminar stress at the  $\pm 45^\circ$  ply interface (where delamination frequently occurs just prior to fracture) is greater in magnitude for the Type I laminate. It happens that the Type I material forms a prefracture pattern involving the  $\pm 45^\circ$  interface, clearly shown in Figs. 11, J, K. The Type II material forms no such pattern. While we cannot say that this difference in behavior is directly attributable to this difference in stress states it certainly is consistent with it. This contrast is further supported by Figs. 43 and 44. They show distributions of the interlaminar stress as a function of distance from the crack tip in the axial direction. It is seen that the calculated values near the tip are fifty percent greater for the Type I laminate, and at a distance of one half ply thickness away they are more than one hundred percent greater. It is quite likely that such a difference is reflected in physical behavior. It is also well to notice that, considering the

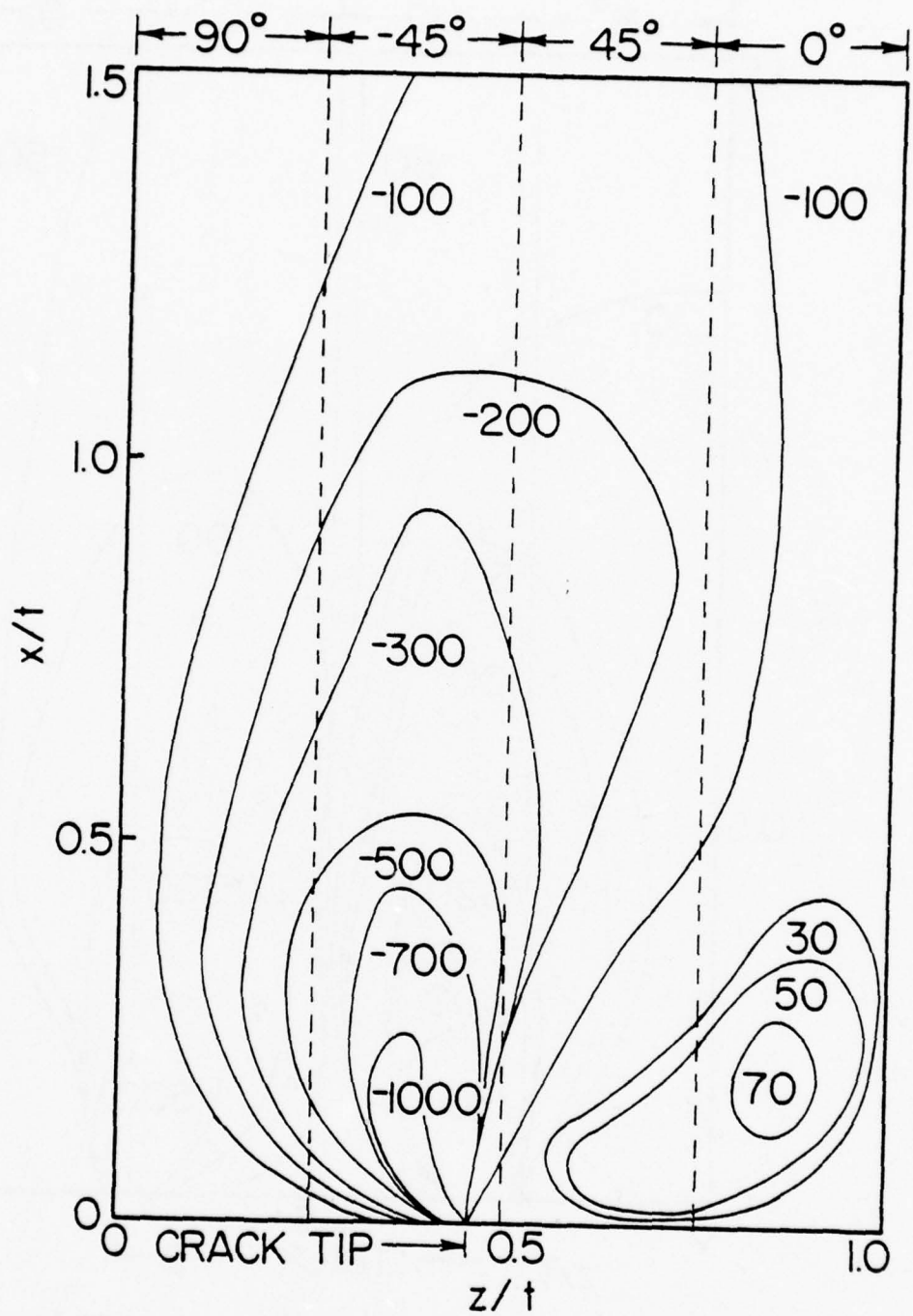


Figure 41. Contours of  $\tau_{xz}$  (psi) for a type I laminate with 90° and -45° ply damage

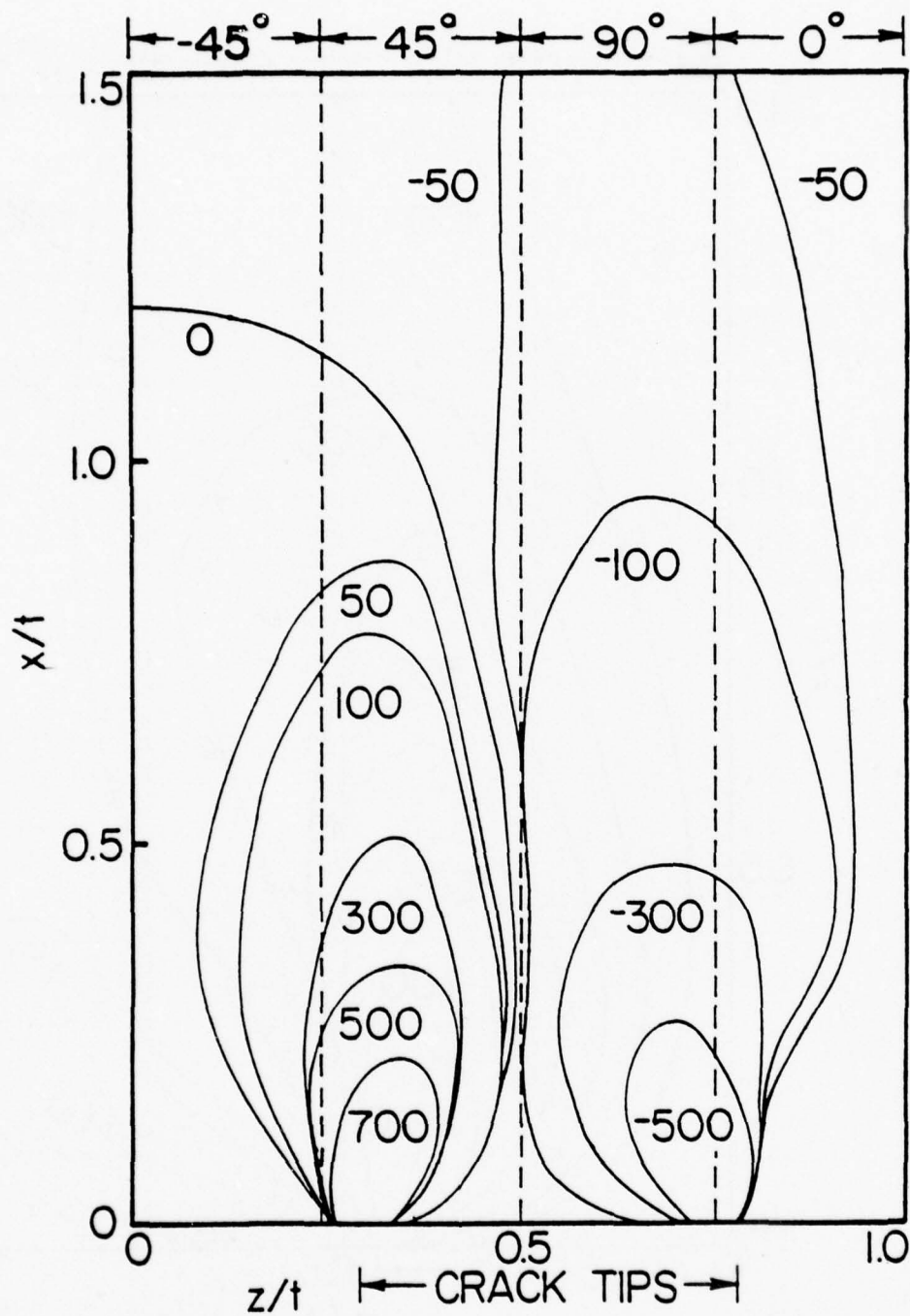


Figure 42. Contours of  $\tau_{xz}$  (psi) for a type II laminate with  $90^\circ$  and  $45^\circ$  ply damage

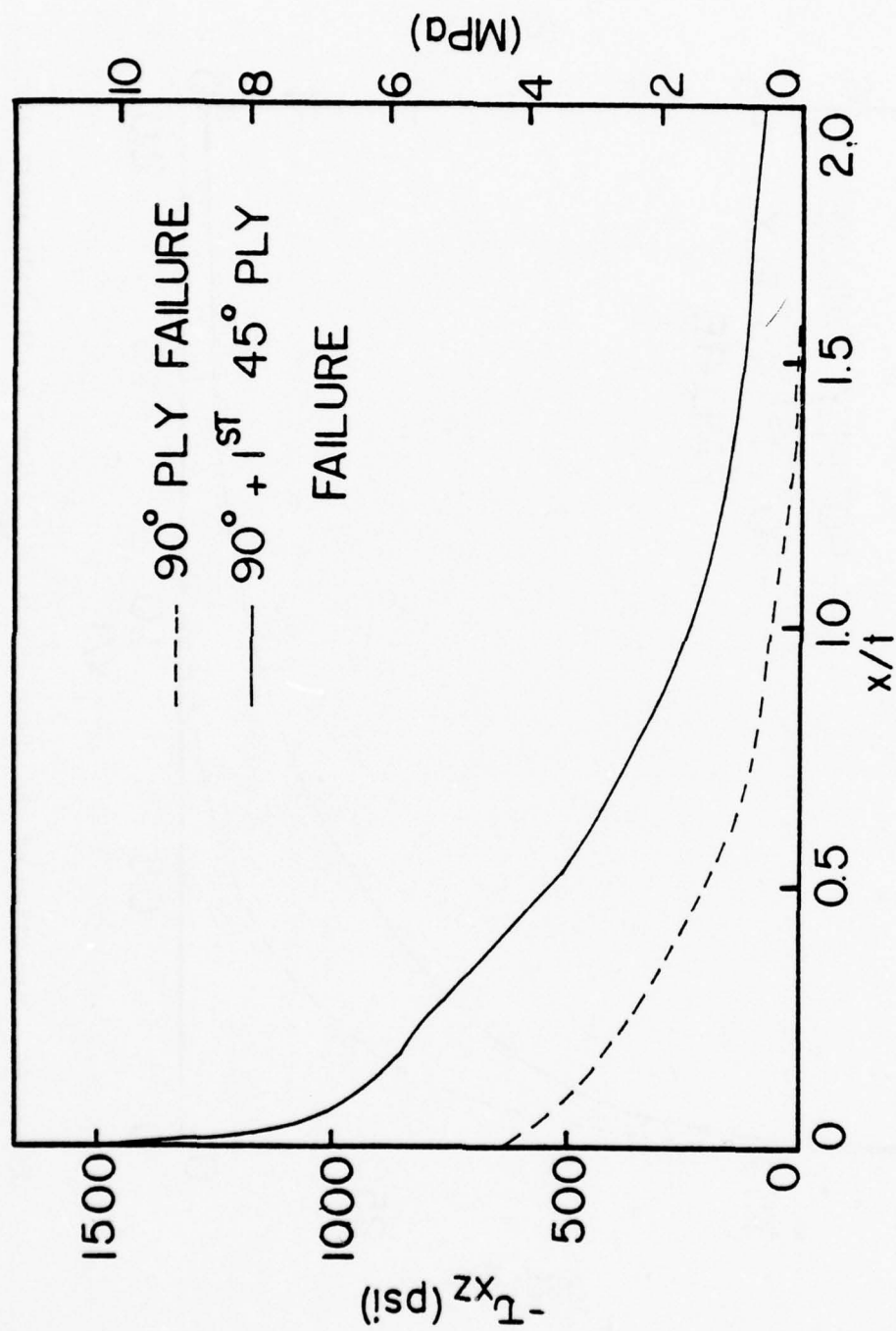


Figure 43. Variation of the shear stress,  $\tau_{xz}$ , with  $x$  directly above the crack tip for damaged type I laminates



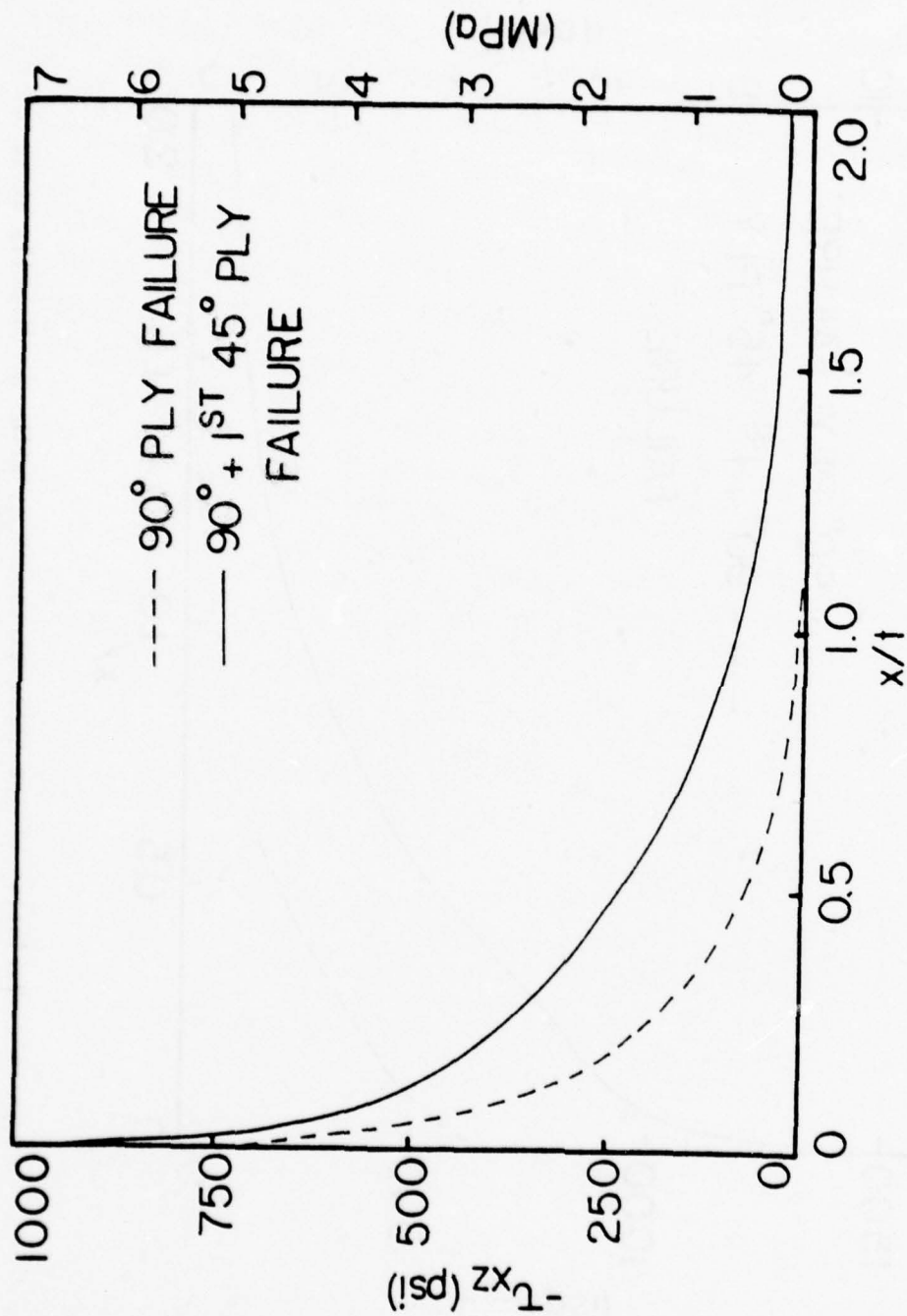


Figure 44. Variation of the shear stress,  $\tau_{xz}$ , with  $x$  directly above the crack tip (within the 0° ply) for damaged type II laminates

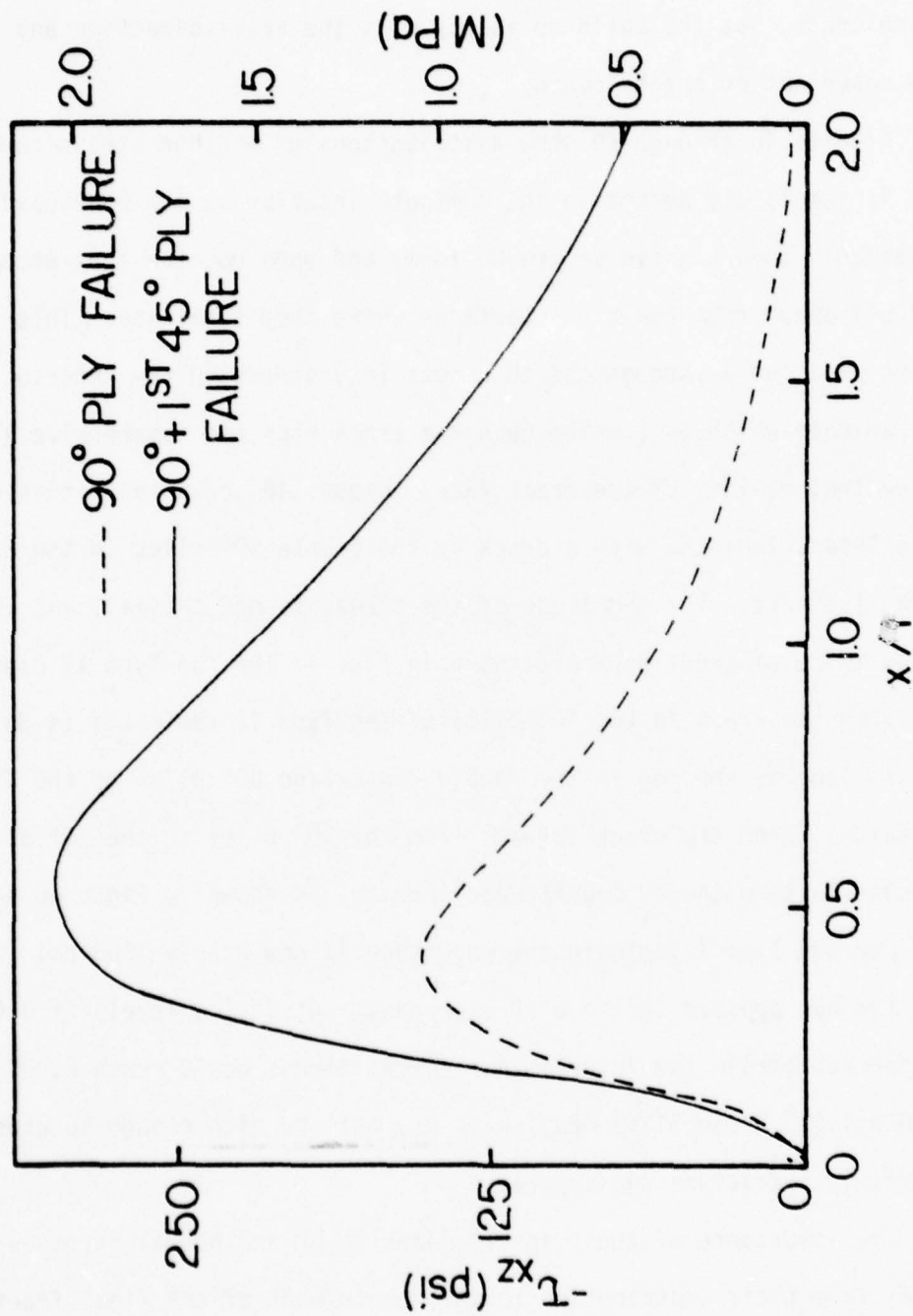


Figure 45. Variation of the shear stress,  $\tau_{xz}$ , with  $x$  above the first node ahead of the crack tip for damaged type I laminates

loading, the magnitudes are significantly large. Figure 45 shows the axial distribution for the Type II laminate at a point just ahead of the crack tip. The symmetry plane brings the stress to zero directly ahead of the crack, but the build-up is rapid in the axial direction and is very dependent on crack length.

Figures 46 through 49 show distributions of another stress component that is completely absent in the laminate interior in the uncracked situation. When transverse cracks form, and open up, the tips attempt to "pull away" from the ply interfaces where they terminate. This action produces a through-the-thickness ( $\sigma_z$ ) stress in the interior of the laminate which is tensile near the crack tips and compressive along the central regions of the crack face. Figure 46 shows the situation for a Type I laminate with a crack in the double 90° plies in the center of the laminate. The magnitude of the stress is not trivial, and is nearly twice as great as those shown in Fig. 47 for the Type II case. Of course the crack in the 90° plies of the Type II laminates is only half as long as the one in the double centerline 90° plies of the Type I laminates. When the crack spreads from the 90° plies to the 45° plies adjacent to them the  $\sigma_z$  magnitudes increase, as shown in Figs. 48 and 49. For the Type I laminate the magnitude is now nearly 1500 psi (10.34 MPa) for our applied strain of 0.1 percent. At design levels of 0.4 or 0.5 percent strain the interlaminar normal stress would reach 6,000 to 7,500 psi (35.34 to 51.68 MPa) which may well be high enough to cause an interlaminar fracture and separation.

The importance of these interlaminar shear and normal stresses arises from their contribution to the development of the final fracture

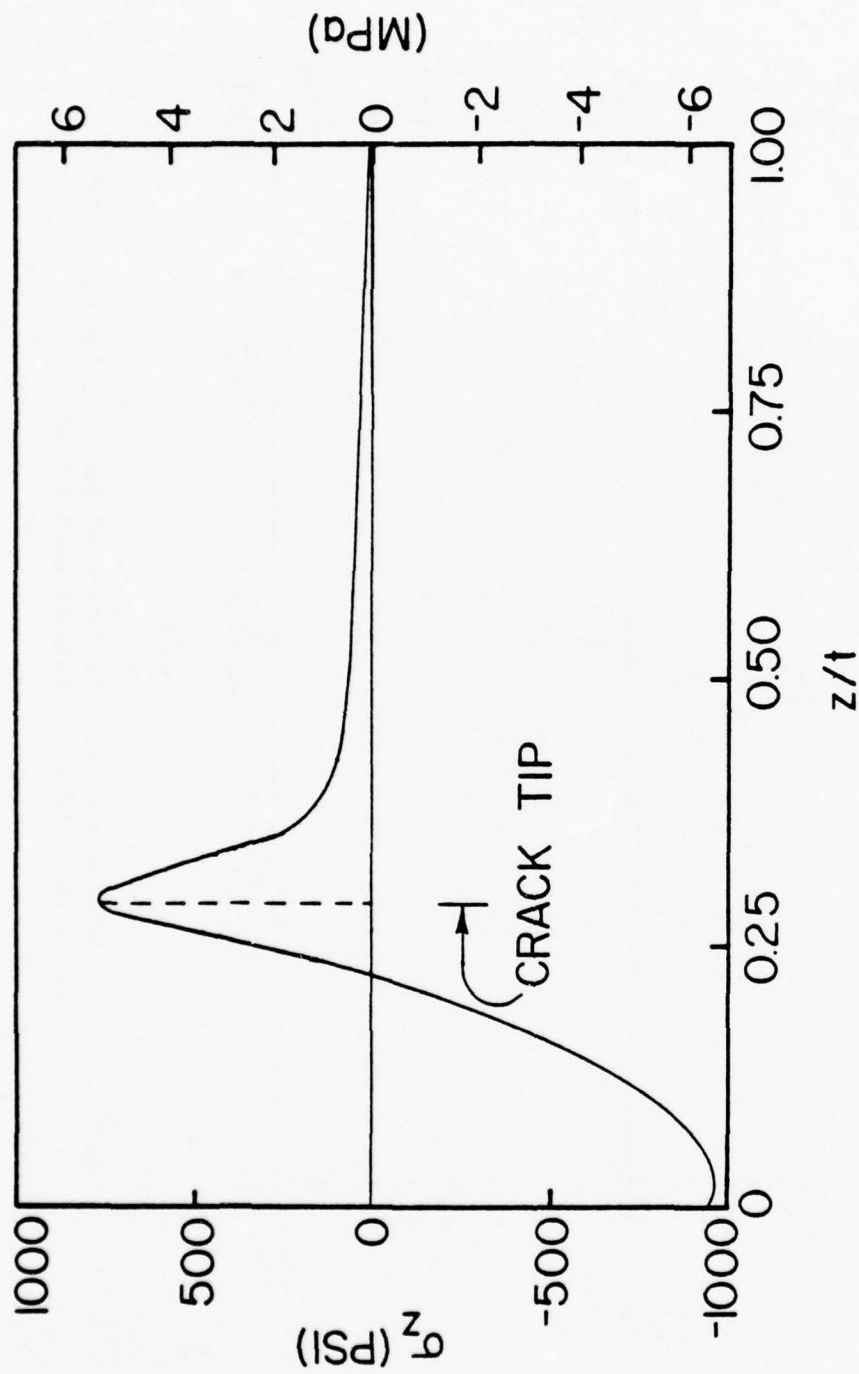


Figure 46. Through-the-thickness variation of the interlaminar normal stress for a type I laminate with 90° ply damage.

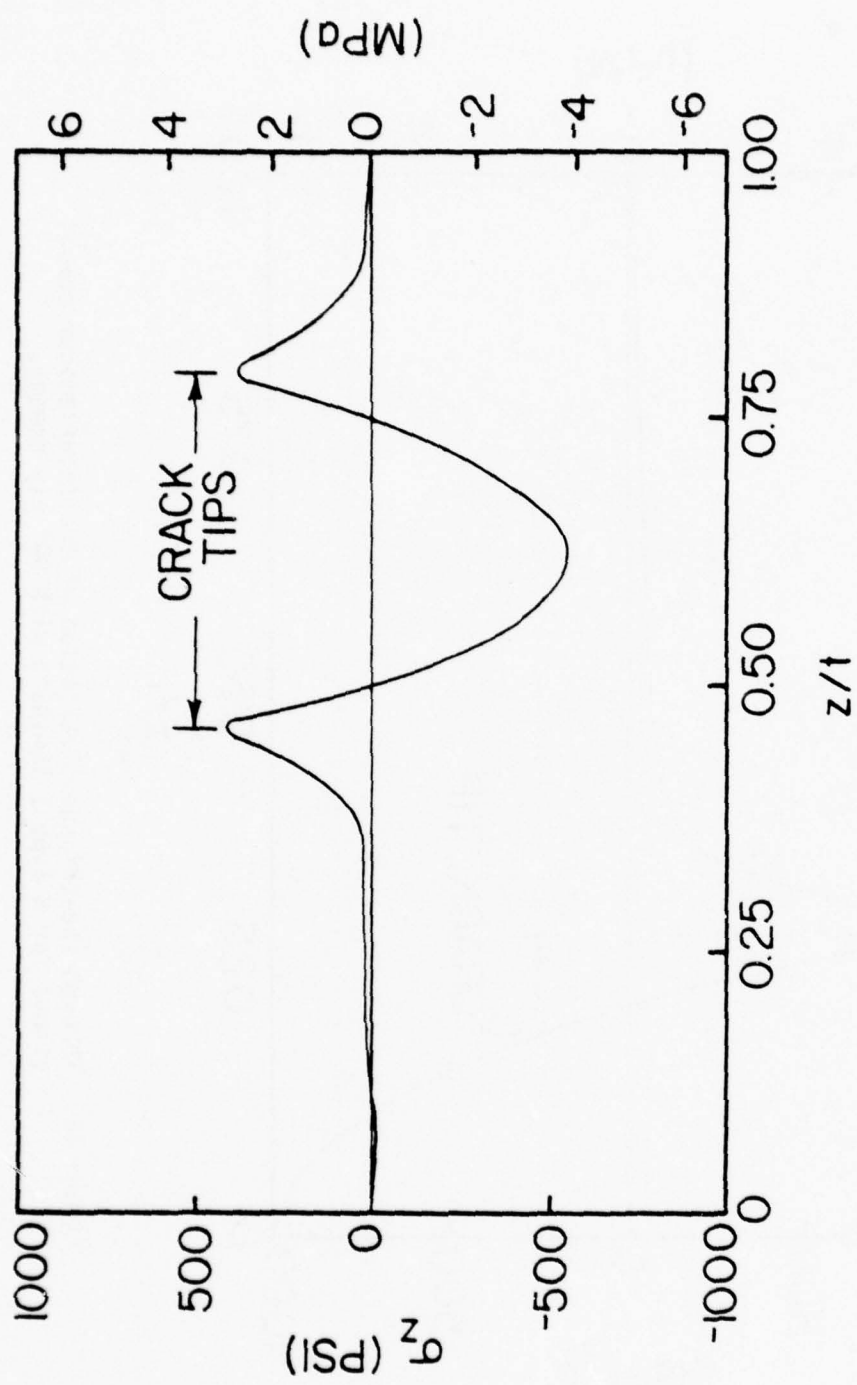


Figure 47. Through-the-thickness variation of the interlaminar normal stress for a type II laminate with 90° ply damage.



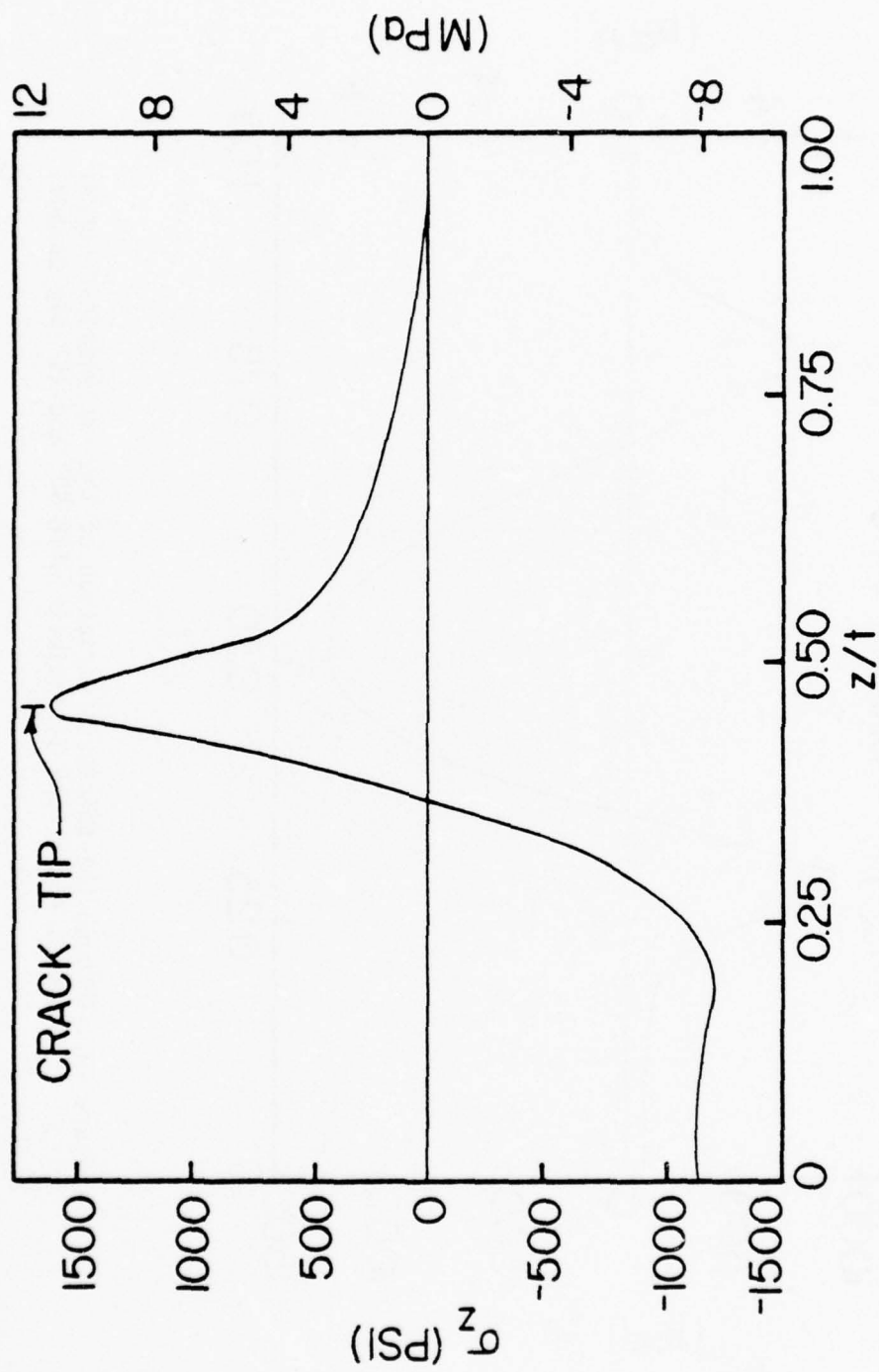


Figure 48. Through-the-thickness variation of the interlaminar normal stress for a type I laminate with 90° and -45° ply damage

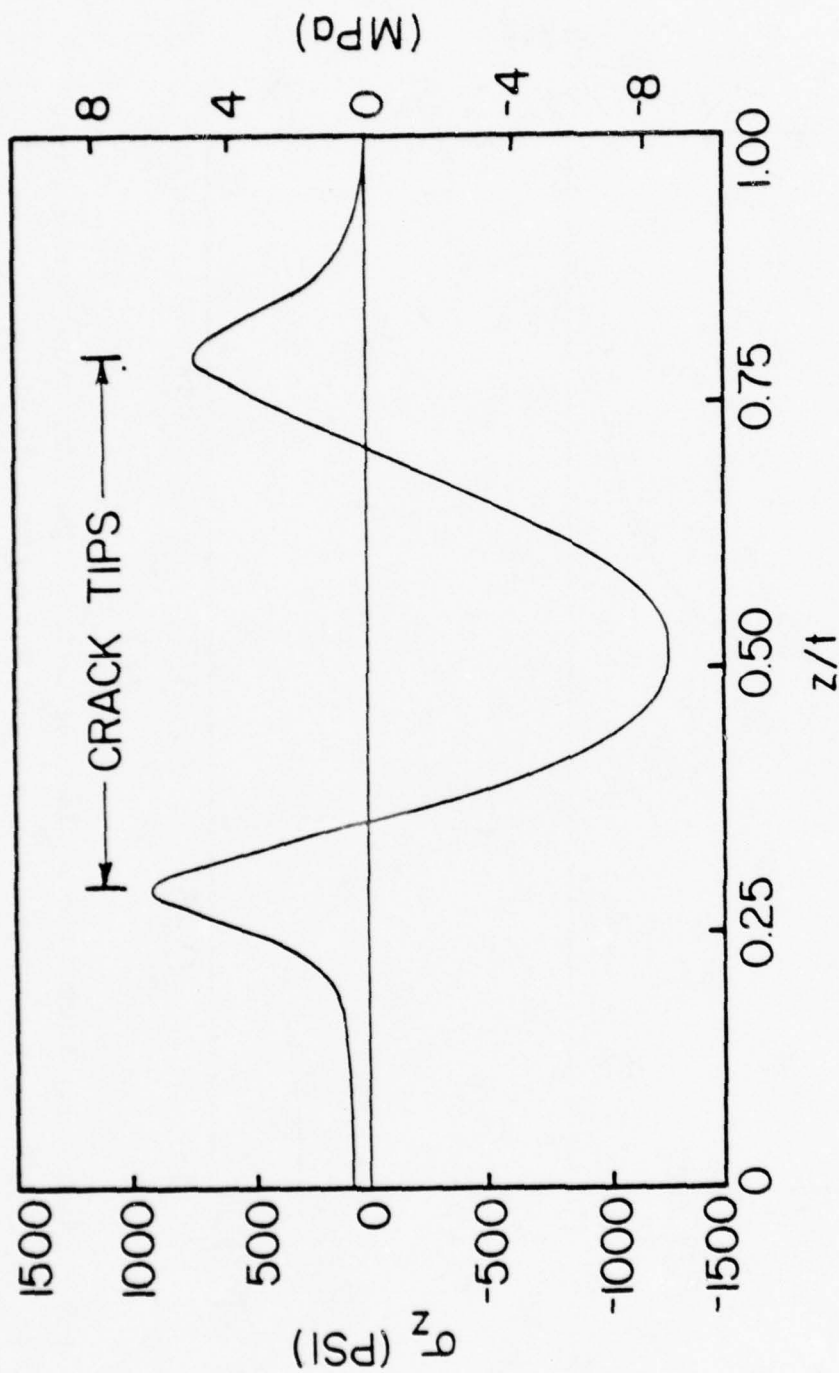
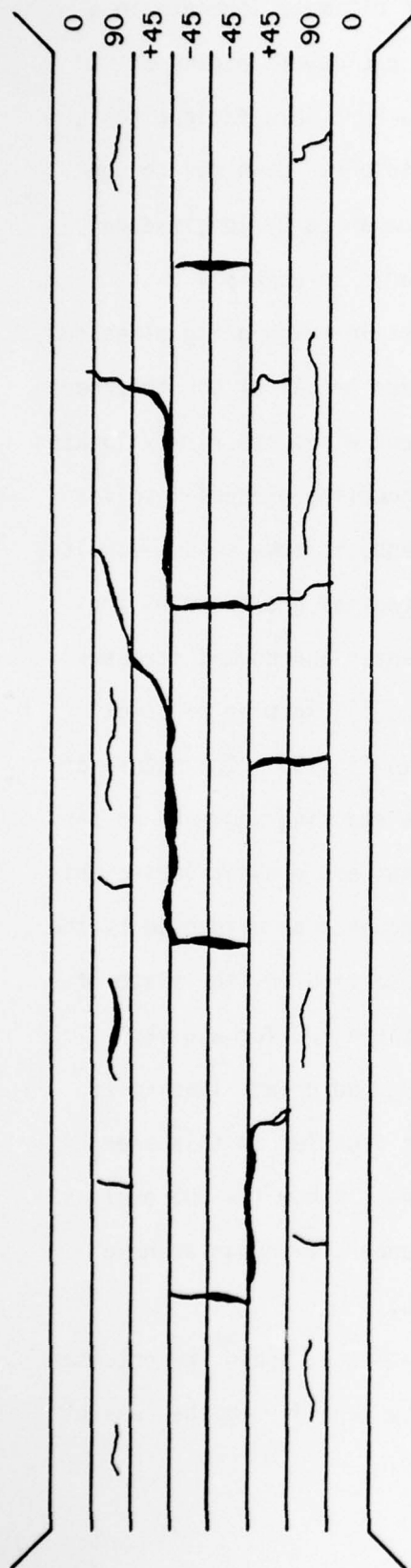


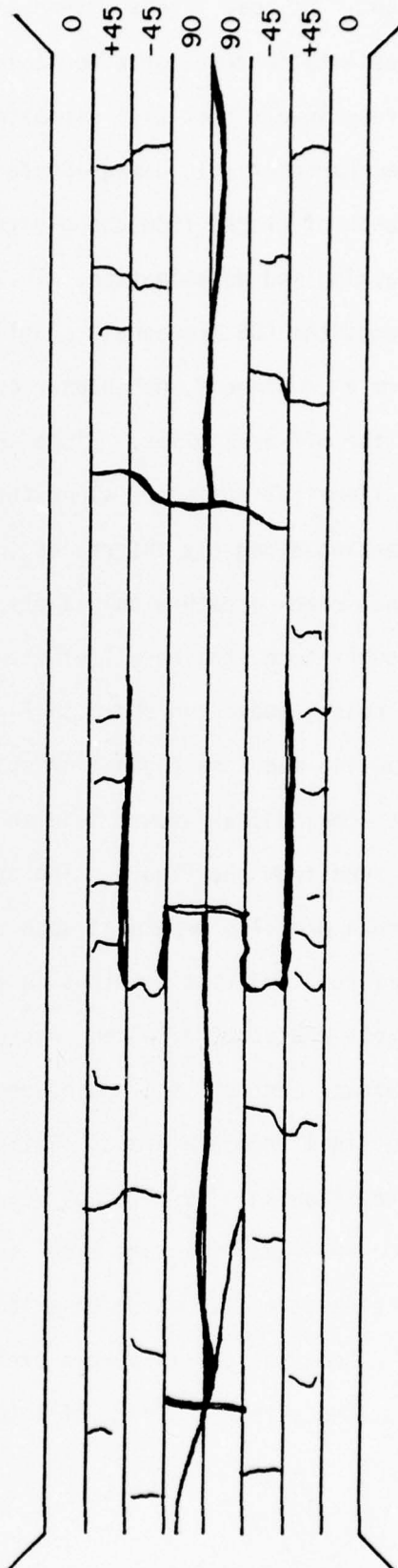
Figure 49. Through-the-thickness variation of the interlaminar normal stress for a type II laminate with 90° and 45° ply damage.

event. At load levels within a few percent of ultimate strength in a quasi-static test, or after a large number of cycles of loading at stress levels that will ultimately produce fracture in a fatigue test, the characteristic damage state (CDS) begins to break down due to the growth of cracks from one ply to the next accompanied by longitudinal cracking and delamination. The transverse cracks in each ply that formed the CDS frequently couple up with cracks in neighboring plies to form a continuous, non-planar crack through part or all of the thickness of the off-axis plies. Since cracks in adjacent plies are rarely located at identical positions along the length this coupling process involves cracking along ply interfaces (delamination) and, in some cases, longitudinal crack growth within a ply. These longitudinal growth modes are thought to be the result of the interlaminar shear and normal stresses discussed above and shown in Figs. 40 through 49. Examples of crack coupling and longitudinal cracking are shown in Fig. 50. The nature of the longitudinal growth is also dependent upon stacking sequence as can be seen from the figure. The stress fields that are present during this growth are also dependent upon the stacking sequence as evidenced by the different CDS that develops in each case. In particular, the state of stress and state of strength created by the stable CDS for a given laminate controls the subsequent crack coupling and growth leading to the final fracture event. This is the present frontier in this area of investigation. We have not yet established exactly how the CDS evolves into the final fracture event in a rational manner, although we have considerable data which describe the evolution.

Some insight into this evolutionary process can, again, be obtained from the stress analysis of interior cracks, by considering the case of



112



# PRE-FRACTURE PATTERNS NEAR FRACTURE SITE

Figure 50. Pre-fracture Crack Patterns Showing A Breakdown of the Characteristic Damage State by Crack Coupling and Longitudinal Cracking

a crack which has extended through the entire thickness of off-axis plies, i.e., only the zero degree plies remain unbroken. Based on our experimental data, and rather simple logic, such a state is the last well-defined condition preceding fracture in a tensile test. Figure 51 shows the distribution of the axial normal stress ahead of what we shall call a through- (the off-axis plies) crack as the tip enters the zero degree ply. Equilibrium requires that the area under the two distributions be the same. The Type I laminate has a higher stress near the crack tip and lower stress away from the tip. If one makes the interpretation that such a state of stress might cause the crack to propagate more readily than the Type II distribution, since the stress near the crack tip is greater, then one would predict that the Type I laminate has lower ultimate strength. The experimental data show that the Type I laminates do have consistently lower strength under both quasi-static and fatigue loading, usually by about six to fourteen percent. Of course, as we have pointed out earlier, the Type I laminate also delaminates which may also contribute to the lesser strength (4). However, we have been unable to directly associate the mechanism of delamination with the mechanism of actual fracture in these laminates, analytically or experimentally. While delamination is much more extensive during fatigue loading than during quasi-static loading, the strength (or residual strength) differences appear to be more directly related to the fact that delamination creates a serious discontinuity along the length in the region of the tabs (or grips) and increases greatly the incidence of grip-related failure.

The interlaminar shear stress ( $\tau_{xz}$ ) distributions for the "through-crack" are shown in Fig. 52 for the Type I laminate. A similar pattern



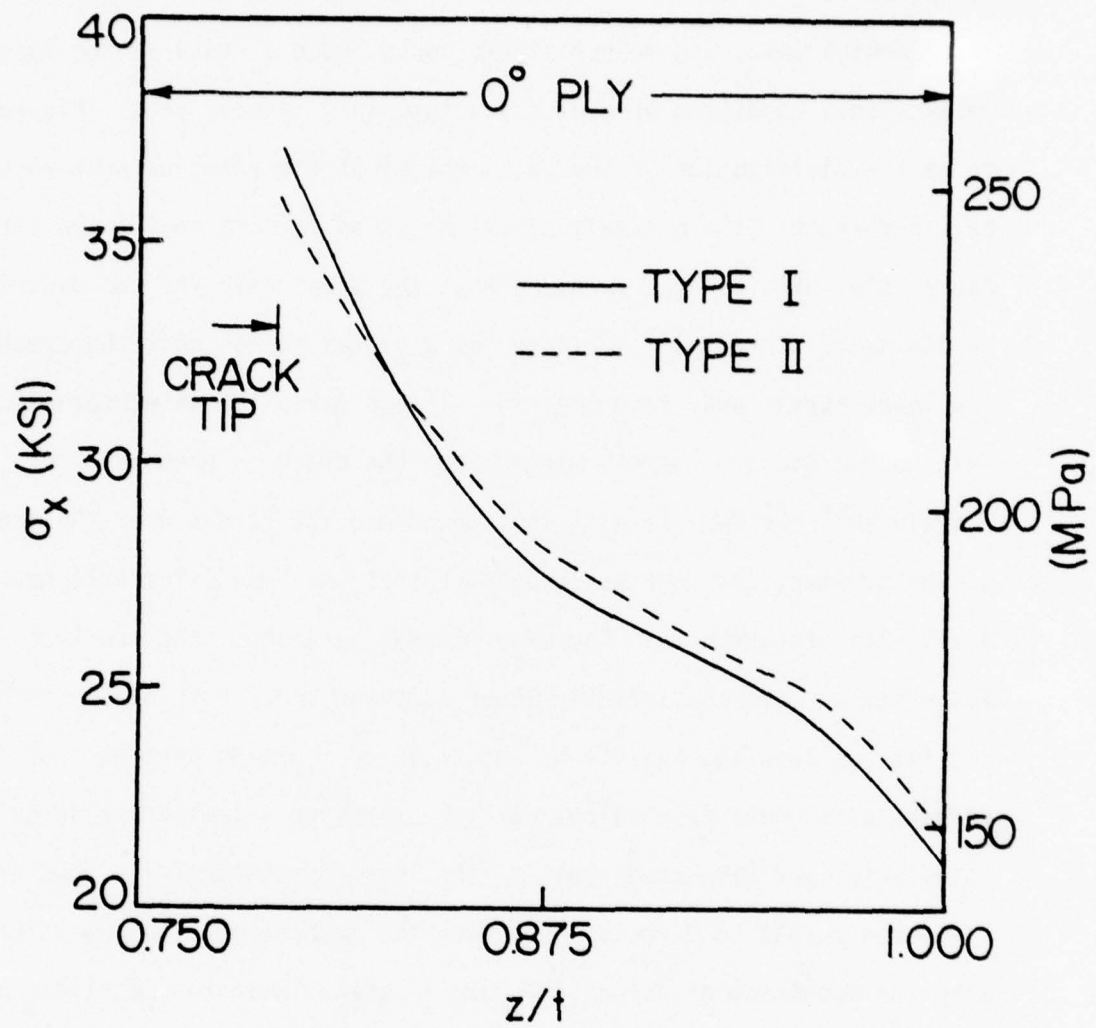


Figure 51. Through-the-thickness variation of  $\sigma_x$  ahead of the crack tip for complete off-axis ply failure. (After the crack extends into the  $0^\circ$  ply.)

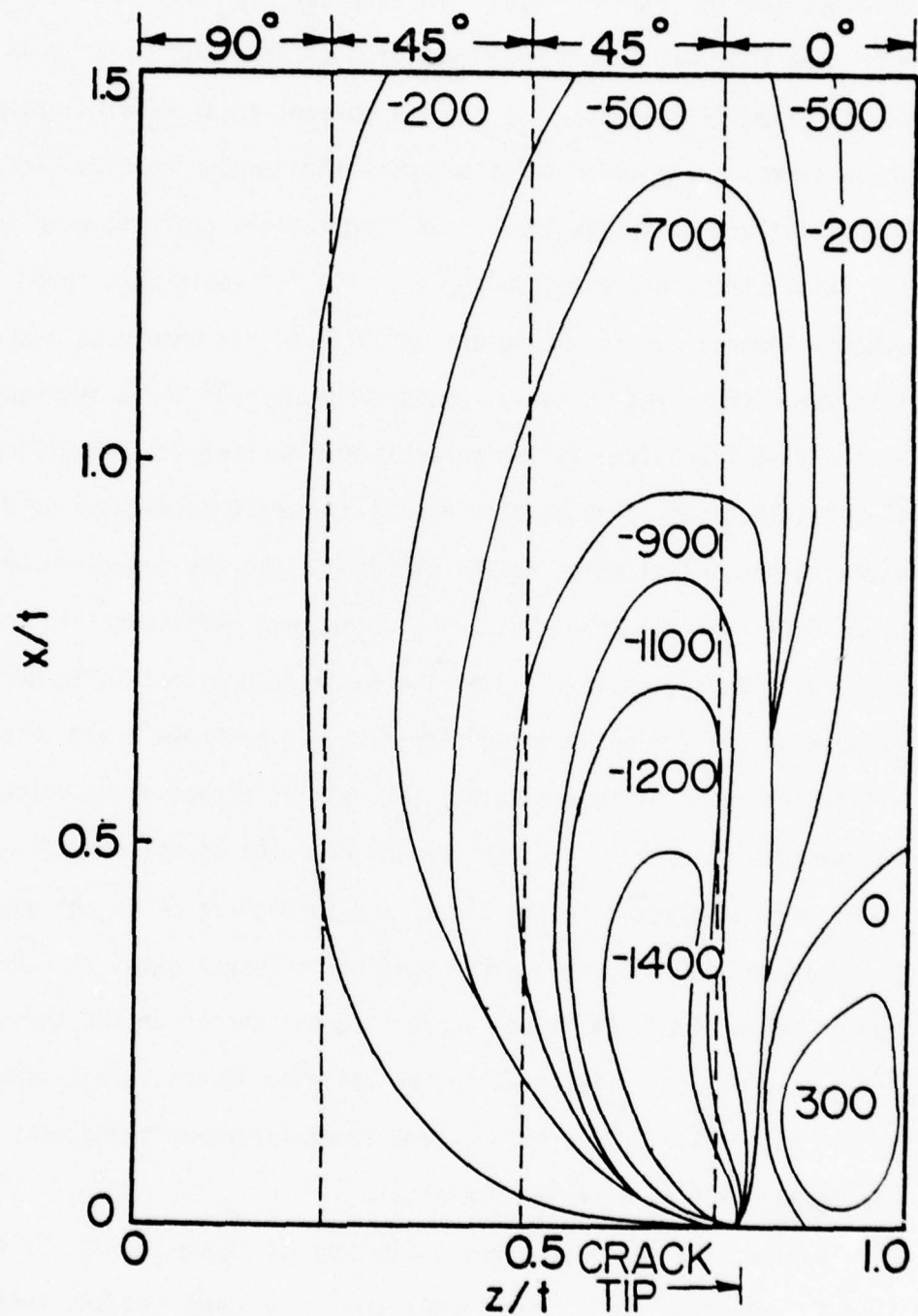


Figure 52. Contours of  $\tau_{xz}$  (psi) for a type I laminate with complete off-axis ply failure.

develops for the Type II case. The stresses near the crack tip reach more than 2000 psi (13.78 MPa) (compared to about 1225 psi (8.44 MPa) for the Type I laminate) for our 0.1 percent axial strain loading. These stresses are quite large and more than enough to cause local matrix failure at design loads. If longitudinal cracking were to occur the axial stress distribution shown in Fig. 51 would be altered, presumably lowered due to the "blunting" effect. It should be emphasized that the differences in the stresses which develop for a through-crack in the Type I and Type II laminates is due entirely to the difference in the distributions of compliance across the crack faces (due to different stacking sequences) which causes differences in the manner in which the crack faces deflect under load, and consequent differences in local stresses. Hence, while the stacking sequence does not influence the in-plane stresses for an undamaged laminate, it can make a significant difference in the in-plane values (as well as out-of-plane values) in the damaged condition. In the present case the lowest stresses in the local region adjacent to the tip of the through-crack in the unbroken plies are produced by having the stiffest off-axis plies (in the longitudinal direction) positioned nearest to the center of the through-crack and most compliant plies next to the unbroken layers. This makes the broken material displace more like a "boot-in-the-mud" and less like the classical crack in a brittle material.

Another interlaminar stress component is shown in Fig. 53 for a Type I laminate. The  $\sigma_z$  magnitudes are quite large and, as mentioned earlier, contribute to local matrix cracking and longitudinal crack growth. The corresponding contours in the longitudinal direction are shown in Fig. 54. The Type II contours are quite similar. One must

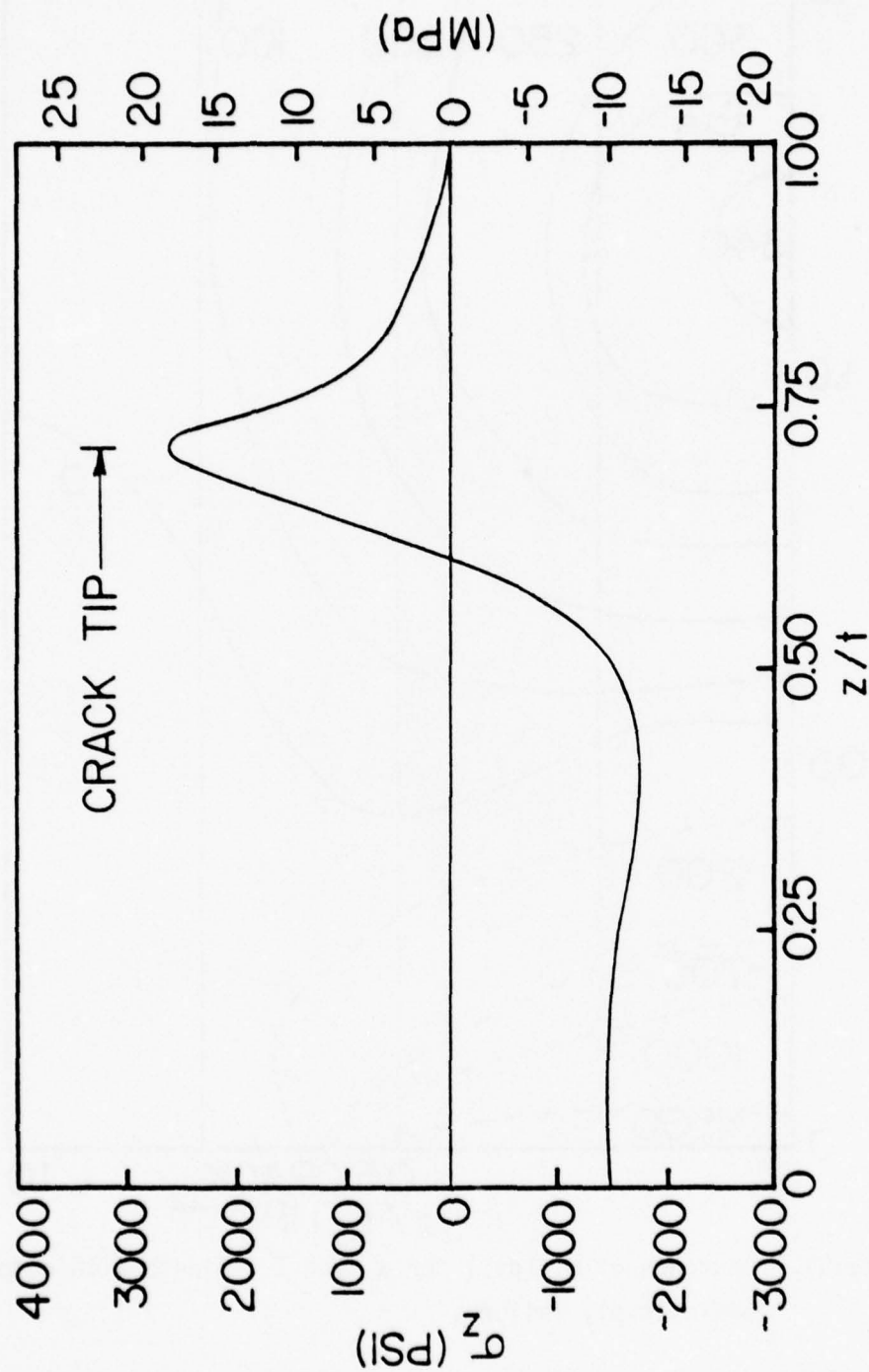


Figure 53. Through-the-thickness variation of  $\sigma_z$  for a type I laminate with complete off-axis ply failure. (Before the crack extends into the  $0^\circ$  ply.)

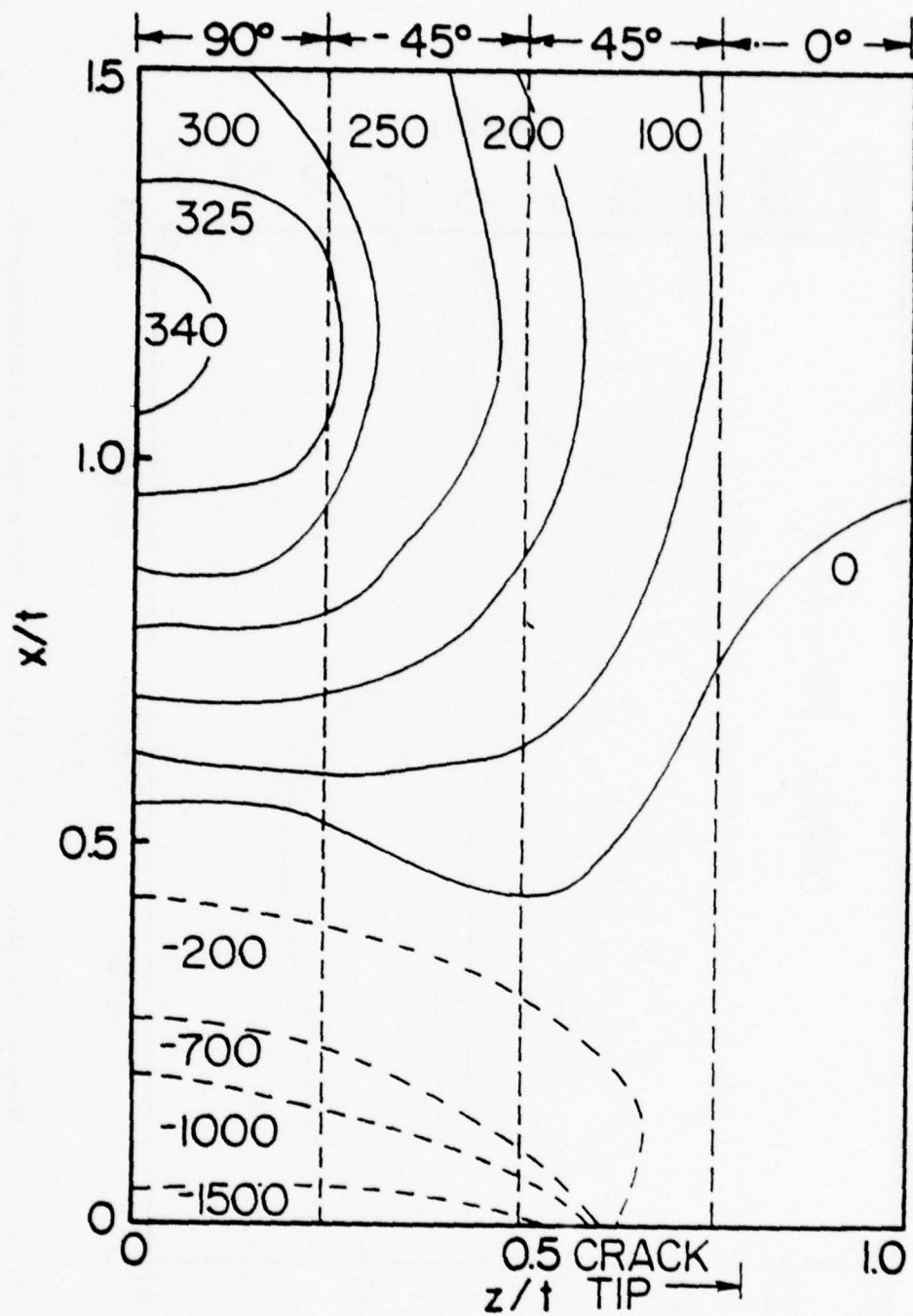


Figure 54. Contours of  $\sigma_z$  (psi) for a type I laminate with complete off-axis ply failure.



remember that these large stresses are in the interior of the specimen, not at the edge, i.e., they will occur for all such laminates in the damaged condition regardless of geometry.

The final observation dealing with our pre-fracture "through-crack" situation is made from the data shown in Figs. 55 and 56. Those plots show strain energy distributions in the unbroken  $0^\circ$  plies of Type I and Type II laminates with all off-axis plies broken, as well as in the broken plies. If we consider the  $0^\circ$  plies only we find that, in the total length shown - about three fourths of a specimen thickness in axial length - the total stored energy is greater for the Type II material than for the Type I laminate. The concentration of strain energy at the "crack tip" is also larger for the Type II case. However, the strain energy per unit length of total  $0^\circ$  ply cross section near the crack position is larger for the Type I case. For the cross section directly ahead of the crack plane it is about sixteen percent larger, with a similar difference along a distance of a ply thickness or so along the longitudinal direction away from the crack face. Since there is little evidence that "crack tip" local stresses control the fracture of  $0^\circ$  plies, and it is generally accepted that some region in front of a flaw tip is collectively involved in strength determination, our results suggest that the Type I stacking sequence should be less strong because of greater strain energy density in the flaw-related  $0^\circ$  ply cross section if that quantity influences fracture. This is consistent with earlier results and with our data.

We have, by no means, determined the complete picture of the mechanics of internal flaws. Perhaps the most obvious need is for attention to

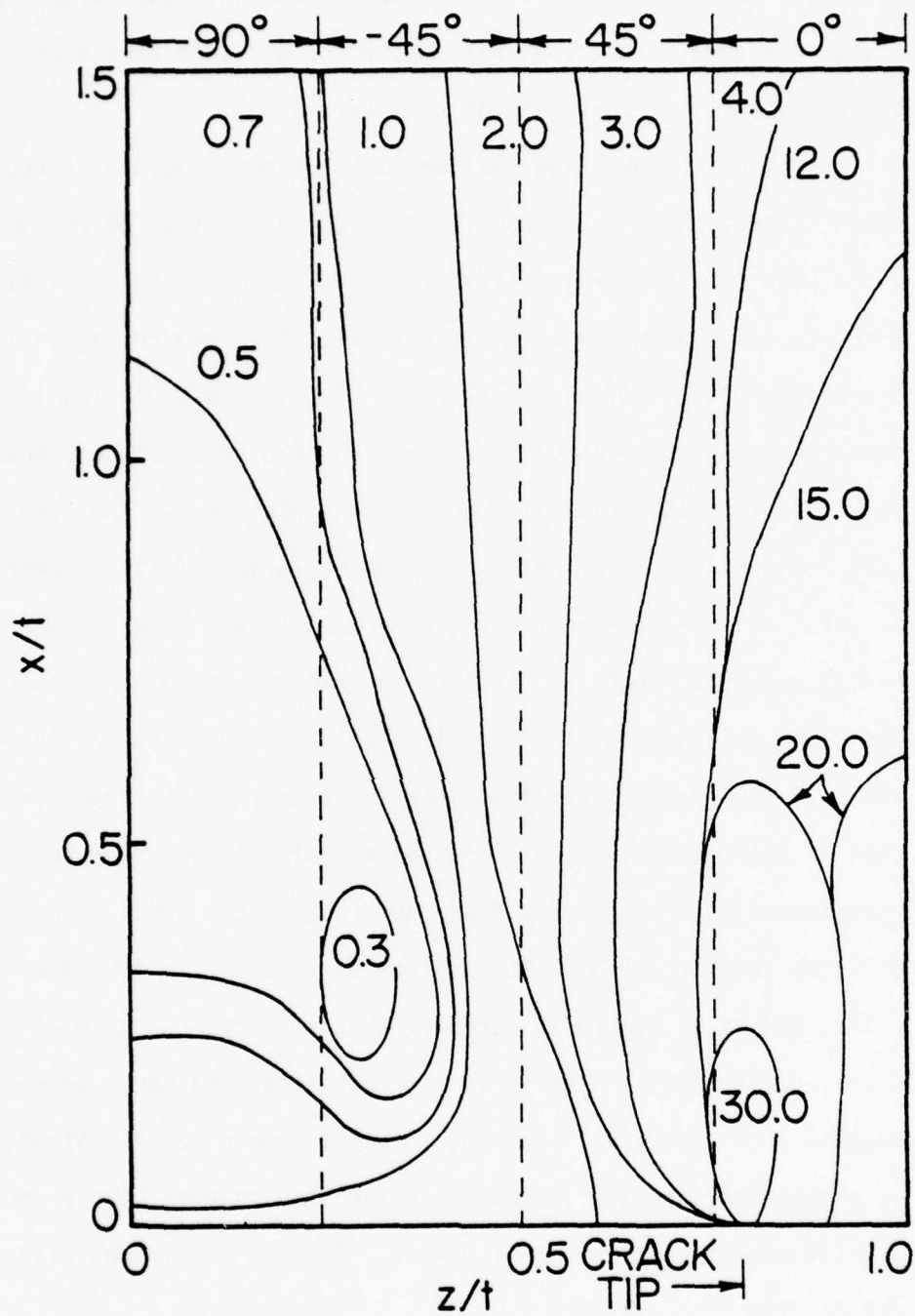


Figure 55. Contours of strain energy (psi) for a type I laminate with complete off-axis ply failure.

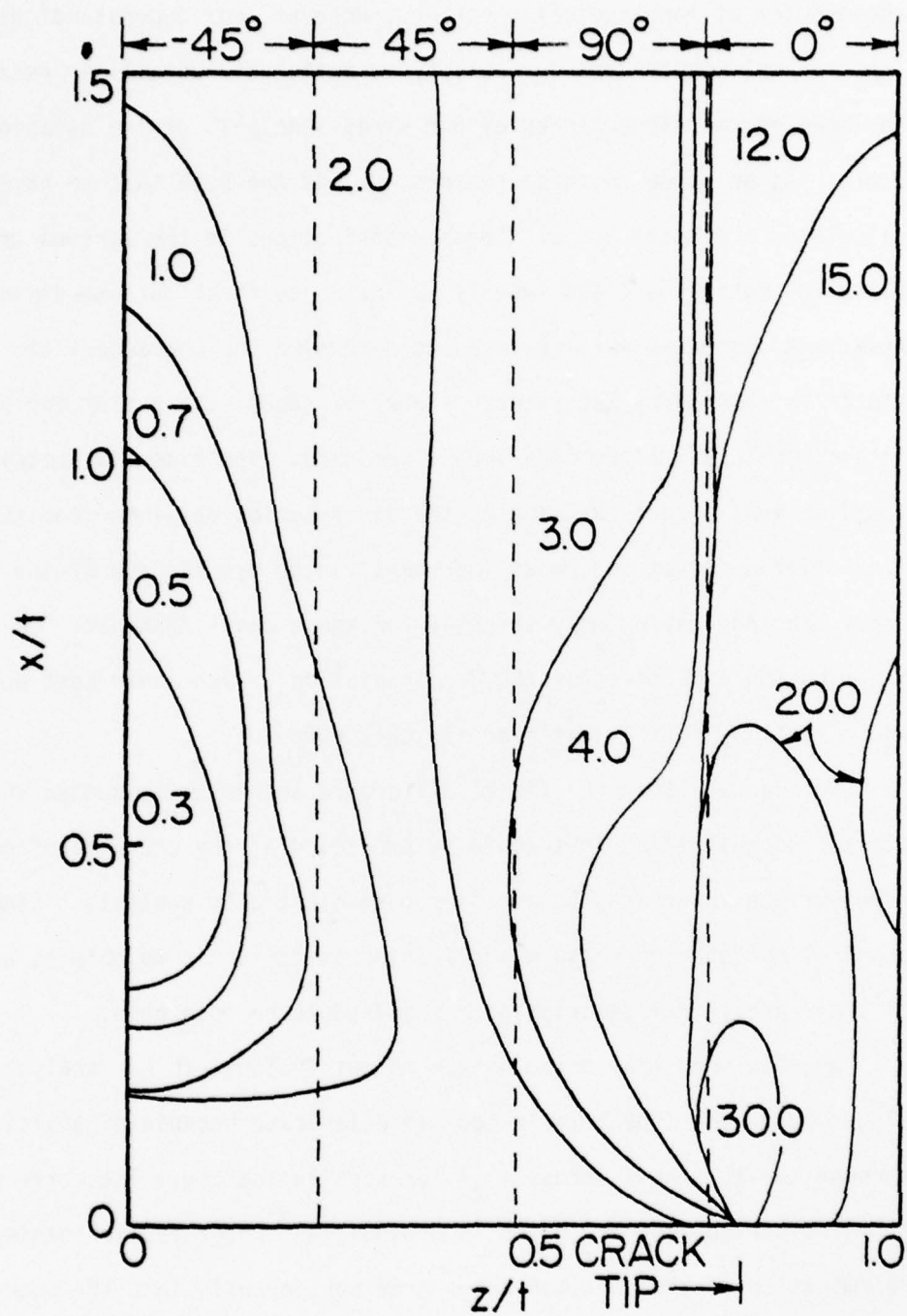


Figure 56. Contours of strain energy (psi) for a type II laminate with complete off-axis ply failure

the problem of longitudinal cracking. However, our understandings of experimental results and our ability to anticipate unfamiliar response has been enormously enhanced by our stress analysis of the damaged state. As an aside to these remarks, we add the note that we have also calculated the axial normal stress distributions in the various cracked plies for both Type I and Type II laminates to check our one-dimensional treatment described earlier, used to determine the characteristic damage states for arbitrary laminates. Figure 57 shows such a plot for a crack in the double  $90^\circ$  plies of a Type I laminate. The essential details of the distribution are the same as the distribution obtained from the simplified analysis and, most importantly, the predictions of the CDS crack spacings differ only slightly for those cases examined. Considering the objectives of the CDS predictions, such added cost and time and effort may not be justified for that purpose.

We also add that the finite difference scheme has expunged the elastic singularities that would be predicted at the crack tips and at free surface interfaces by a closed form elasticity analysis. Since physical evidence of these singularities is difficult to obtain, a loss of their analytical descriptions is judged to be tolerable.

We also note that delamination is not included in our analysis of the CDS. The Type I laminates did delaminate because of positive through-the-thickness stress ( $\sigma_z$ ) for tensile loading. The corresponding stress distributions are given in Appendix A. Under cyclic loading the delamination of the specimen edges grew continuously into the specimen. As delamination continued transverse cracking of the off-axis plies stopped in the delaminated regions. Additional details of this behavior appear in reference 10.

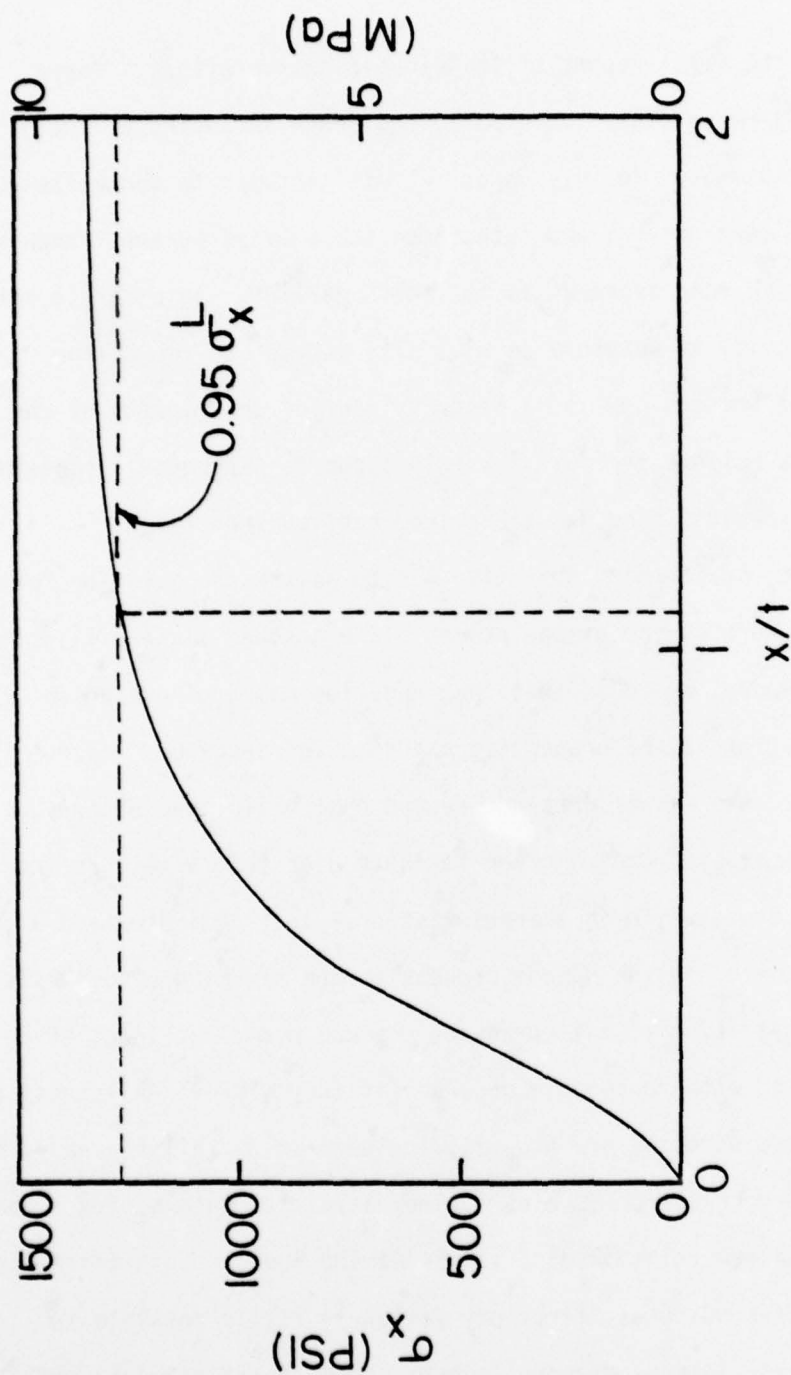


Figure 57. Variation of  $\sigma_x$  with the distance from the crack surface for a type I laminate with  $90^\circ$  ply damage.



## SECTION V

### SUMMARY AND CLOSURE

This is the final report of this investigative effort. Three earlier yearly reports have been published, each including a list of detailed conclusions. In this report we will attempt to summarize our findings on a more general and integrated scale by using the framework of our objectives and approach as set forth earlier. In order to retain as much continuity as possible we will also attempt to reduce the results of the program down to a reasonably brief description of the conclusions we believe the data strongly support. Appendix I contains a list of more specific findings taken from earlier reports.

Our first and foremost objective was to answer the question "precisely what is the nature of the damage process in unnotched angle-ply laminates"? For graphite epoxy, we found that that question has a unique answer for each unique set of lamina properties and stacking sequence. Except to a minor degree, the answer does not depend on tensile load history, i.e., we were able to establish that a given laminate does form a well defined, unique damage state which is characteristic of that laminate type alone.

The first step in the damage process is the cracking of off-axis plies. The initiation of this cracking process occurs at loads which can be predicted with reasonable accuracy if thermal residual stress and moisture-related stresses are properly included in a "failure analysis" using a standard criterion such as maximum strain or interactive theories such as the Tsai-Wu relationship, at the lamina level. This initiation is normally referred to as "first ply failure." It is possible to design for stress levels intended to avoid such "first ply failure." For quasi-isotropic laminates, however, first ply failure of "dry" laminates

may occur at about 20 ksi (137.8 MPa). Also, there are always some cracks in the off-axis plies before loading. Most troublesome, however, is the fact that first ply failure does not appear to have any physical significance. Cracks do not form throughout an off-axis ply at one load level, but over a wide range of loads (or cycles at one load). So the laminate condition overall at first ply failure cannot be uniquely described.

If loading continues beyond the initiation of cracking in a given off-axis ply, or if the load is cycled with an amplitude just beyond the quasi-static level associated with crack formation, additional cracks form, generally in planes perpendicular to the load axis and to the specimen surface, through the thickness of a given ply and (although there may be exceptions) across the entire specimen width for uniform loading of a plate specimen. The number of such cracks increases until the rate of new crack formation begins to drop off sharply and finally stops entirely, i.e., the number of cracks remains essentially constant thereafter. The reason for this equilibrium state is found to be that the crack formation process creates, systematically, a more-or-less regular array of cracks in each off-axis ply with each crack being spaced apart from those around it by equal distances along the specimen length with a variability defined by variations in local strength, variations in local geometry, and variations in local stiffness due to such things as fiber volume fraction fluctuations. There is a unique crack spacing for each lamina in a given laminate, and when this spacing is reached the crack formation process stops, for that layer alone. This well defined damage state consisting of stable regular arrays of cracks in the off-axis plies forms for cyclic loading as well as quasi-static loading; it is

always the same state. It is independent of hygroscopic or thermal residual stresses, and does not depend on geometry except for stacking sequence. We have come to call this state the characteristic damage state (CDS) of the laminate. It can be thought of as the heterogeneous material counterpart of the single crack in homogeneous materials. It controls the state of strength and state of stress from which final fracture develops. Since it is well defined it is amenable to analysis. We have developed two analysis schemes, one quite simple, for predicting the CDS of any arbitrary laminate.

Strength, life and stiffness are all affected by CDS formation. Stiffness is influenced in the same way that the compliance changes for single crack growth in homogeneous materials, except that CDS formation begins very early in the life of a component and may be nearly complete before any significant strength reduction occurs, in contrast to the single crack case. Hence, stiffness changes (in all four independent in-plane stiffness values) may be large and will generally occur early. Strength, as we suggested above, may not be significantly influenced by CDS formation. If these regular arrays of cracks form and remain stable the strength is relatively unchanged. When the cracks begin to couple up from ply to ply to form cracks through the thickness of all of the off-axis plies strength reduction does occur. Changing the stacking sequence of the broken off-axis plies changes the resulting stress in the unbroken  $0^\circ$  plies suggesting a source of stacking sequence effects on strength. Such effects were observed. The final fracture process remains a frontier of knowledge. The exact nature of that event or the events immediately preceding it have not been established. Strength

is controlled by fiber breaks in the  $0^\circ$  plies and these breaks occur in the stress state created by the CDS but the mechanism is not known to us, especially not the triggering mechanism.

Life of the laminate is more difficult to define. If life is defined by stiffness change, and it may be in many engineering situations, CDS formation can be directly and quantitatively related to life. If life is defined by residual strength then we have a missing link in the results of our work, the unknown mechanism, mentioned earlier, which relates the CDS and its stress field to the final failure event. We know coupling and possibly delamination is involved but all the pieces of the puzzle do not yet fit, if we do in fact have all of the pieces.

The mechanics of our findings can be represented by fairly firm analysis since our damage state is well defined. We are able to predict the CDS, enabling us to anticipate the damaged condition of any laminate before failure and prior to testing. Estimates of stiffness change, strength and, in some cases, life, can be made from such information. Design philosophies can also be developed based on such an analysis. Testing of materials can be reduced. Perhaps the most important point is that we are able, for the first time, to quantitatively define and analyze a damaged state that has real generality in composite materials, even for fatigue loading.

The list of unanswered questions remains long. What, exactly, does happen when these materials fracture? What triggers the fracture event and what actually controls it? Until we are able to answer such questions we will never be able to intelligently design materials, i.e., optimize stacking sequences, create the best hybrid materials, design for reliability,



etc. An especially important aspect of this issue is how the CDS is related to fiber failure in the  $0^\circ$  plies. Then we can also ask, "what happens when we have a complex stress state such as in the neighborhood of a notch"? The philosophy behind the CDS indicates that it should not depend on the nature of the applied stress state, except as that state controls the degree of CDS development. We need to know if that is the case. There is also the question of other material systems; does the CDS form in other composite material laminates? While we know it does in some cases the question has not been answered completely.

Perhaps the most important question is "can the CDS concept be used as a basis for a mechanistic "mini-mechanics" approach to the description and prediction of the strength, stiffness, and life (or reliability) of composite materials." Or stated another way, "can the CDS philosophy be developed so as to provide a rational (*mechanics*) approach to describing the behavior of composite materials in the sense that fracture mechanics serves that purpose for homogeneous materials"? While our prejudice suggests an affirmative answer to that question, we do feel strongly that the question at least deserves to be answered.



## APPENDIX A

Although Type I and Type II laminates were both quasi-isotropic, there is a great difference between the through the thickness or  $z$  stress distributions. To establish the nature of those distributions, the laminate analysis was combined with the approach of Pagano and Pipes (10). Normal stresses in the  $z$  direction were of primary concern because of the possibility of delamination in the instance that  $\sigma_z$  is positive. The  $\sigma_z$  stresses are determined by the moments caused by  $\sigma_y$  (transverse) stresses in the plane of the laminate. The  $\sigma_y$  distribution for the Type I laminate layup is shown in Fig. A1. The thermal residual stresses are shown by the solid curve and the broken curve represents the total stresses due to the thermal residual stress plus a 4.45 kN (1 kip) axial load. In general, there is a tensile  $\sigma_y$  stress in the outer three layers and compressive stress in the  $90^\circ$  ply next to the center-line of the specimen. The  $\sigma_z$  distribution which results for this layup is shown in Fig. A2. Again, the solid curve is the thermal residual stress and the broken curve represents the values when an axial load of 1 kip is applied. The  $\sigma_z$  values are tensile throughout the thickness. At an applied load of 4.45 kN (1 kip) the tensile stress at the interface between the  $90^\circ$  and  $-45^\circ$  ply reaches a value of about 68.94 MPa (10 ksi) which should initiate delamination if a simple maximum stress criterion is applied. If it is argued that thermal residual stresses are relaxed near the specimen edge (for which these plots apply), then delamination may occur at a higher load. However, a load of at least 4.45 kN (1000 lb.) (an applied stress of at least 158 MPa) should be required to initiate delamination in these specimens.

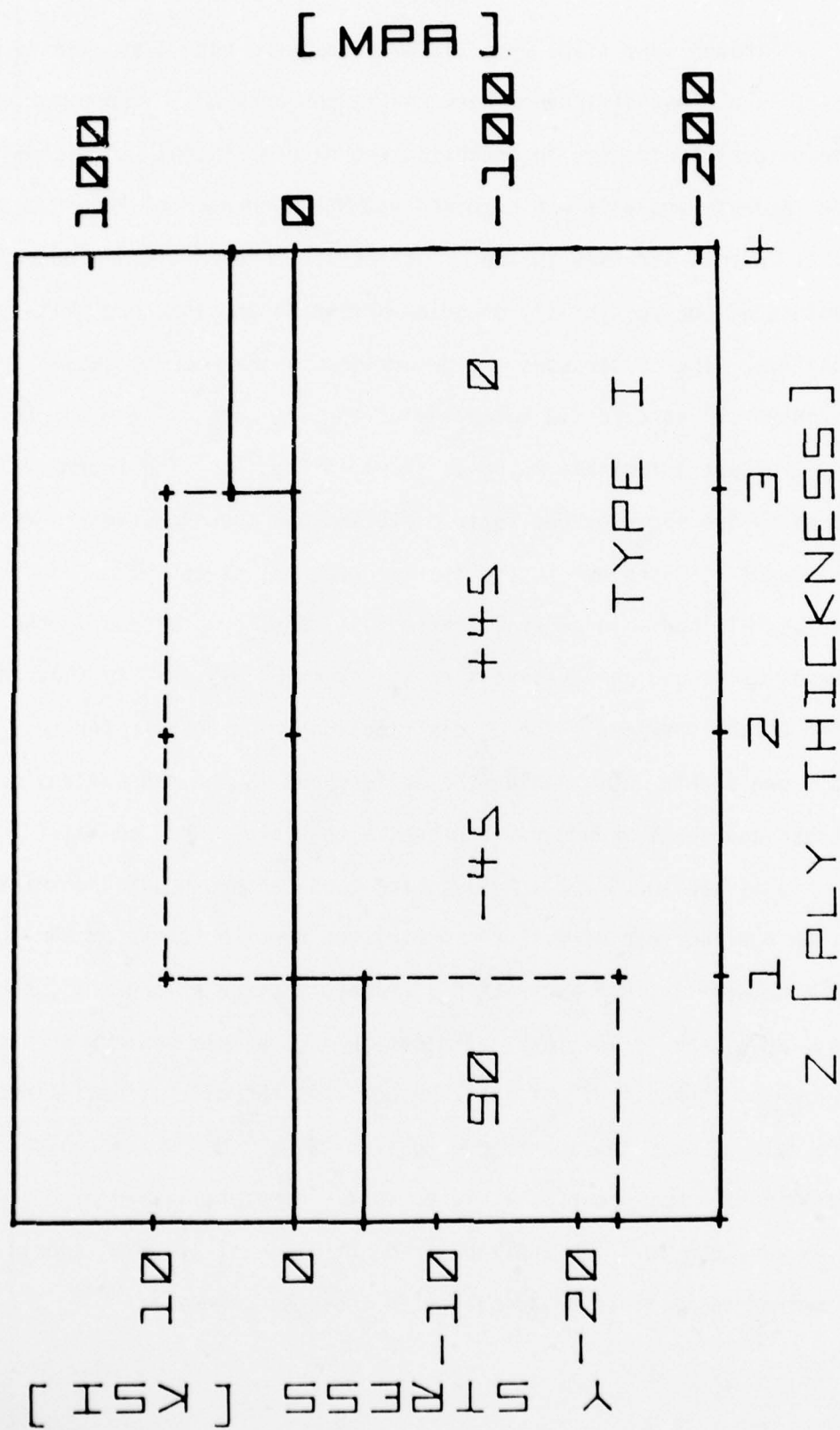


Figure A1. Transverse in-plane normal stress in a  $[0, \pm 45, 90]_s$  laminate. The thermal residual stresses are shown by the solid lines while the stresses due to a 4.45 kN applied load are shown by the dotted lines.

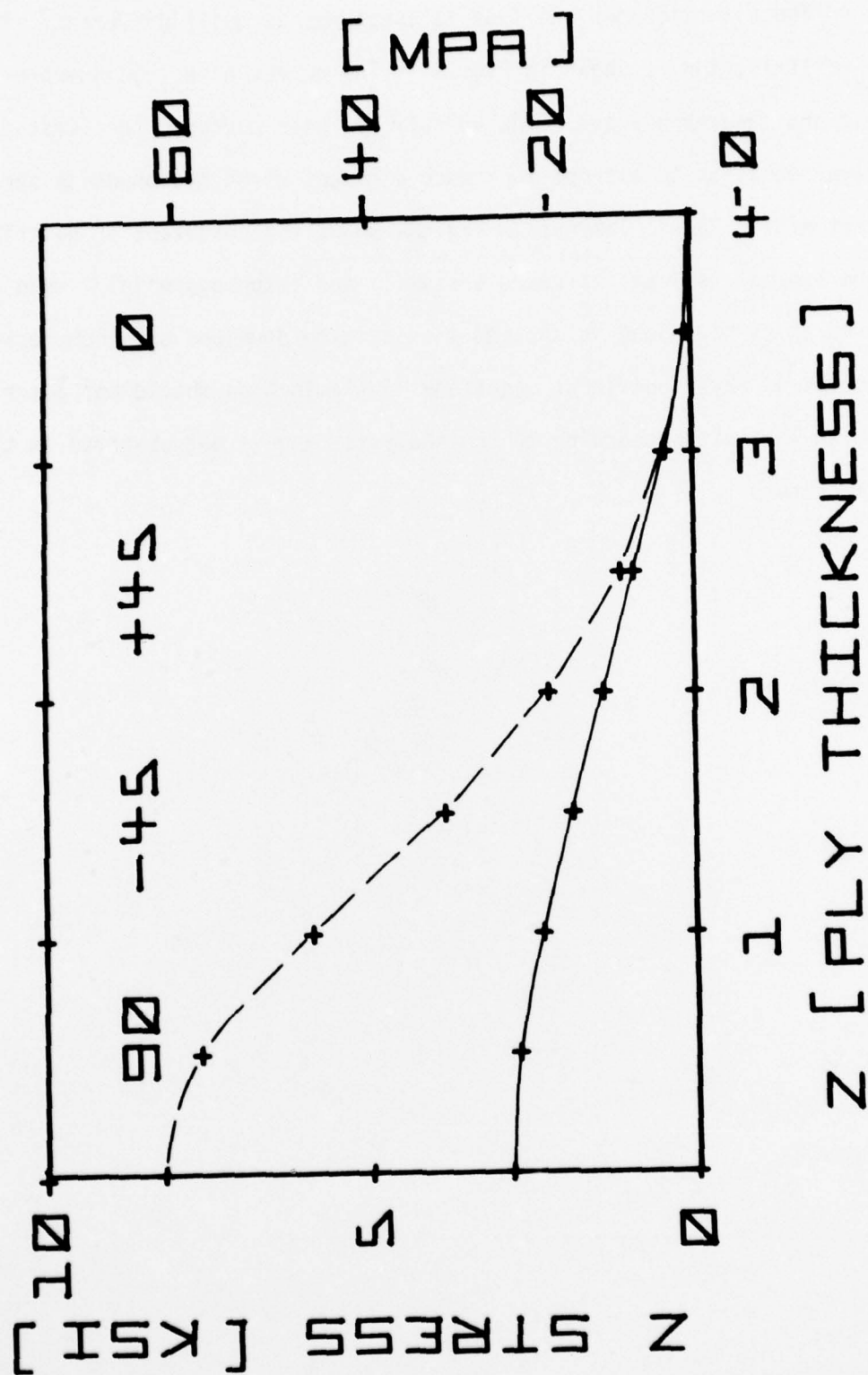


Figure A2. Through-the-thickness " $\sigma_z$ " stress distribution for a  $[0, \pm 45, 90]_s$  laminate.

The situation for the Type II specimens is quite different. The  $\sigma_y$  distribution is shown in Fig. A3. The curves have the interpretations described above. The 90° ply has been moved to the first underlayer position to attempt to induce a moment which has opposite sense to that of the Type I laminate. Fig. A4 shows the resultant  $\sigma_z$  distribution. The thermal residual stresses are small and inconsequential. When a 4.45 kN (1 kip) load is applied the laminate develops only compressive stress of any significant magnitude. Delamination should not occur for these laminates according to the analysis, and is not observed in the laboratory.



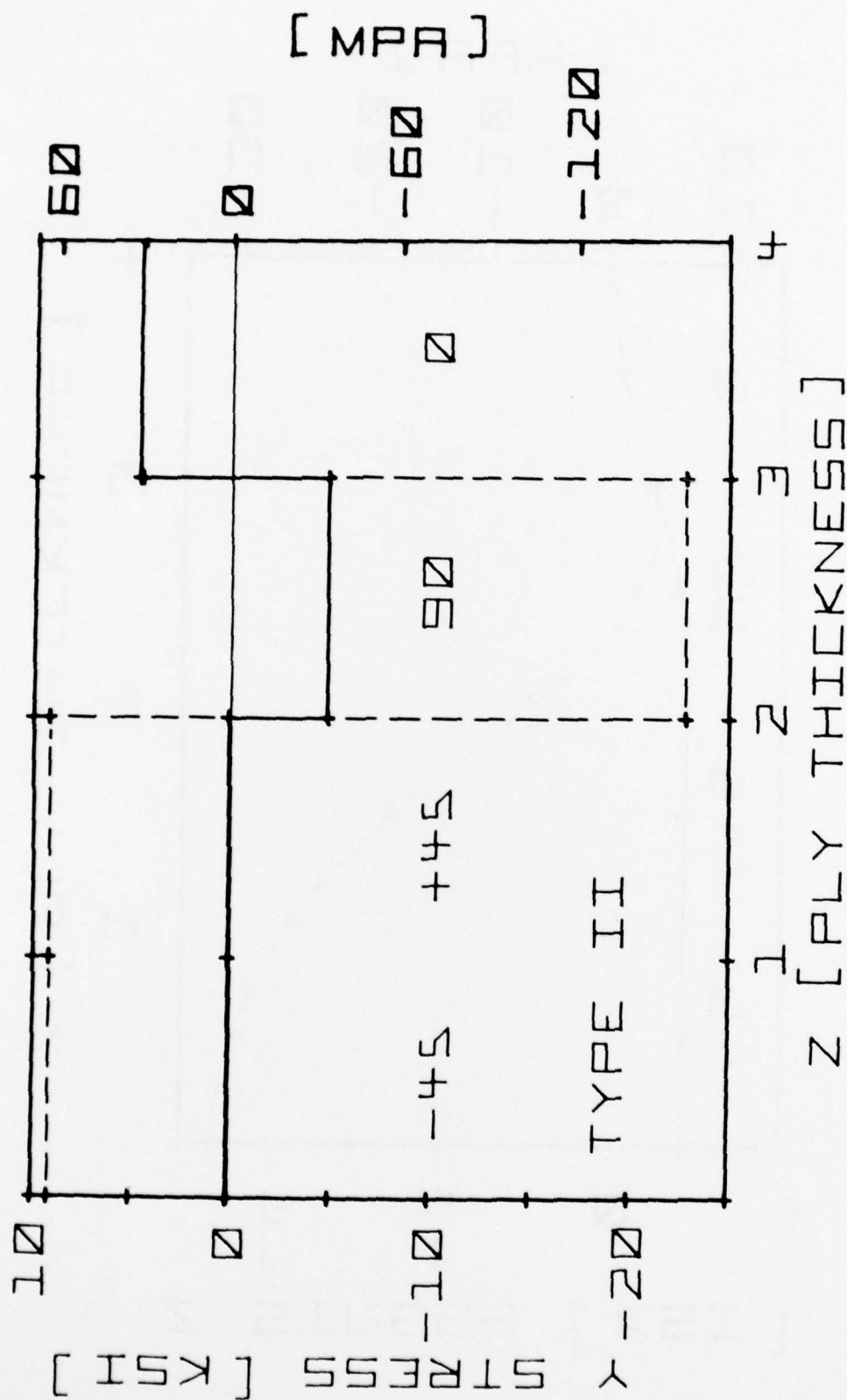


Figure A3. Transverse in-plane normal stress in a  $[0,90,\pm45]_s$  laminate. Solid lines show thermal residual stresses while dotted lines show the stresses under a 4.45 kN applied load.



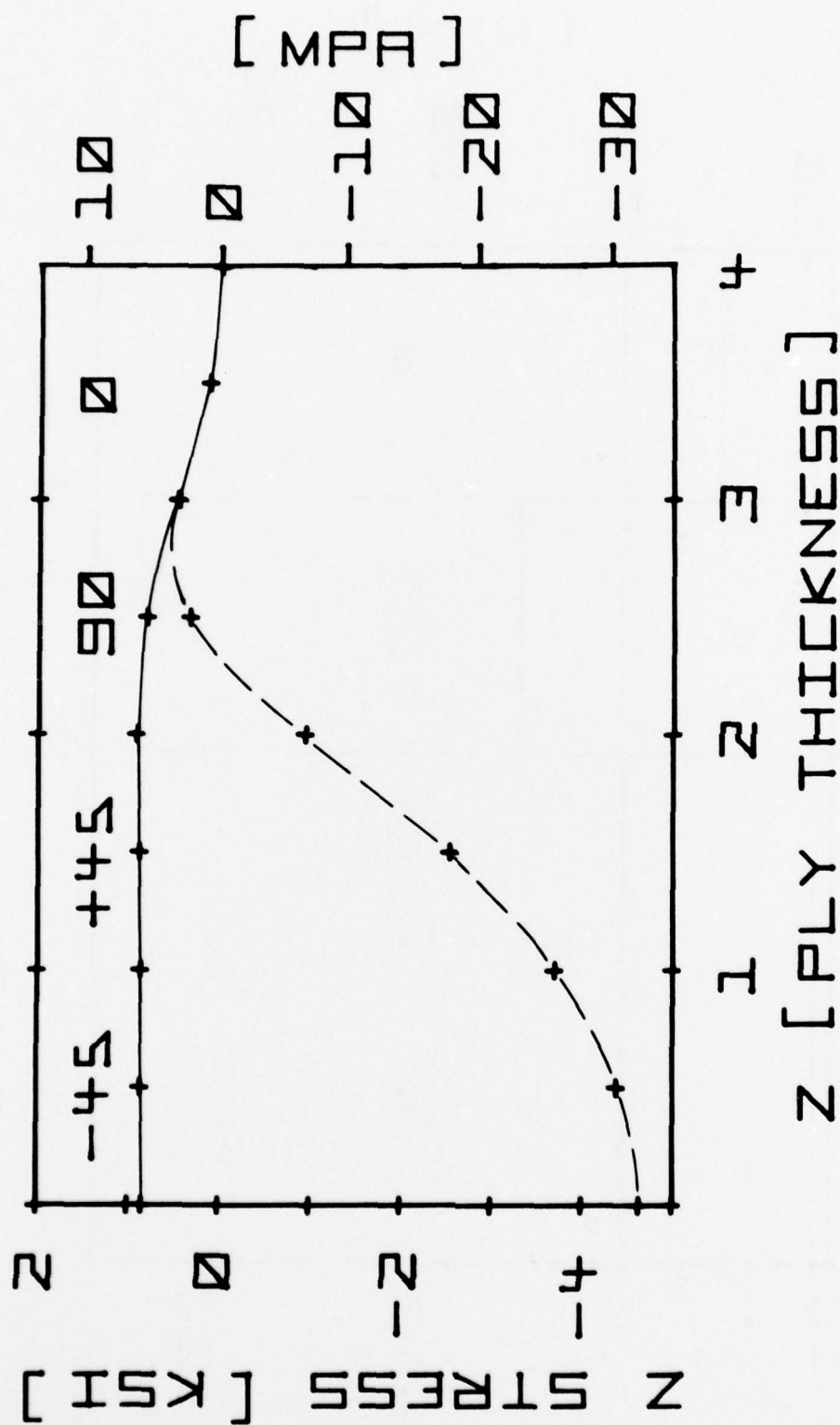


Figure A4. Through-the-thickness " $\sigma_z$ " stress distribution for a  $[0, 90, +45]_s$  laminate.

## REFERENCES

1. Smith, C. W., "Limitations of Fracture Mechanics as Applied to Composites," Inelastic Behavior of Composite Materials, Proc. 1975 ASME Winter Annual Meeting, Houston, Texas, C. T. Herakovitch, Ed., pp. 151-169.
2. Reifsnider, K. L., Henneke, E. G., II and Stinchcomb, W. W., "Defect-Property Relationships in Composite Materials," AFML-TR-76-81, April 1976.
3. Reifsnider, K. L., Henneke, E. G., II and Stinchcomb, W. W., "Defect-Property Relationships in Composite Materials," AFML-TR-76-81, A052358 Part II, June 1977; Part III, June 1978.
4. Hayford, D. T., "Theory of Ultrasonic Diffraction by Damage Developed in Thin Laminated Composites," Thesis, Master of Science, College of Engineering, Virginia Polytechnic Institute and State University, September 1977.
5. Hayford, D. T., Henneke, E. G., II, "A Model for Correlating Damage and Ultrasonic Attenuation in Composites," to appear in Composite Materials Testing and Design, STP 674, ASTM, 1978.
6. Jones, T. S., "Thermographic Detection of Damaged Regions in Fiber-Reinforced Composite Materials," Thesis, Master of Science, Virginia Polytechnic Institute and State University, April 1977.
7. Zweben, C., "On the Strength of Notched Composites," Journal of Mechanics and Physics of Solids, Vol. 19, pp. 103-116, 1971.
8. Kulkarni, S. V., McLaughlin, P. V., Jr., and Pipes, R. B., "Fatigue of Notched Fiber Composite Laminates," NASA CR-145039, April 1976.
9. Talug, A., "Analysis of Stress Fields in Composite Laminates with Interior Cracks," Thesis, Doctor of Philosophy, College of Engineering, Virginia Polytechnic Institute and State University, September 1978.